1-1-2004

Engineering viscoelastic properties of novel protein hydrogels.

Jill K. Sakata
University of Massachusetts Amherst

ENGINEERING VISCOELASTIC PROPERTIES OF NOVEL PROTEIN HYDROGELS

A Dissertation Presented
by
JILL K. SAKATA

Submitted to the Graduate School of the
University of Massachusetts Amherst in partial fulfillment
of the requirements for the degree of

DOCTOR OF PHILOSOPHY

February 2004

Polymer Science and Engineering

ENGINEERING VISCOELASTIC PROPERTIES OF NOVEL PROTEIN HYDROGELS

A Dissertation Presented

by

Jill K. Sakata

Approved as to style and content by:

David A. Tirrell, Chair

David A. Hoagland, Member

Horst H. Winter, Member

Thomas J. McCarthy, Department Head
Polymer Science and Engineering Department

DEDICATION

To my family, for their constant support and for instilling in me a belief that with God, all things are possible.

ACKNOWLEDGEMENTS

There are many people who have contributed to my scientific education and have made it possible for me to come to this crossroad in my life. I must begin by thanking my advisor, David Tirrell. He has provided me freedom to explore science from the perspective of a researcher and a teacher, and allowed me to work independently without hesitating to offer help whenever asked. I extend my sincere thanks to my committee members, David Hoagland and Henning Winter. I have been constantly encouraged and supported by both, and am thankful for their thoughtful advice and continued interest in my work.

The members of the Tirrell group, past and present, have provided many friendships as well as fruitful scientific discussions. First, I would like to thank Wendy Petka for efforts to spark my interest in this project, as well as her continued friendship and support in continuing this work. I thank Kathy DiZio, Kristi Kiick, David Flanagan, Karen Guhr, Jeff Linhardt, Wendy Naimark, and Nandita Sharma, for their friendship, especially during the move from Amherst to Pasadena. Thanks to Wei Shen for so much diligent work on aspects of this project that provided understanding in areas I did not explore. I thank Hanna, Isaac, Kent, Marissa, Pin, Rebecca, Sarah, Soojin, and Yi and all of the Tirrell group for being friends as well as co-workers.

I would like to thank many people who I worked with as collaborators, or who provided helpful advice to advance my research. John Crocker provided software for the single particle tracking system, as well as helpful advice about

the microscope apparatus and microrheology in general. Justin Gallivan studied a new application of this system to protein-polymer hybrids. Jim Harden introduced the idea of single particle tracking to characterize these proteins. Molly Stevens and Stephanie Allen have provided new methods to examine the molecular interactions of the leucine zipper domains. Eileen Spain has been a wonderful support during the last stages of my writing.

Most importantly, I thank God for blessing me with a wonderful family, both immediate and extended, and a loving husband. Their unconditional love and support continues to amaze me.

ABSTRACT

ENGINEERING VISCOELASTIC PROPERTIES OF NOVEL PROTEIN HYDROGELS

FEBRUARY 2004

JILL K. SAKATA, B.S., HARVEY MUDD COLLEGE

M.S., UNIVERSITY OF MASSACHUSETTS AMHERST

Ph.D., UNIVERSITY OF MASSACHUSETTS AMHERST

Directed by Professor David A. Tirrell

Hydrogels are of interest to the biomedical field because the hydrated networks can provide a physiological environment where biological species can survive or grow. Genetic engineering of protein polymers—a synthetic technique which provides a superior level of synthetic control without compromising natural composition—was used to prepare materials of the general architecture, rod-coil-rod. A naturally occurring motif, the leucine zipper, describes the rod domain. The leucine zipper can self-assemble when two amphipathic helices come together and are stabilized by contact along their hydrophobic face. The acidic leucine zipper domain, denoted 'A,' contains mostly glutamic acid in residues which flank the hydrophobic interface. A polyelectrolyte protein, of the repetitive sequence [$(AG)_3$PEG], defines the coil domain, denoted 'C.' AC_{10}Acys displayed reversible gelation as a function of pH and temperature, thus three aspects of the viscoelastic behavior were investigated.

The gelation properties were studied by single particle tracking, which monitors the Brownian motion of fluorescent particles imbedded in a protein hydrogel or suspended in a protein solution.

First, the physical crosslinks in an $AC_{10}Acys$ hydrogel network were diplaced by the addition of a leucine zipper domain, Atrp. A 2.23 mM $AC_{10}Acys$ hydrogel behaved as an elastic gel at pH 8.5, but upon addition of 1.13 mM Atrp, a viscous solution was obtained.

Second, the effect of charge of the leucine zipper domains were examined using, $AC_{10}Acys$, and $BC_{10}Bcys$, where 'B' denotes a basic leucine zipper domain. Both proteins form viscous solutions at 1.78 mM, pH 8.5 or pH 7.4, however, upon combination of $AC_{10}Acys$ and $BC_{10}Bcys$, a stiff elastic gel is formed.

Finally, a series of triblock proteins with increasing midblock length were genetically engineered to study the influence of midblock length on the gelation behavior of triblock proteins. The pH and concentration dependences of gelation of AC_xAcys, where x = (20, 30, 40, 50), were examined by single particle tracking. Whereas $AC_{10}Acys$ was found to gel around 2.23 mM, pH 8.0, the concentration required for gelation decreases to 1.27 mM for the protein with the longest midblock length, $AC_{50}Acys$.

TABLE OF CONTENTS

LIST OF TABLES

LIST OF FIGURES

CHAPTER 1

INTRODUCTION

Polypeptides that adopt specific three dimensional structures, display unique biological functions, or self-assemble to higher order aggregates are interesting for biomaterials applications and can be synthesized by genetic engineering. The work described herein aims to elucidate the relationship between the microstructure of triblock protein polymers and the macroscopic properties of their resulting bulk materials. The general architecture of the triblock is defined by two leucine zipper end blocks separated by a water soluble polyelectrolyte spacer. Leucine zipper domains are able to associate into dimers or higher order aggregates, physically crosslinking chains to form a network. The polyelectrolyte coil domain hydrates the region surrounding the aggregates, creating a swollen hydrogel.

This body of work addresses questions of how changes in microstructure affect the macroscopic properties of triblock protein hydrogels. First, the ability to impede network formation by adding rod end blocks into a rod-coil-rod gel addresses the hypothesis that network formation is a function of leucine zipper association (*1*). Second, the viscoelastic properties of the protein hydrogel are examined as a function of electrostatic changes in the leucine zipper domain. Triblock proteins comprised of sequences which differ in 24 of 232 residues are examined independently and in combination to create a new method for induced network formation. Third, the viscoelastic properties of a series of proteins containing the same leucine zipper end blocks are examined with respect to increasing polyelectrolyte midblock length.

1.1 Synthetic Physical Gels

The material properties of a homopolymer, which is synthesized from a single type of monomer, can be altered by covalently linking one homopolymer chain with another. Often, two polymers with opposite characteristics (i.e. glassy and rubbery) are combined to improve the bulk properties. Microphase separation is controlled at the molecular level—covalently linking homopolymers will limit aggregate sizes of the different phases. A common illustration of this idea is found in styrene-butadiene-styrene triblock (SBS) copolymers. Phase separation is limited by the covalent connectivity between the styrene and butadiene blocks (*2*). The rigid styrene microphases prevent flow, while the rubbery butadiene regions impart elasticity. Rigid phases are analogous to covalent crosslinks in a chemical gel, but lack the specific functionality imparted by the chemical crosslinking agents.

Thermo-reversible gels, such as SBS terpolymers, differ from chemically crosslinked networks in that the junction points in the gel result from secondary, or non-covalent, interactions between chain segments. The interactions are largely due to van der Waals forces or hydrogen bonding and can be disrupted by an increase in temperature. A similar temperature dependence is observed in biological systems; folded proteins, such as enzymes, remain in their native state at physiological temperature but denature with an increase in temperature.

The gel point for a polymeric system with chemical crosslinks is defined by Flory as the point when the weight-average molecular weight can be considered infinite, or an infinite network is formed (*3*). In the case of physical gels, the crosslinks are able to

exchange at some time scale, so that an infinite network may be present on one time scale, but at longer times, the network is freely exchanging. Thus, viscous character is observed at long times, but an elastic network may be observed at shorter times. Green and Tobolsky (*4*) described a basic theory for transient networks, which was experimentally examined by Annable and coworkers (*5, 6*) using hydrophobic ethoxylated urethane (HEUR) polymers that associate into physical gels. Hydrophobes cap the ends of polyethylene-glycol polymers to comprise the HEUR polymer, which forms micelles in dilute aqueous solutions. Hydrophobe end blocks comprise the interior of the micelles and the polyethylene-glycol midblocks form the corona, shielding the hydrophobes from the aqueous environment. As the concentration increases, hydrophobic end blocks can bridge two micelles, effectively acting as crosslinkers. The rate of hydrophobe exchange in and out of a micelle defines the relaxation time of the viscoelastic network—this relaxation time is the reciprocal of the disengagement rate (*5*).

1.2 Protein Hydrogels

Biosynthetic polymers which display reversible gelation are of interest as biomaterials for applications in wound healing, drug delivery, or cellular encapsulation. Although natural materials, such as fibrin, or collagen, are widely available and generally biocompatible, the mechanical properties of their resulting materials often vary from batch to batch. The variation in processing presents a potential drawback for reliable preparation of naturally derived materials. In contrast, synthetic polymers, such as

poly(ethylene oxide) or poly(methyl methacrylate) afford greater synthetic control, but sometimes at the expense of biocompatibility.

It is of interest, therefore, to use biosynthetically prepared protein polymers which display reversible gelation. This synthetic technique exploits nature's ability to synthesize monodisperse samples of polypeptides with precisely defined sequence, length, and tacticity—a feat not yet achieved using conventional polymer synthesis methods. Recombinant DNA technology was used to create protein polymers that are naturally derived and biodegradable, but at the same time may be readily modified with precise synthetic control.

Genetically engineered polymers provide the opportunity to create systems which are biologically compatible, retain biological function, display sensitivity to temperature and pH, and require low concentrations of material to form a physical gel. More importantly, structure-property relationships can be studied directly by eliminating the uncertainty in the polydispersity and tacticity of the sample.

Exploiting the ability of proteins to fold, self-assemble, and associate through specific binding, Petka designed artificial proteins that form reversible hydrogels under physiological conditions (*1*). The proteins are triblock copolymers generally described as rod-coil-rod copolymers, where the rod end blocks self-associate according to the leucine zipper motif and the coil is a water soluble polyelectrolyte described by a random coil conformation. This design provides the advantages of crosslinks, which self assemble according to a defined biological motif. The network formed by these triblock proteins is transient, owing to the reversibility of the end block aggregation and the ability of the individual chains to exchange among aggregates.

Coiled coil motif

The leucine zipper motif, a molecular coiled coil, is modeled as a two stranded rope. Crick first described the packing scheme for a coiled coil in terms of knobs (side chains of the individual residues) on one chain that align into the holes (groove) of the second chain. The most efficient packing is achieved when individual chains wrap around each other with the individual axes tilted approximately 20° from the coiled coil axis (*7*). The coiled coil motif was also suggested for the structure of tropomyosin, on the premise that non-polar groups align at the interface between helices in the coiled coil.

Not until 1972 (*8, 9*) did the amino acid sequence of tropomyosin verify Crick's proposal that the hydrophobic residues would be found at the coiled coil interface. The tropomyosin helix is characterized by a sequence of heptad repeats, $(abcdefg)_n$, in which nonpolar residues occupy **a** and **d** positions, while polar amino acids reside in the **e** and **g** positions. As the protein folds into a 7_2 helix, a hydrophobic face is formed by alignment of the **a** and **d** residues. This structure is stabilized by forming a dimer (two helices), where the two hydrophobic faces effectively exclude water from the inter-helical interface.

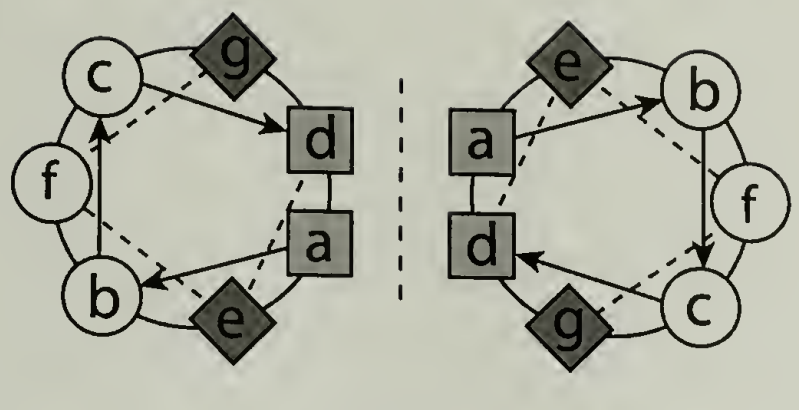

Figure 1.1 Helical wheel representation of a coiled coil dimer. The hydrophobic interface formed between **a** and **d** residues is illustrated with a dotted line. Residues flanking the hydrophobic interface, **e** and **g**, can stabilize or disrupt the hydrophobic interaction by their electrostatic interactions.

The stabilization of the coiled coil dimer can be enhanced or disrupted by electrostatic interactions between the **e** and **g** residues which flank the hydrophobic interface formed by the **a** and **d** residues (*10, 11*). By changing the electrostatic interactions of the **e** and **g** residues, one can tailor the stability of the artificial leucine zipper domains to create networks sensitive to different pH or temperature conditions.

Various groups have synthesized sequences which follow the general leucine zipper pattern to study the stability of coiled coil proteins (*10-14*). Circular dichroism spectroscopy has been adopted as the general method for coiled coil characterization because of the simplicity of its secondary structure—the α-helix. The stability of the folded structure is recorded in terms of the $t_{½}$, the temperature at which half of the protein is denatured. Tropomyosin analogues have been used to investigate the influence of : (i) disulfide bonding (*15, 16*), (ii) substitution of alternative nonpolar residues in the **a** and **d** positions of the heptad repeat (*15*), (iii) length of the coiled coil domain (*17*). Both disulfide bonds and increased hydrophobicity of **a** and **d** residues resulted in increased

stability, however, increases in coiled coil length did not result in proportional increases in stability.

A subclass of coiled coils, characterized by leucine residues in approximately 80% or more of the **d** positions, were named leucine zippers to describe how interdigitation of leucine residues facilitates the dimerization of two helices (*18*). This model assumes that the helices are out of register with each other and oriented in antiparallel fashion. A 30 amino acid peptide sequence—the leucine zipper domain of the yeast transcription factor GCN4—was synthesized and analyzed to examine this claim. The protein consists of domains for various functions, including one for DNA recognition and one that dimerizes by the leucine zipper motif. O'Shea and co-workers synthesized the leucine zipper region of GCN4 with a cysteine at either the NH_2 or the COOH terminus of the peptide (*19*). Preference for parallel or antiparallel dimers was determined by identifying the combination of cysteine terminal peptides resulting in disulfide bonded dimers. Results indicated that the helices were oriented parallel to each other, thus contradicting the leucine zipper motif proposed by Landshultz (*20*). X-ray diffraction patterns of crystals formed from the synthetic GCN4 peptide confirmed that the hydrophobic residues do not interdigitate, but instead align side by side, adding another subclass of proteins to those described by a coiled coil motif (*21, 22*). Although the leucine zipper mechanism was not confirmed, the name is still used to describe coiled coil proteins that contain leucine residues in at least 80 percent of the **d** positions in the heptad repeat. Further studies of GCN4, tropomyosin, their synthetic analogues, and other coiled coil proteins have elucidated factors which affect association and stabilization of coiled coils and have given insight to *de novo* protein design (*20, 23-28*).

Protein Design

Information about the association of coiled coils, the reversible nature of triblock copolymer gels, and the ability to synthesize polypeptides of exact sequence, tacticity and molecular weight provided incentive to create a new class of artificial proteins that self assemble into pH- and thermal-reversible hydrogels (*29*). The leucine zipper domain described by Petka *et al.* (*1*) consists of six heptad repeats, with glutamic acid occupying the majority of the **e** and **g** positions. Under acidic conditions, changes in protonation stabilize the leucine zipper dimer. Gelation of triblock protein samples follows the trend of leucine zipper folding—at room temperature and pH 8.0, an elastic hydrogel forms, which transitions to a viscous liquid as the pH increases above pH 9.5. The hydrogel was found to lose elastic properties with increasing temperature, with viscous behavior observed at 55 °C (*1*).

These triblock protein polymers were prepared by recombinant DNA technology. This synthetic strategy affords the ability to prepare monodisperse samples of protein polymers, where the molecular uniformity extends to tacticity and sequence (*30*). This method provides an opportunity to study the relationship between microstructure and bulk properties without the need to consider the influence of differences among molecules in the sample (*31-33*). Not only can one modify regions of the polymer—incrementally adding or removing blocks, or adding new functionality—but one can also substitute amino acids in the sequence with analogues that expand the chemical functionality beyond the 20 naturally occurring residues (*34*).

In this work we examine the role of the water soluble spacer by increasing its length from 10 to 50 repeats. Our synthetic technique allows us to change the water soluble coil independent of the leucine zipper domains.

1.3 Characterization Techniques

1.3.1 Circular Dichroism

Circular dichroism spectroscopy (CD) was used to determine the secondary structure of protein solutions at pH 7.4 in phosphate buffered saline. This technique reports the ellipticity, θ, which represents the difference in absorbance observed for left and right circularly polarized light. The spectrum of any protein can be simply described as the superposition of the fractional amount of each type of structure multiplied by the mean residue ellipticity, $[\theta]$, observed for the pure component at any wavelength:

$$[\theta] = f_H[\theta]_H + f_\beta[\theta]_\beta + f_R[\theta]_R \quad (1)$$

where $[\theta]$ is the overall molar ellipticity, f_H, f_β, and f_R are the fractions of each structural component, and $[\theta]_H$, $[\theta]_\beta$, and $[\theta]_R$ are the reference values for pure helix, β-sheet or random coil, respectively (*35*). A CD spectrum for a helix in the 250-190 nm region has a characteristic double minimum around 222 and 208, and a maximum near 190, which represent the n-π^*, the π-$\pi_\parallel^*$ and the π-$\pi_\perp^*$ transitions, respectively (*36*). In contrast, the random coil structure is characterized by a spectrum which has a small maximum near 230 nm, and decreases from zero beginning around 212 nm. Chen and coworkers (*35*)

examined the contribution of helix, β-pleated sheet and random coil forms to the overall CD spectrum.

1.3.2 Microrheology

The pioneering work of Pine and Weitz (*37, 38*) has illustrated a non-invasive technique to measure the rheological properties of materials including colloidal suspensions, gels (*39-41*), and colloidal glasses (*42*). Diffusing wave spectroscopy uses dynamic light scattering to determine the thermal fluctuations of a colloidal suspension of microspheres in a viscoelastic medium. The motion of the microspheres can be determined by the autocorrelation function of the scattering, and from that the mean square displacement as a function of time is calculated.

This technique was used to characterize a hydrogel prepared from a triblock protein prepared by Petka (*1, 29*). The mean square displacement (MSD) of the microspheres suspended in the protein solution is monitored as a function of time. For a viscous solution, the microspheres are unrestricted, thus the MSD will increase linearly with time. In contrast, an elastic medium will restrict the motion of the microspheres, resulting in a plateau in the MSD vs. time. The plateau can also be used to estimate the modulus of the medium, based on the assumption that the thermal energy of the beads is related to the sheer creep compliance by $J(t) = (\pi a/k_B T) \langle r^2(t) \rangle$, where a is the radius of the particle, $k_B T$ is the thermal energy, and $\langle r^2(t) \rangle$ is the MSD as a function of time.

Using this procedure, AC_{10}Acys proteins were shown to be effective in forming pH and temperature reversible hydrogels. The non-covalent nature of the crosslinks in

the $AC_{10}Acys$ hydrogel is manifested as a transition from a plateau in the mean square displacement as function of time, to a constantly increasing MSD with time. It was of interest, however, to find a similar characterization method that would require smaller sample volumes.

Particle tracking is widely used in biophysics to track the movement of membrane bound proteins. Submicron or micron sized beads are coated with proteins that will bind to specific molecules in the cell membrane, then the beads are tracked using video microscopy. Prior to the development of single particle tracking, analysis of molecular motions was limited to the ensemble averaged values, preventing directed motions from being identified separately from simple Brownian diffusion. Using video-enhanced light or fluorescence microscopy, various groups demonstrated the ability to track individual particles in cells (*43*), attached to biological molecules such as kinesin (*44*), or attached to cell surface receptors (*45*). One of the attractions of this technique is the ability to identify single trajectories of motion.

This technique has been recently been applied to the rheological study of cellular components, such as actin gels (*39, 41, 46*). There are many factors that make this technique attractive for the study of rheology of the cell—the non-invasive nature of the experiment, the small sample requirements, and the ability to automate the tracking analysis.

1.4 Summary

Biosynthetic techniques provide an alternative method to prepare hydrogels which exceed the level of control achieved by traditional polymer synthesis, with the advantages observed for naturally derived materials. Specifically, the self-assembly of leucine zipper domains is exploited to create a reversible network that form as a function of their folding behavior.

1.5 References

1. W. A. Petka, J. L. Harden, K. P. McGrath, D. Wirtz, D. A. Tirrell, *Science* **281**, 389-392 (1998).

2. K. te Nijenhuis, Ed., *Thermoreversible Networks: Viscoelastic Properties and Structure of Gels*, vol. 130 (Springer-Verlag, New York, 1997).

3. P. J. Flory, *Principles of Polymer Chemistry* (Cornell University Press, Ithaca, NY, 1953).

4. M. S. Green, A. V. Tobolsky, *J. Chem. Phys.* **14**, 80-92 (1946).

5. T. Annable, R. Buscall, R. Ettelaie, D. Whittlestone, *J. Rheol.* **37**, 695-726 (1993).

6. T. Annable, R. Buscall, R. Ettelaie, *Colloid Surface A* **112**, 97-116 (1996).

7. F. H. C. Crick, *Acta Crystallogr.* **6**, 689-697 (1953).

8. R. S. Hodges, J. Sodek, L. B. Smillie, L. Jurasek, *Cold Spring Harb. Sym.* **37**, 299-310 (1972).

9. R. S. Hodges, J. Sodek, L. B. Smillie, L. Jurasek, *P. Natl. Acad. Sci. USA* **69**, 3800-3804 (1972).

10. K. J. Lumb, P. S. Kim, *Science* **268**, 436-438 (1995).

11. P. Lavigne *et al.*, *J. Mol. Biol.* **254**, 505-520 (1995).

12. E. Durr, I. Jelesarov, H. R. Bosshard, *Biochemistry-US* **38**, 870-880 (1999).

13. J. Moitra, L. Szilak, D. Krylov, C. Vinson, *Biochemistry-US* **36**, 12567-12573 (1997).

14. P. B. Harbury, T. Zhang, P. S. Kim, T. Alber, *Science* **262**, 1401-1406 (1993).

15. R. S. Hodges, A. K. Saund, P. C. S. Chong, S. A. St.-Pierre, R. E. Reid, *J. Biol. Chem.* **256**, 1214-1224 (1981).

16. N. E. Zhou, B. Y. Zhu, C. M. Kay, R. S. Hodges, *Biopolymers* **32**, 419-426 (1992).

17. S. Y. M. Lau, A. K. Taneja, R. S. Hodges, *J. Biol. Chem.* **259**, 13253-13261 (1984).

18. W. H. Landschultz, P. F. Johnson, S. L. McKnight, *Science* **240**, 1759-1764 (1988).

19. E. K. O'Shea, R. Rutkowski, P. S. Kim, *Science* **243**, 538-542 (1989).

20. E. K. O'Shea, R. Rutkowski, I. Walter F Stafford, P. S. Kim, *Science*, 646-648 (1989).

21. E. K. O'Shea, J. D. Klemm, P. S. Kim, T. Alber, *Science* **254**, 539-544 (1991).

22. R. Rasmussen, D. Benvegnu, E. K. O'Shea, P. S. Kim, T. Alber, *P. Natl. Acad. Sci. USA* **88**, 561-564 (1991).

23. N. E. Zhou, C. M. Kay, R. S. Hodges, *J. Biol. Chem.* **267**, 2664-2670 (1992).

24. S. Cohen *et al.*, *J. Am. Chem. Soc.* **112**, 7832-7833 (1990).

25. R. S. Hodges, N. E. Zhou, C. M. Kay, P. D. Semchuk, *Peptide Res.* **3**, 123-137 (1990).

26. J. W. Bryson *et al.*, *Science* **270** (1995).

27. W. D. Kohn, C. T. Mant, R. S. Hodges, *J. Biol. Chem.* **272**, 2583-2586 (1997).

28. R. S. Hodges, *Biochem. Cell Biol.* **74**, 133-154 (1996).

29. W. A. Petka, Ph.D. dissertation, University of Massachusetts, Amherst (1997).

30. J. G. Tirrell, D. A. Tirrell, M. J. Fournier, T. L. Mason, in *Protein-Based Materials* K. McGrath, D. Kaplan, Eds. (Birkhauser, Boston, 1997) pp. 61-102.

31. K. P. McGrath, M. J. Fournier, T. L. Mason, D. A. Tirrell, *J. Am. Chem. Soc.* **114**, 727-733 (1992).

32. M. Krejchi *et al.*, *Science* **265**, 1427-1432 (1994).

33. S. Yu *et al.*, *Nature* **389**, 167-170 (1997).

34. Y. Tang, D. A. Tirrell, *J. Am. Chem. Soc.* **123**, 11089-11090 (2001).

35. Y.-H. Chen, J. T. Yang, K. H. Chau, *Biochemistry-US* **13**, 3350-3359 (1974).

36. N. R. Kallenbach, P. Lyu, H. Zhou, in *Circular Dichroism and the Conformational Analysis of Biomolecules* G. D. Fasman, Ed. (Plenum Press, New York, 1996) pp. 201-259.

37. T. G. Mason, H. Gang, D. A. Weitz, *J. Mol. Struct.* **383**, 81-90 (1996).

38. D. A. Weitz, J. X. Zhu, D. J. Durian, H. Gang, D. J. Pine, *Phys. Scripta* **T49**, 610-621 (1993).

39. J. Xu, A. Palmer, D. Wirtz, *Macromolecules* **31**, 6486-6492 (1998).

40. F. Gittes, B. Schnurr, P. D. Olmsted, F. C. MacKintosh, C. F. Schmidt, *Phys. Rev. Lett.* **79**, 3286-3289 (1997).

41. J. Xu, V. Viasnoff, D. Wirtz, *Rheol. Acta* **37**, 387-398 (1998).

42. E. R. Weeks, J. C. Crocker, A. C. Levitt, A. Schofield, D. A. Weitz, *Science* **287**, 627-631 (2000).

43. H. Geerts *et al.*, *Biophys. J.* **52**, 775-782 (1987).

44. J. Gelles, B. J. Schnapp, M. P. Sheetz, *Nature* **331**, 450-453 (1988).

45. C. M. Anderson, G. N. Georgiou, I. E. G. Morrison, G. V. W. Stevenson, R. J. Cherry, *J. Cell Sci.* **101**, 415-425 (1992).

46. T. G. Mason, K. Ganesan, J. H. vanZanten, D. Wirtz, S. C. Kuo, *Phys. Rev. Lett.* **79**, 3282-3285 (1997).

CHAPTER 2

SINGLE PARTICLE TRACKING

2.1 Introduction

Diffusing wave spectroscopy (DWS), pioneered by Weitz and co-workers (*1, 2*), is a light scattering technique that analyzes Brownian of colloidal suspension of particles in order to observe their mean square displacement (MSD)as a function of time. The time evolution of the MSD provides information about the viscoelastic character of the medium (*3*). In a Newtonian fluid, the MSD of the probe particles will increase linearly with time, whereas in an elastic material, the MSD will reach a plateau value typically at low frequency for chemical gels (*4*), or at some intermediate frequency for transient networks (*5*).

Researchers have extended the DWS technique to single particle tracking (SPT), a technique that uses video microscopy, rather than light scattering, to determine particle displacements directly (*6-8*). Although microrheology has been used to analyze both chemical (*4, 9*) and biological gels (*10, 11*), its utility may be appreciated in cases where small sample volumes are desirable. Diffusing wave spectroscopy, used to analyze the AC_{10}Acys protein (*5*), requires volumes of 0.3-0.5 mL, while single particle tracking can be performed on samples less than 20 μL, making it an attractive alternative. For example, a high-throughput screening technique has been developed to analyze the rheological properties of a library of copolypeptide solutions (*12*).

Single particle tracking also affords the ability to analyze the movement of proteins within the cell membrane (*13-15*). Because the motion of particles or proteins is determined by direct observation, rather by an autocorrelation function of the ensemble of particles, new information can be derived that was not previously accessible. For example, two-particle tracking was developed to address the possibility that the probe particle will perturb the local environment and thus provide misleading information about the rheological properties of the material (*16, 17*). In particular, two-particle tracking is effective for probing inhomogeneous materials (*18*), and results from Crocker et al. indicate that previous analyses of F-actin, shown to vary sample-to-sample (*11*), or as a function of probe chemistry (*19*), may not accurately describe the true bulk behavior. Recently, the technique has been used to probe the interior of living cells, using natural cellular components as probe particles (*20*).

A single particle tracking apparatus was assembled in the interest of using small sample volumes, building an instrument that could be used in our lab, and developing a method to assess the viscoelastic properties of protein gels. A fluorescence microscope was used to visualize fluorescent microspheres, and their motion was digitally recorded. The digitized movies were transferred to a Linux workstation running IDL (Research Systems, Inc., Boulder, Colorado). Particle tracking routines, written by Crocker and Grier (*6*) were used in IDL to analyze digital movies. The software was designed to: a) determine particle positions, b) connect particle positions to form trajectories, and c) determine mean square displacement from trajectories. Reported herein are the results of calibrating the microscope for digital to real space distance, and viscosity determination

using the single particle tracking apparatus and software package provided by John Crocker.

2.2 Apparatus

2.2.1 Fluorescence Microscopy

Red carboxylate-modified fluorescent polystyrene beads (0.5 μm) were purchased from Molecular Probes (Eugene, OR). The proprietary dye is incorporated into the interior of the bead, resulting a highly fluorescent bead that is subject to minimal photobleaching. The beads were visualized under epi-fluorescence illumination using a Zeiss Axiovert 100 microscope, equipped with a 100 watt high pressure mercury Oriel Q Arc Lamp.

In the epi-fluorescence mode, light is passed through the objective and onto the sample. Fluorophores that were excited by the illumination emitted light of a longer wavelength, which was collected by the objective to create the fluorescent image (*21*). A TRITC/DiI filter cube (Chroma Technology, Rockingham, VT) was used to excite and detect red fluorescent microspheres (maximally excited at 580 nm with emission at 605 nm). The cube contains a narrow bandpass filter (535 nm center with 50 nm width) to limit the spectral range of the excitation beam. Light was directed through the objective onto the sample by a dichromatic beam splitter. This prism discriminates illuminating light from emitted light along the path from the sample back into the objective, using a filter which blocks wavelengths shorter than 565 nm. Finally, the reflected beam is

directed through a second bandpass filter (610 nm center with 75 nm width) before reflection into the observation tube. Although the filter set is not optimized for the maximal excitation and emission for the microspheres, the total fluorescence is bright enough to achieve high a signal to noise ratio sufficient for this analysis.

Images were observed using a 40x/1.4-NA oil immersion Plan Neofluar (Zeiss) objective and were recorded using a Dage-MTI CCD-72 camera attached to a 4x F/Axioline TV-Tube (Zeiss). The camera was attached to a JVC mini-dv recording deck (Figure 2.1) through a BNC to s-video connector. Two components define the image signal—luminance, or the brightness of the image and chrominance, the relative ratio of hues, which define the color of the image. The Dage-MTI camera records an analogue signal in black and white, so the connection for the BNC was directed to the luminance feed of the s-video converter, leaving the chrominance feed empty.

Figure 2.1 Zeiss Axiovert 100 fluorescence microscope equipped with Oriel Q 100 watt mercury arc lamp for illumination and mounted on a vibration isolation table. The lateral phototube is fitted with a Dage-MTI CCD-72 camera, which feeds into a JVC digital video recorder. Movies are transferred to an iMac DV before particle tracking analysis in IDL.

2.2.2 Digital Video

The analog signal from the CCD camera was converted to a digital movie using the JVC digital video recorder (Figure 2.1). The CCD signal is fed into a control box, which controls the gain and black level. Relative brightness and contrast can be adjusted before archiving the movie to digital video tape. Alignment of the illumination into the microscope determines the overall quality of the image, and the gain and black level adjustments provide a finer level of control to achieve the highest signal to noise. Movies were digitally recorded at a 4:1 compression ratio using the DV-NTSC CODEC, a standard for American television broadcast, which uses 500 TV lines at a frame rate of 29.97 frames per second. The CODEC is the type of compression-decompression

software that the video deck uses to translate the compressed digital signal to the images that are displayed on the monitor or television screen.

Digital video was transferred to an iMac-DV computer, with an external 40 GB hard drive, using Firewire™ and Adobe Premiere 5.1 software. Movies were captured using the OS9 systems disk, with the following capture settings: 640 x 480 image size; 24 bit pixel depth; 29.97 frames per second; DV-NTSC compressor; Quick time device; most (5) quality; 30 frames per second non-drop frame time code.

2.3 Single Particle Tracking Analysis

Digitized movies were analyzed using routines written in IDL by Crocker and Grier (*6*) (with Eric Weeks) and are documented in a tutorial website: http://glinda.lrsm.upenn.edu/~weeks/idl/. Details of the particle tracking algorithms are thoroughly described by Crocker and Grier and will not be reiterated. The figures and description provided herein illustrate the application of the analysis software to data obtained from the home-built instrument. This section details the image processing steps to quantify the motion of a colloidal suspension of fluorescent beads in ethylene glycol, which was used as a calibration standard.

2.3.1 System Requirements

Because high resolution images recorded at video frequency are required for the most accurate results, a minimum of 1 GB of RAM and 40 GB hard drive space is a necessity. The large amount of RAM will provide a large buffer for storing data on the the particle positions and subsequent determination of the tracks. When RAM has been limited to 128 MB, the tracking procedure was unable to compare complete sets of particle positions over more than two time steps, effectively truncating the data.

Table 2.1 System Requirements

Hardware or Software	Suggested	Actual
Processor	Pentium 4, or fastest available; dual processors for multiple users	Pentium 4
RAM	1 GB, minimum 2 GB for multiple users	1 GB
Hard drive	60 GB minimum	2x 40 GB drives
Platform to run IDL	Unix or Linux	Linux

Suggested hardware and software are listed in Table 2.1, along with the components used for the particle tracking apparatus described here. With this system, two or three sets of data could be processed simultaneously. Running more than three IDL sessions at one time, however, resulted in significantly slower processing speed.

2.3.2 Software

The series of movie files was transferred to the Linux computer and processed in IDL. The apparatus was calibrated to determine the conversion from the digital representation (in pixel values) to real space (in microns), then the viscosity of ethylene glycol was determined to check the accuracy of the particle tracking procedure.

2.3.3 Calibration

Two calibrations are detailed in the following sections. First, the microscope was calibrated by viewing a diffraction grating under two different magnifications to calculate the ratio of microns to pixels. Second, an ethylene glycol sample was analyzed with the particle tracking software to determine the time dependent evolution of the mean square displacement (MSD). For a viscous solution, this relationship should be linear and directly related to the diffusion coefficient. Using the Stokes-Einstein equation, the viscosity can be calculated from the linear fit to the plot of the MSD vs. time.

2.3.3.1 Microscope

The system was calibrated by first determining the micron to pixel ratio. A 200 line per mm diffraction slide was observed under 40x magnification using the Plan Neofluar objective with and without the 4x magnifying TV tube (Figure 2.2).

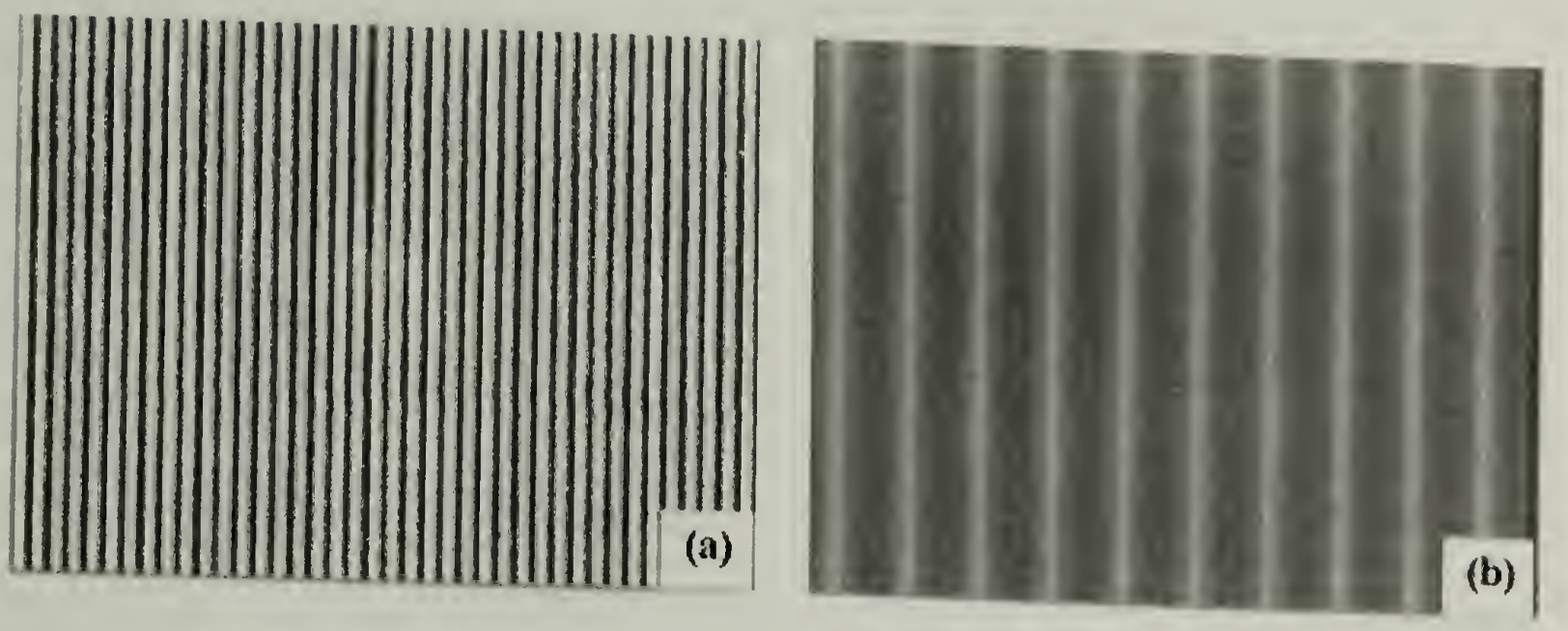

Figure 2.2 Diffraction pattern, 200 lines/mm, viewed with 40x Plan Neofluar objective in bright field (a) without and (b) with 4x F/Axiolin TV-Tube. Microscope images calibrated as 0.33 μm per pixel for 40x magnification and 0.083 mm per pixel for 160x magnification.

Images were recorded as digital video by the method described in Section 2.2. Single frames of the diffraction pattern were exported as uncompressed TIFF images using Adobe Premiere software. The micron to pixel ratio was determined from two images of the lines, in either the vertical or the horizontal direction. NIH Image software was used to measure the edge to edge distance between lines in pixel values. A total of five measurements spanning the image, (i.e. one line, two lines, four lines, and 10 lines) were averaged to determine the micron to pixel ratio—0.33 microns per pixel for 40x magnification or 0.083 microns per pixel for 160x magnification.

2.3.3.2 Ethylene Glycol

To verify the calibration from digital image to real space, and to test the accuracy of viscosity measurements using the single particle tracking software, the Brownian motion of 0.56 μm beads was tracked in ethylene glycol. Samples were prepared by

centrifuging 10 μL of red fluorescent beads (0.56 μm, 2 % solids, 2 mM NaN_3), Molecular Probes, and removing the buffer by pipetting. The beads were resuspended in 100 μL of ethylene glycol by vortexing. A grease chamber (thickness ~1-2 mm) was prepared on a microscope slide and 6 μL of the ethylene glycol solution with beads was transferred to the center of the chamber. A number 1 ½ cover slip (18 mm x 18 mm) was used to seal the top of the chamber.

The sample was visualized under 160x magnification (40x objective and 4x TV tube) and movies were recorded to mini-dv tape and transferred to an iMac DV hard drive for analysis.

Upon transfer from the digital video deck to the iMac computer, the movie remained in the compressed form. The analysis, however, requires that the image be uncompressed. More specifically, the images must be in TIFF format, written from NIH-Image. The analysis procedure saves all frames of a movie to the RAM buffer, so it is unreasonable to write movies longer than 10 seconds and still maintain reasonable processing speed. For this reason, a series of uncompressed movies, each exactly five seconds long, were exported from the original three minute movie in the uncompressed TIFF format using Adobe Premiere. The series of movies generated in Adobe Premiere was translated into NIH Image format using a macro written in NIH Image (Appendix A), which opens each movie and saves it as a stack of TIFF images (black and white, with no sound file). Each file contains 150 images, with a total size of 49.3 MB per file.

Figure 2.3a shows one frame of the original fluorescence image recorded to a digital movie file. Before analyzing the entire movie, the fitting procedures are applied to one frame of the movie to test the validity of the applied settings.

The first analysis procedure, the bpass function, was used to idealize the image—reducing random noise due to digitization and restoring the particle image to its ideal representation. Since pixels are both square as well as integer value representations of brightness (in a 640 x 480 TIFF image), the digital representation contains less information than the original image, however, the image of a fluorescent bead is easily fit to a two dimensional Gaussian surface. The image before (Figure 2.3a) and after (Figure 2.3b) idealizing illustrates the reduction in noise and the change in the sphere appearance.

In practice, two integer values are entered with the original image using the **bpass** function (i.e., bpass(a,1,11), where a=NIH image file). The first value can be roughly described as the full width at half max of the Gaussian surface applied to fit the particle. For 0.5 μm beads visualized under 160x magnification, this value is set to 1 or 2. The second number, approximated as the diameter of the particle, usually falls between 9 and 13.

(a)

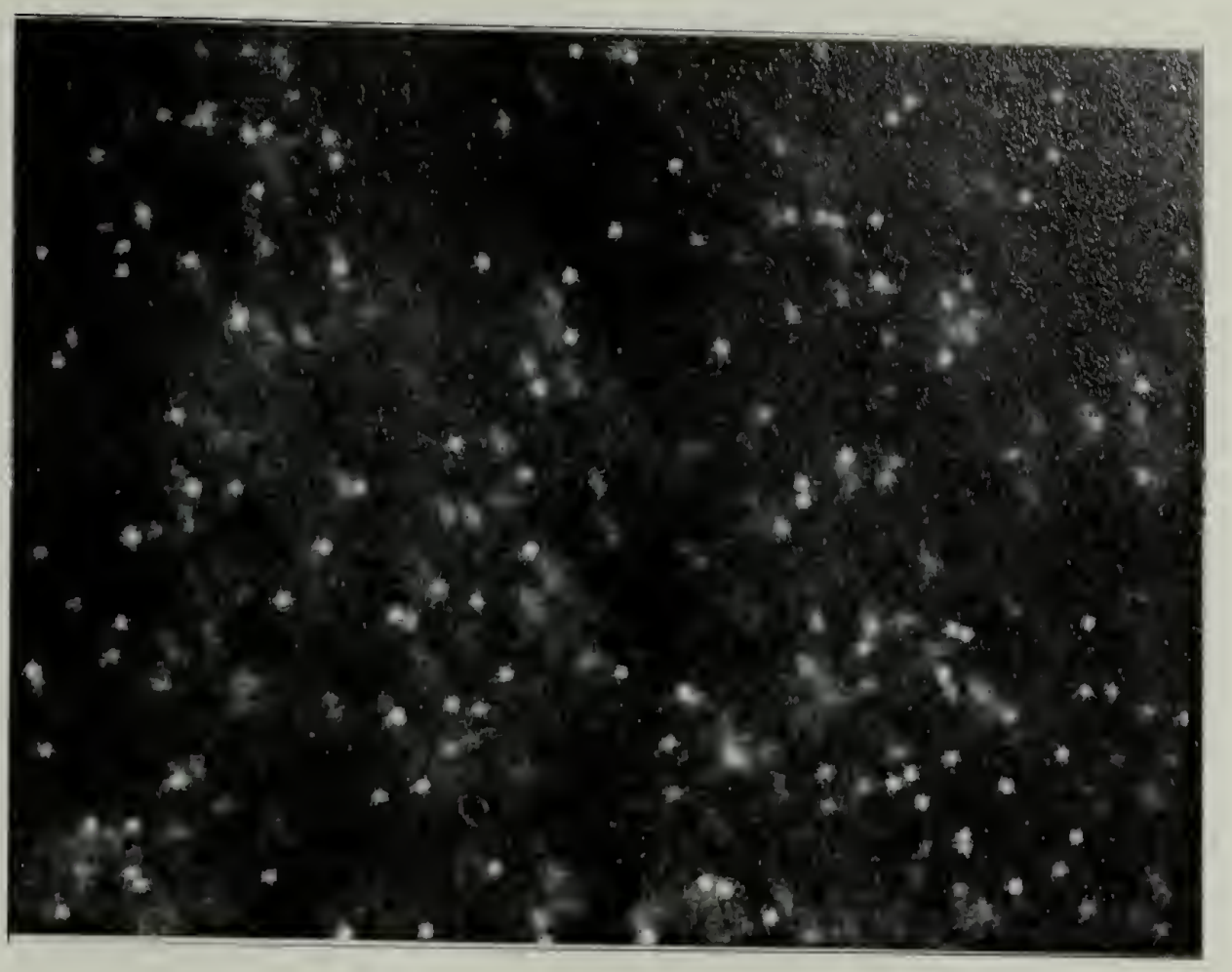

(b)

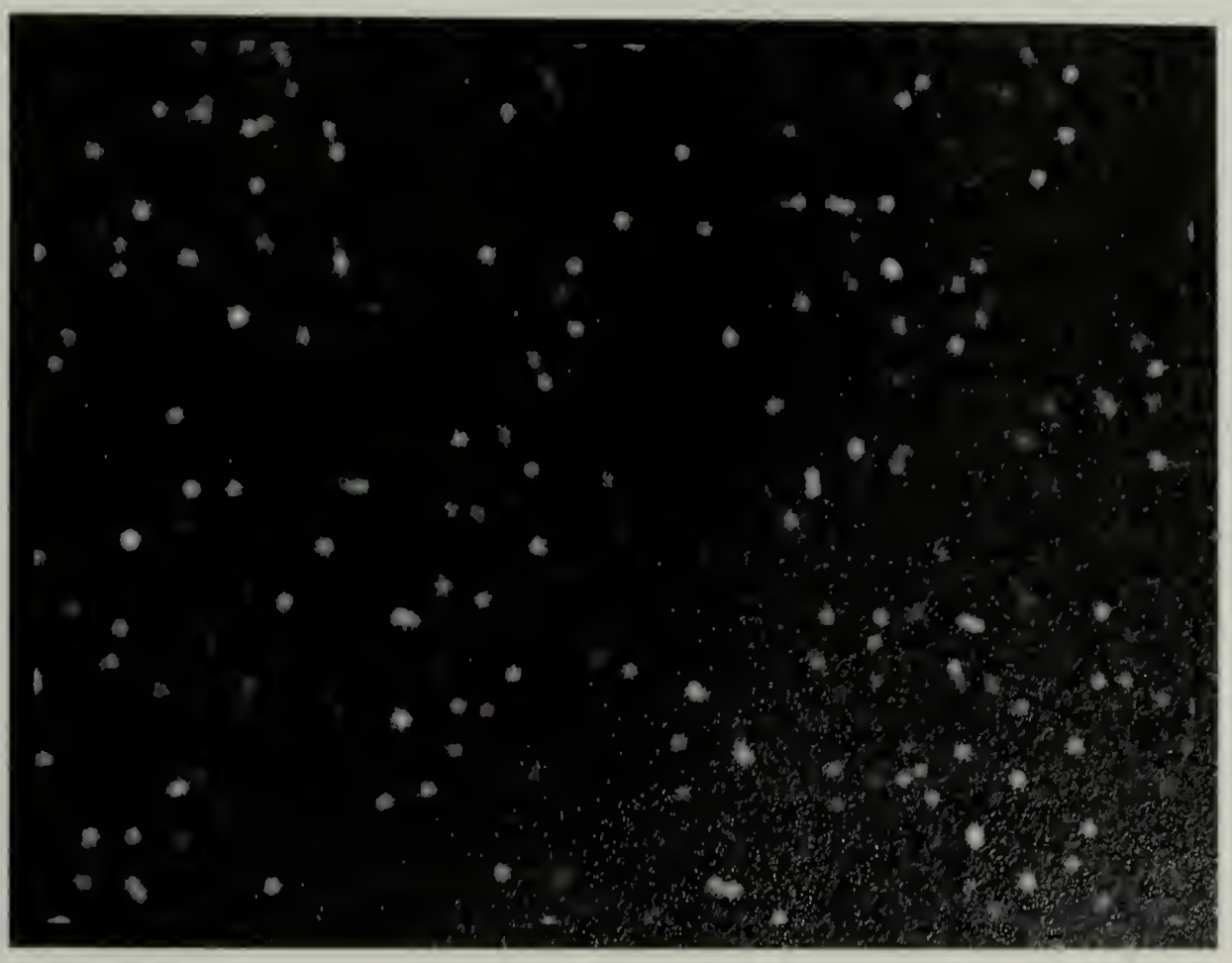

Figure 2.3 Fluorescence image of ethylene glycol with 0.56 μm beads viewed under 160x magnification (a) before and (b) after convolve function applied.

Overall brightness was used to discriminate particles from background noise. The images in Figure 2.4 illustrate the number of features identified (a) before and (b) after a brightness weighted threshold was applied. In the first image, features, or potential particle positions, are identified by the location of the red dots overlayed on the original image. The second image shows the features identified using the threshold option. Following the identification of the proper threshold value which returns the largest assignment of particles over noise, the particle positions were determined for the entire set of movie files.

(a)

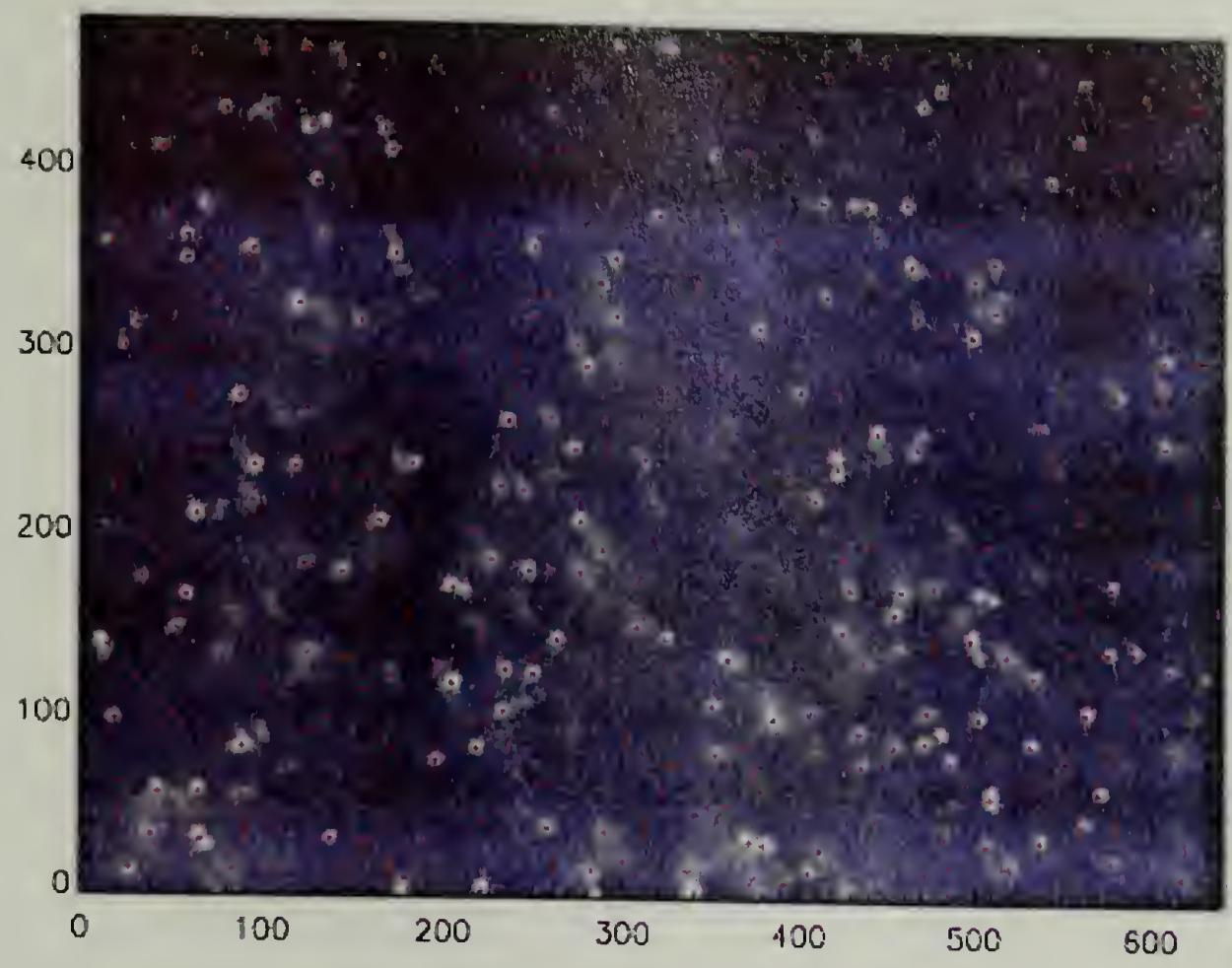

(b)

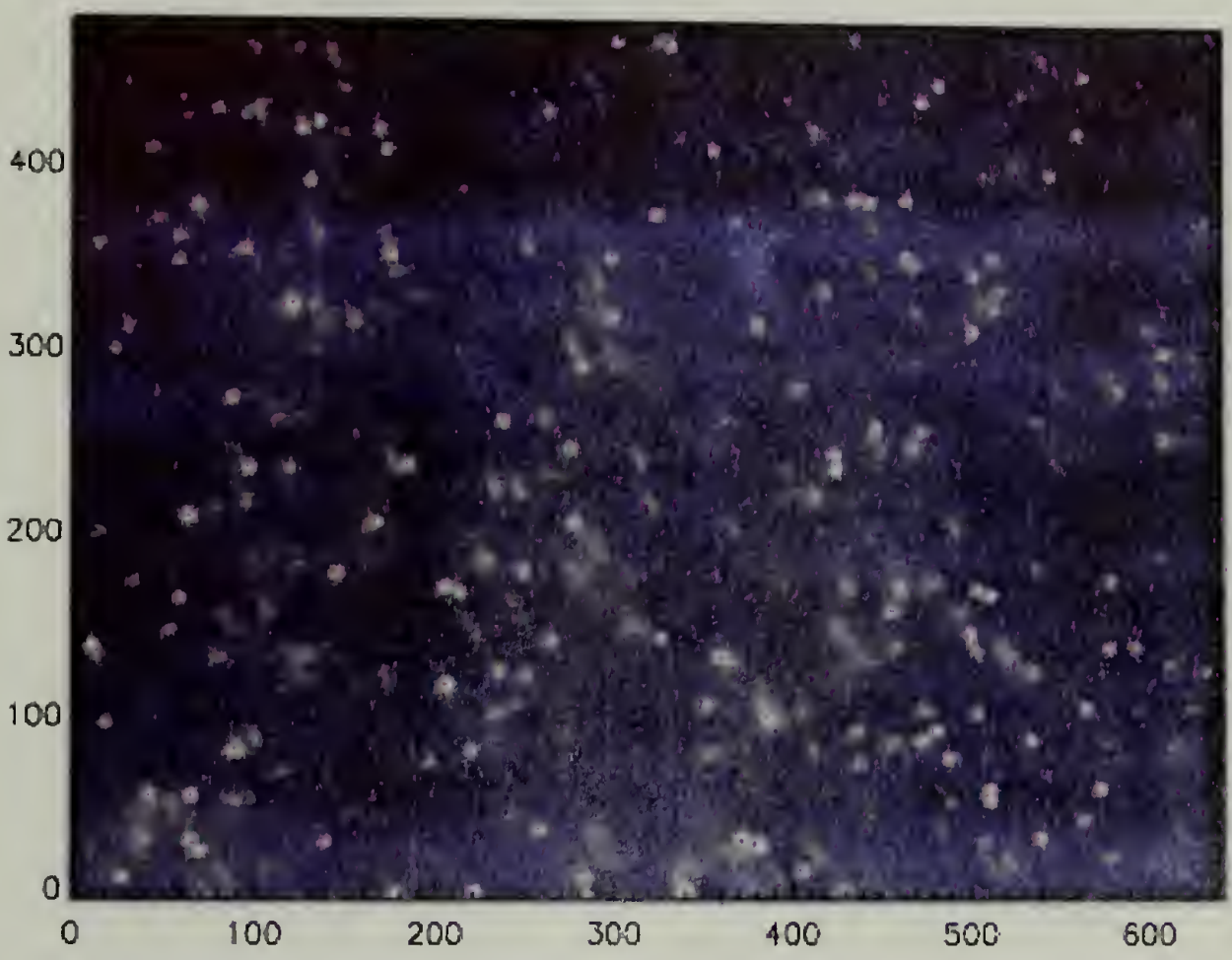

Figure 2.4 Particle identification for 0.56 µm fluorescent beads in ethylene glycol viewed under fluorescence,160x magnification (a) before and (b) after threshold analysis.

After the correct parameters were determined to identify the location of particles in the image, the **jpretrack** function was applied to the entire set of movies. This procedure incorporated noise reduction, particle image idealization, and particle identification into one function, outputting a text file containing the positions of particles from each frame in a five second movie. Temporarily, the data were written to individual files for each five second movie. The series was later concatenated into one file with the frame number consecutively written for the entire series.

Before determining the trajectories of the particles, a final procedure was used to discriminate particle locations from any noise which may have been falsely assigned to a particle position by the **jpretrack** procedure. Simply, the distribution of the brightness and size of each particle were displayed and used to select a population representing particles of similar brightness and size. For example, in the display of the size vs. brightness, double particles will show similar size to individual particles, but display double the intensity, or brightness. The most accurate mean squared displacement is determined by a population of particles that are equal in size, so it is important to reject the population of double particles. The **cutcat** procedure, used to concatenate the individual text files containing the particle position data, also provides an option to cut a polygon to select a population of particle positions based on a plot of the size vs. brightness. This final selection tool was used prior to determination of the trajectories.

The trajectories were determined using the **track** procedure. In this routine, particle positions are compared from one from to the next consecutive frame, by examining the space, *r*, (designated by the user) from the particle's center. The *good enough* option allows the user to provide a minimum number of steps that the trajectory

must exceed to be considered in the final data set. By setting this value to a minimum of 10, noise, due to random flicker from the camera, can be eliminated. For particles that lie at the edge of the focal plane, and come in and out of focus, the trajectory can be maintained even if the particle is out of the field of view. The *memory* option will designate the number of frames that the particle may be allowed "missing" before the trajectory is ended. For particles in a stiff, elastic medium, the memory may be set to 0 or 1, while particles in a low viscosity fluid may require a *memory* value of 3 or higher. Finally, the *erode* option is used to drop a set number (usually 1 or 2) of particle positions from the beginning and end of each trajectory. This option reduces the possibility of incorporating noise into the beginning or end of a trajectory.

(a)

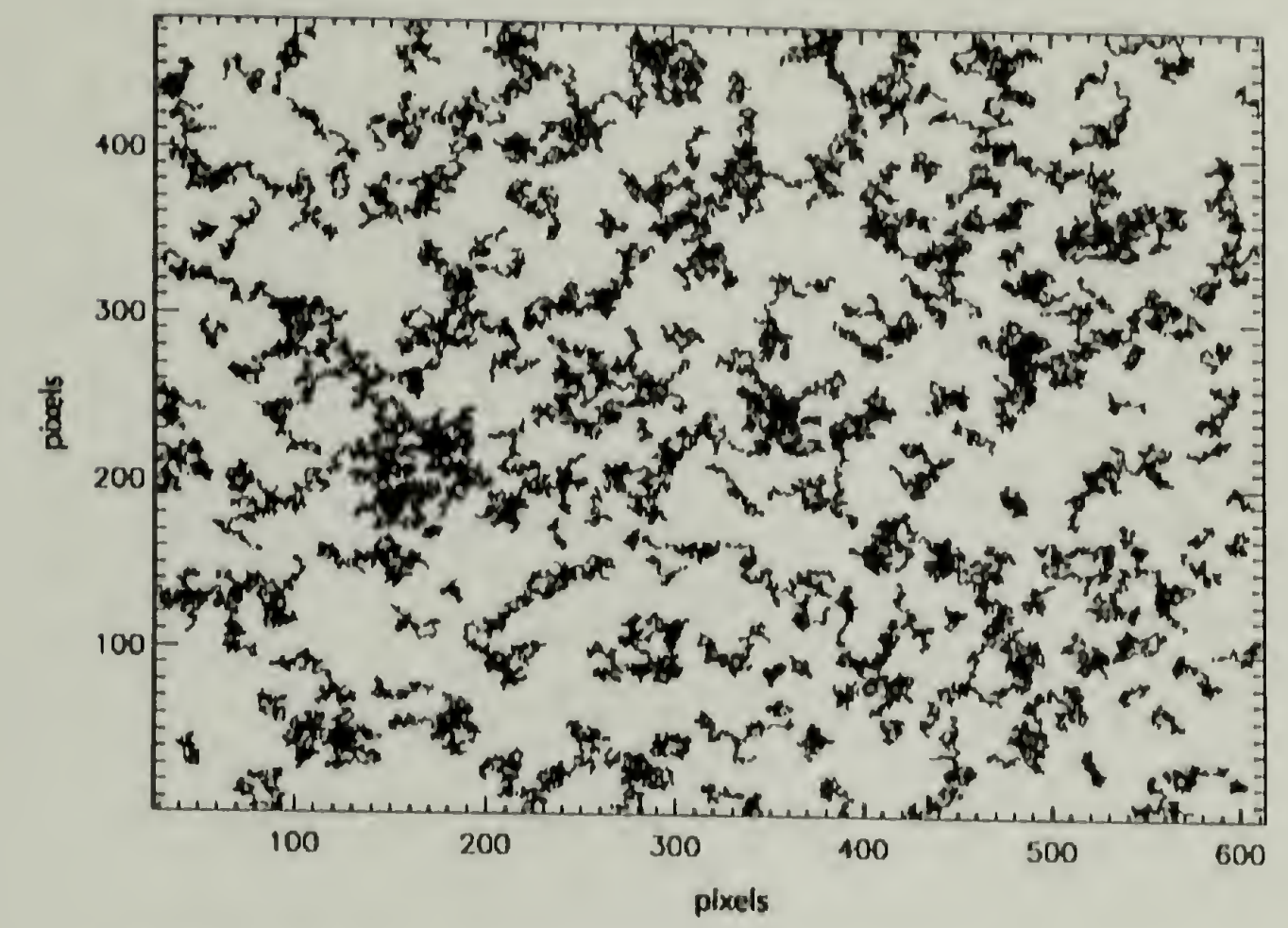

(b)

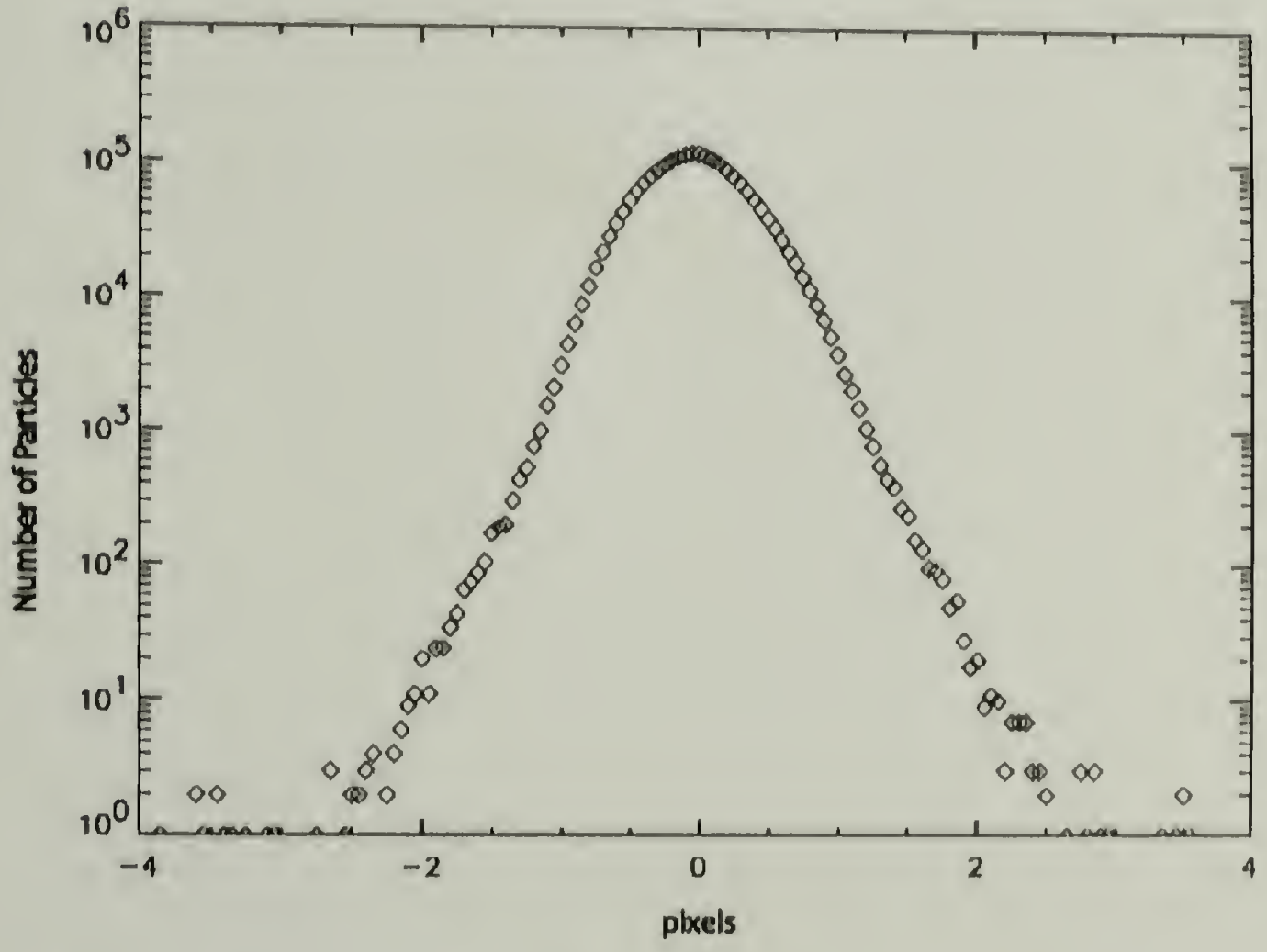

Figure 2.5 (a) Particle trajectories longer than 500 steps shown as a function of pixel position (640 x 480) as determined for 0.56 μm particles in ethylene glycol. (b) Histogram of displacement for one time step determined from the particle trajectories shown in (a).

Figure 2.5a illustrates the trajectories observed for particles in the ethylene glycol sample described. The distribution of displacements for one time step is shown in Figure 2.5b, and indicate that a single population of particles were traced by this analysis. For data that include a population of noise, two outlying distributions of particle displacements are usually observed at plus or minus five pixels. In cases where noise was tracked with the particles, a new data set was selected using the cutcat procedure before proceeding to determine the MSD as a function of time from the trajectories.

After verifying the trajectories accurately describe the particle motion and not noise, the evolution of the MSD is determined as a function of time and reported on a log-log plot (Figure 2.6). In a purely viscous solution, the MSD varies linearly with time, resulting in a slope of one for a log-log representation of the data. The diffusion coefficient is determined from the intercept.

$$\langle \Delta r^2(t) \rangle = 6\ Dt$$

$$\log \langle \Delta r^2(t) \rangle = \log 6D + \log t$$

Assuming an isotropic medium, the movement of particles in the x and y directions should be equal, as should the movement in three dimensions, $\Delta x = \Delta y = \Delta z$. Standard video is generated by scanning half of the image (odd lines or even lines) at double the frequency, 60 Hz, of the video rate (*21*). The odd and even fields are combined to represent the complete picture at 30 Hz. Since the two fields are taken at twice the frequency of video rate, the particle position may be different for the individual fields as compared to the full frame at 30 Hz. In low viscosity solutions, particle positions can vary between the even and odd fields, requiring the full image to be

deinterlaced before analysis (*6*). Because the fields are made of horizontal lines, the resolution in the x direction is greater than the y direction, therefore, only the x direction is used to determine the MSD as a function of time.

Although the tracking routine determines the motion of the beads in the projected xy plane, and the data represents motion only in the x direction, the movement in the z direction is accounted for because the $\langle \Delta r^2 \rangle$ measured in two dimensions is 3/2 the $\langle \Delta r^2 \rangle$ value in 3 dimensions.

$$\langle \Delta r_{2D}^2 \rangle = \langle \Delta x^2 \rangle + \langle \Delta y^2 \rangle \qquad \text{2 D}$$

$$\langle \Delta r_{3D}^2 \rangle = \langle \Delta x^2 \rangle + \langle \Delta y^2 \rangle + \langle \Delta z^2 \rangle \qquad \text{3 D}$$

For isotropic behavior, $\langle \Delta x^2 \rangle = \langle \Delta y^2 \rangle = \langle \Delta z^2 \rangle$,

$$\langle \Delta r_{2D}^2 \rangle = 2\langle \Delta x^2 \rangle \text{ and } \langle \Delta r_{3D}^2 \rangle = 3\langle \Delta x^2 \rangle,$$

$$\langle \Delta r_{3D}^2 \rangle = 3/2 \langle \Delta r_{2D}^2 \rangle$$

To determine the diffusion coefficient from the $\langle r^2 \rangle$, consider Fick's law and the Stokes-Einstein equation.

$$D(t) = \langle \Delta r_{3D}^2 \rangle / (6t)$$

$$D_0 = \frac{k_B T}{6\pi\eta\sigma}$$

where η is the viscosity of the medium and σ is the radius of the sphere.

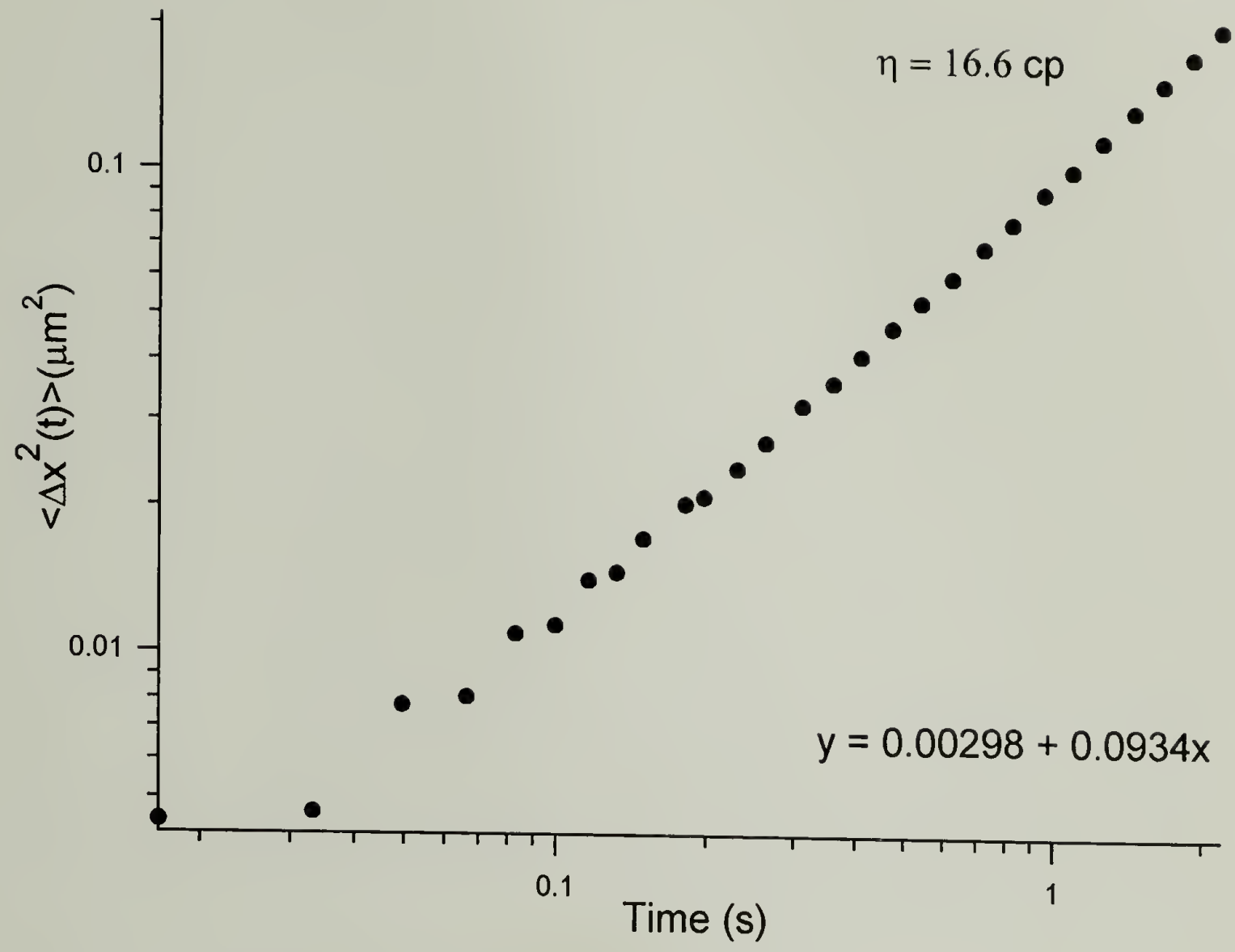

Figure 2.6 Mean squared displacement as a function of time for 0.56 μm beads in ethylene glycol.

Figure 2.6 shows the log-log representation of the MSD vs. time. The equation shown at the bottom right, however, is the linear fit to the data for a linear-linear plot. From the slope of the linear-linear fit, the viscosity was caculated according to the Stokes-Einstein equation.

Deviations at short time observed in Figure 2.6 show a systematic error that may result from deinterlacing. Samples of higher viscosity do not require deinterlacing, as long as the particle displacement is not significant at 60 Hz.

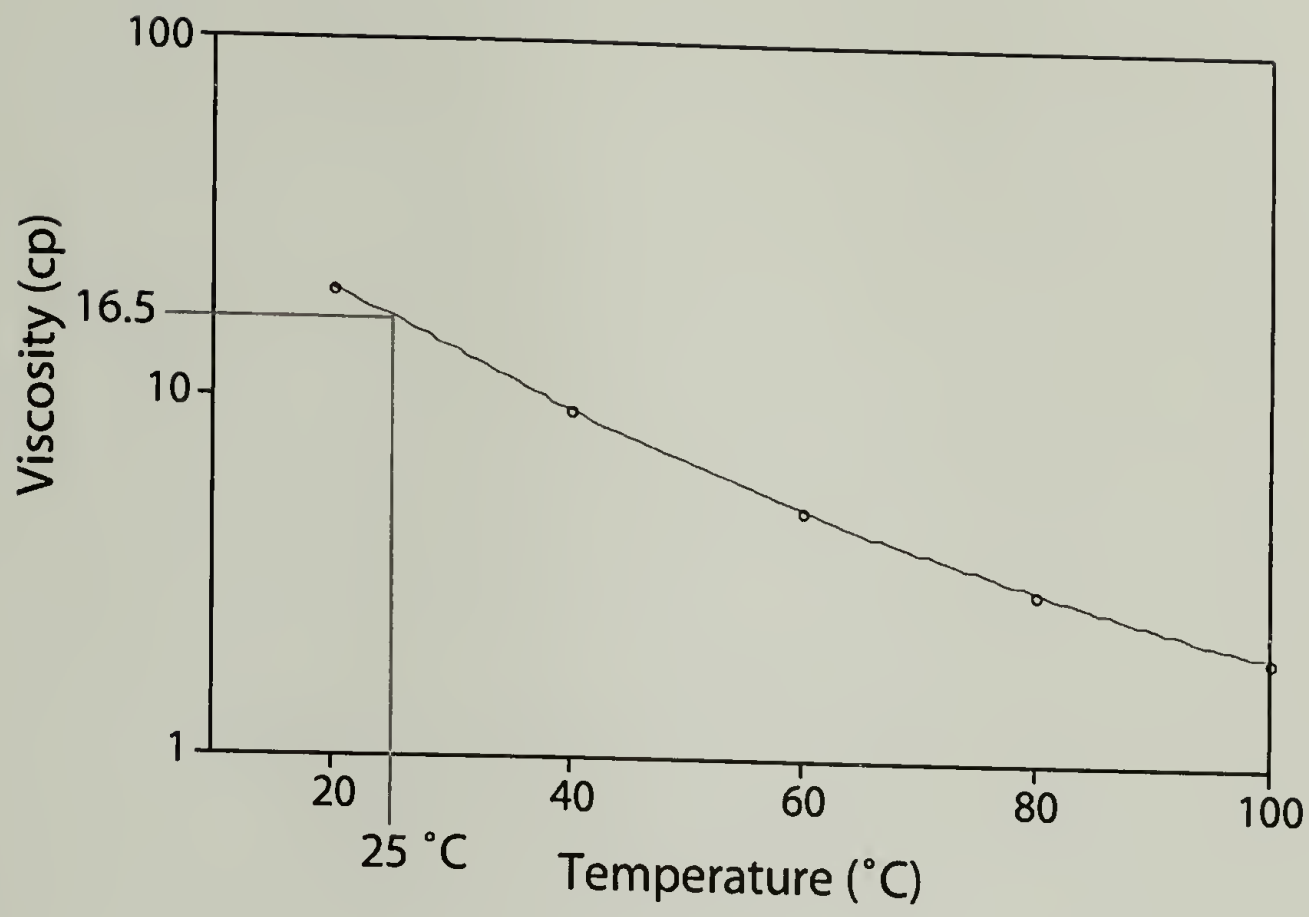

Figure 2.7 Viscosity of ethylene glycol as a function of temperature.

The viscosity determined for ethylene glycol for this method is in agreement to less than 1 % of that determined from the CRC Handbook of Chemistry (*22*), as shown in Figure 2.7. This demonstration illustrates the utility of the apparatus for determining the viscosity of a solution. The demonstration of tracking under 160x magnification is important, since most samples have limited motion and require analysis under the highest magnification. For samples of lower viscosity, water, for example, may require analysis using 40x magnification. In this series of experiments, however, the samples have either high viscosity or are viscoelastic, so the 40x magnification was not used.

2.4 References

1. T. G. Mason, H. Gang, D. A. Weitz, *J. Mol. Struct.* **383**, 81-90 (1996).
2. D. A. Weitz, J. X. Zhu, D. J. Durian, H. Gang, D. J. Pine, *Phys. Scripta* **T49**, 610-621 (1993).
3. H. Qian, *Biophys. J.* **79**, 137-143 (2000).
4. T. Narita, A. Knaebel, J.-P. Munch, S. J. Candau, *Macromolecules* **34**, 8225-8231 (2001).
5. W. A. Petka, J. L. Harden, K. P. McGrath, D. Wirtz, D. A. Tirrell, *Science* **281**, 389-392 (1998).
6. J. C. Crocker, D. G. Grier, *J. Colloid Interf. Sci.* **179**, 298-310 (1996).
7. F. Gittes, B. Schnurr, P. D. Olmsted, F. C. MacKintosh, C. F. Schmidt, *Phys. Rev. Lett.* **79**, 3286-3289 (1997).
8. B. Shnurr, F. Gittes, F. C. MacKintosh, C. F. Schmidt, *Macromolecules* **30**, 7781-7792 (1997).
9. B. R. Dasgupta, S. Y. Tee, J. C. Crocker, B. J. Frisken, D. A. Weitz, *Phys. Rev. E* **65**, 1-10 (2002).
10. J. Xu, V. Viasnoff, D. Wirtz, *Rheol. Acta* **37**, 387-398 (1998).
11. T. Gisler, D. A. Weitz, *Phys. Rev. Lett.* **82**, 1606-1609 (1999).
12. V. Breedveld, D. J. Pine, *J. Mater. Sci.* **38**, 4461-4470 (2003).
13. M. J. Saxton, K. Jacobson, *Annu. Rev. Bioph. Biom.* **26**, 373-399 (1997).
14. M. J. Saxton, *Biophys. J.* **67**, 2110-2119 (1994).
15. M. Goulian, S. M. Simon, *Biophys. J.* **79**, 2188-2198 (October 1, 2000, 2000).
16. A. J. Levine, T. C. Lubensky, *Phys. Rev. Lett.* **85**, 1774-1777 (2000).
17. A. J. Levine, T. C. Lubensky, *Phys. Rev. E* **6501**, 1-13 (2002).
18. J. C. Crocker *et al.*, *Phys. Rev. Lett.* **85**, 888-891 (2000).
19. J. L. McGrath, J. H. Hartwig, S. C. Kuo, *Biophys. J.* **79**, 3258-3266 (2000).
20. A. W. C. Lau, B. D. Hoffman, A. Davies, J. C. Crocker, T. C. Lubensky, *Phys. Rev. Lett.* **91**, art. no.-198101 (2003).

21. S. Inoue, K. R. Spring, *Video Microscopy: The fundamentals* (Plenum Press, New York, ed. 2nd, 1997).

22. R. C. Weast, *Handbook of Chemistry and Physics* (CRC Press, Boca Raton, FL, 1988), vol. 1st Student Edition.

CHAPTER 3

SYNTHESIS AND CHARACTERIZATION OF AC_xA AND AC_xB PROTEINS

3.1 Introduction

Following the synthetic strategy used to prepare the triblock protein, $AC_{10}Acys$ (*1*), a series of new proteins was designed where the midblock length was increased incrementally. The modular nature of the gene construction by recombinant DNA technology provided a simple method for preparing genes encoding triblock proteins varying in size from 22kD to 54kD.

The general architectures of the triblock proteins are described as AC_xAcys or AC_xBcys, where x = 10, 20, 30, 40, or 50 repeats of $[(AG)_3PEG]$, and cys indicates a cysteine residue at the C-terminus of the protein (*1*). The water soluble polyelectrolyte coil was first prepared by McGrath *et al.* (*2*). McGrath showed that the proteins containing the peptide sequence, $[(AG)_3PEG]_x$ (designated C_x), had no regular secondary structure in the solid state, as evidenced by x-ray crystallography. To examine the role of midblock length on the gelation of AC_xAcys proteins, the random coil block was increased incrementally. Two types of leucine zipper end-blocks were used to prepare the triblock proteins: **A**, which contains a majority of glutamic acids in the **e** and **g** positions of the heptad repeat, or **B**, in which lysine is found in the majority of these flanking residues.

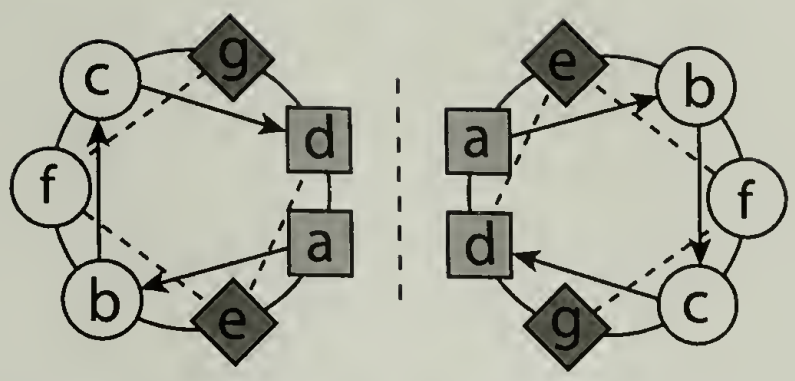

A: **e** and **g** = Glu (9 of 12 residues) **B: e** and **g** = Lys (9 of 12 residues)

Figure 3.1 Helical wheel representation of a coiled coil dimer, indicating the difference between **e** and **g** residues for A and B leucine zipper domains.

3.2 Experimental Work

3.2.1 Genetic Strategy to Prepare New DNA Constructs

Recombinant plasmid, pWAPL2, a pUC-18 derived cloning vector with an inserted DNA sequence containing multiple restriction sites, was used to create all recombinant genes described in this chapter (*1*). The advantage of the pWAPL1 vector is that it can be cut at *Spe*I, a unique restriction site, leaving two *Spe*I overhangs, while the gene to be inserted can be cut at one end with *Nhe*I and at the other end with *Spe*I. *Nhe*I and *Spe*I are compatible cohesive ends, so ligation of the overhangs results in a sequence not recognized by either restriction enzyme. Conversely, ligating two *Spe*I ends or two *Nhe*I ends should maintain the specificity of either restriction enzyme to recognize that site after ligation. Introducing genes by this manner, the *Spe*I and *Nhe*I sites remain unique because the inserted gene will ablate one end, where *Spe*I/*Nhe*I ligate, and maintain the opposite end, where *SpeI* is ligated with to its complement. Multiblock domains were prepared using the *Spe*I site to introduce genes encoding the polyelectrolyte coil or the acidic or basic leucine zipper domain. *Bam*HI was used to

excise the recombinant gene from the cloning vector for transfer into the expression vector.

Preparation of Cloning Strategy Figures

Figures (3.2, 3.3 and 3.4), illustrating the strategy for cloning, were prepared using MacPlasmap and Adobe Illustrator software programs. MacPlasmap provides a simple method for preparing illustrations of recombinant plasmid DNA. The program is available at http://www.cellbiol.com/soft.php or other molecular biology sites containing downloads for freeware programs. A picture file of the recombinant plasmid image was exported from MacPlasmap and placed in Adobe Illustrator™. Several layers of the imported image were redundant and thus deleted before preparing the schematics shown in Figures 3.2, 3.3 and 3.4.

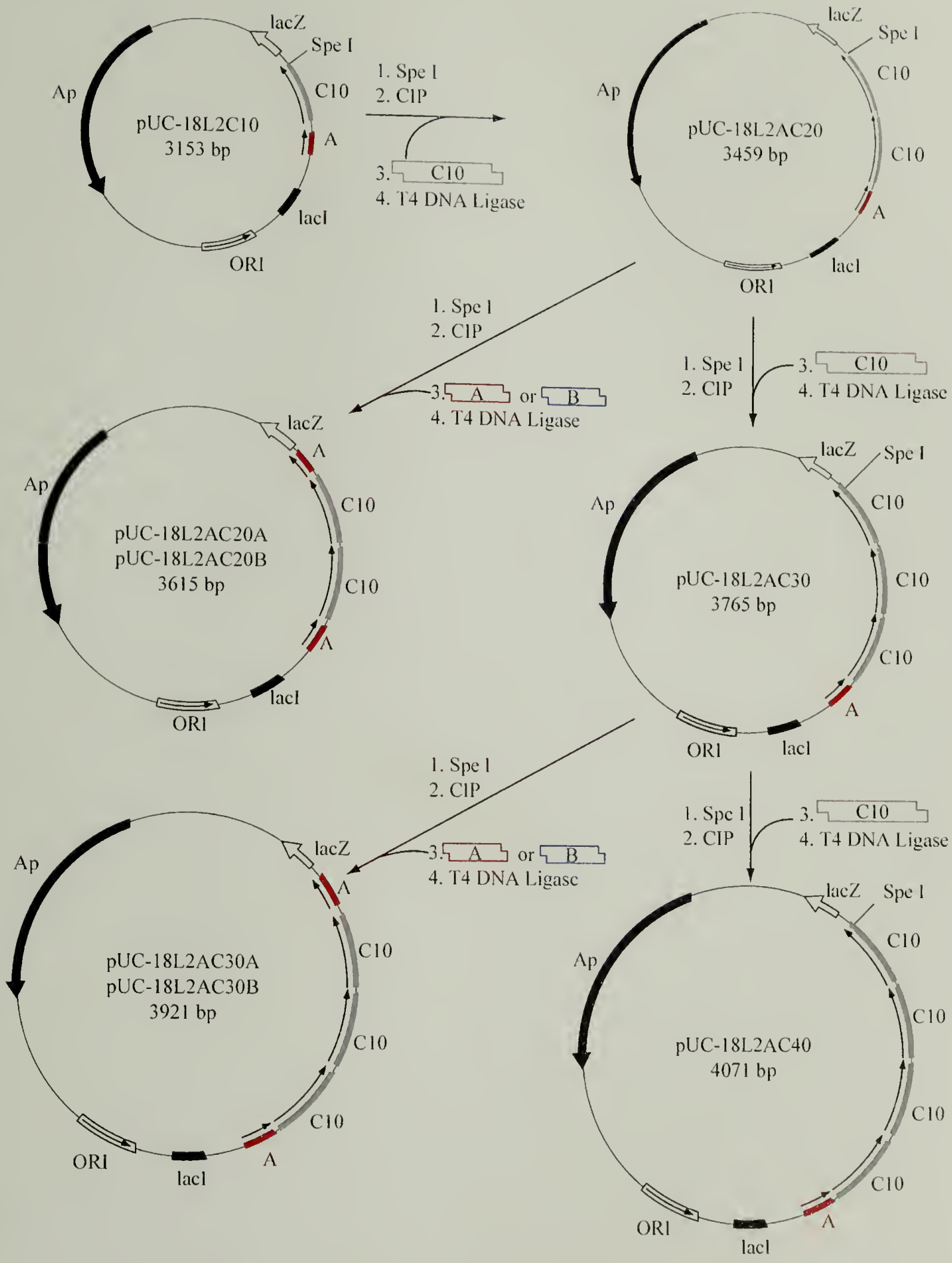

Figure 3.2 Strategy for cloning genes encoding $AC_{20}Acys$, $AC_{20}Bcys$, $AC_{30}Acys$, $AC_{30}Bcys$ protein sequences into pUC-18 cloning vector.

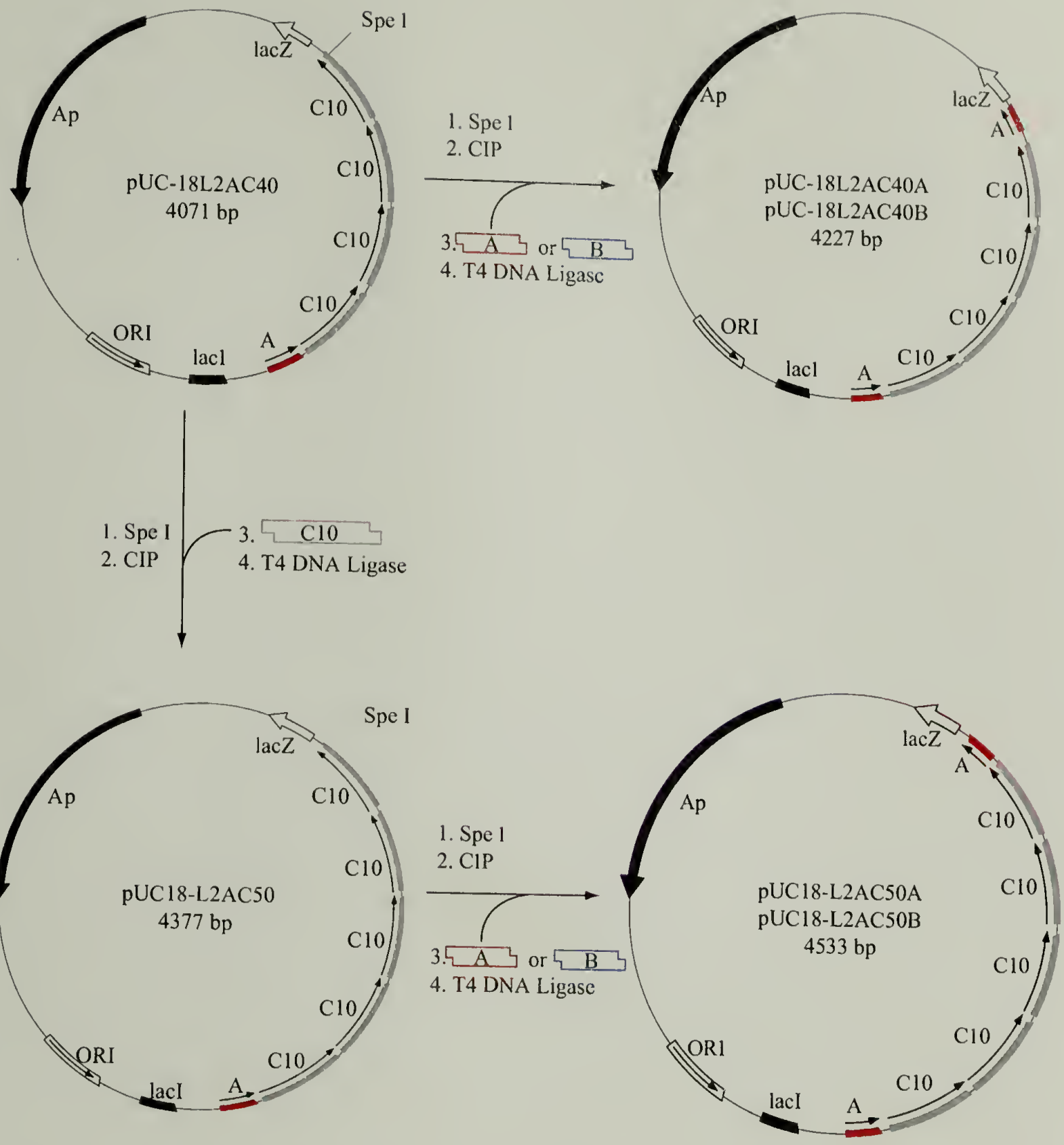

Figure 3.3 Strategy for cloning $AC_{40}Acys$, $AC_{40}Bcys$, $AC_{50}Acys$, $AC_{50}Bcys$ in pUC-18 cloning vector.

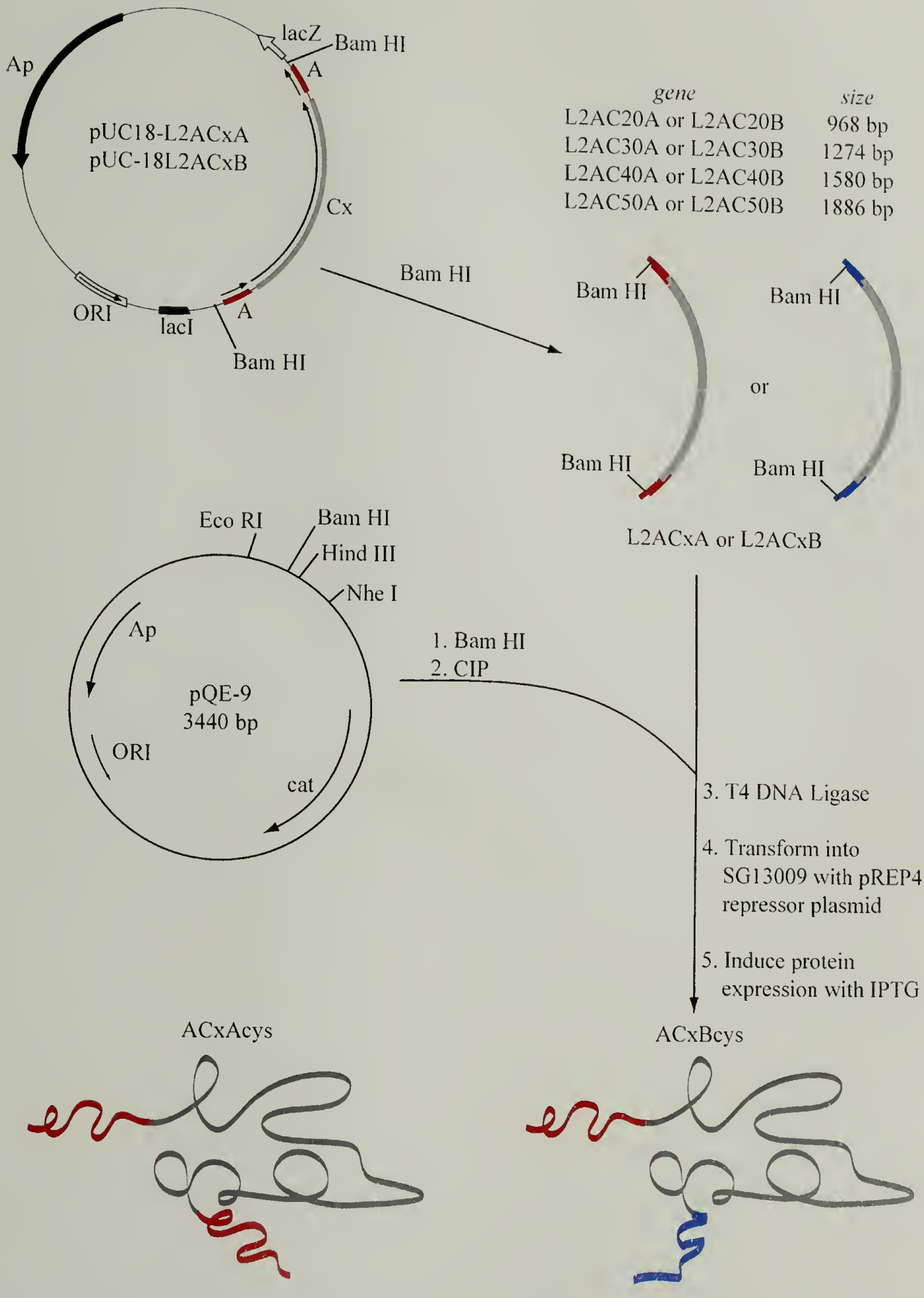

Figure 3.4 Strategy for preparing AC_xAcys and AC_xBcys proteins from recombinant genes.

3.2.2 DNA Modification by Recombinant Technology

T4 DNA ligase, calf intestinal alkaline phosphatase (CIP), base pair standards, protein standards, and all restriction enzymes were obtained from New England Biolabs(NEB, Beverly, MA). Expression plasmid DNA, pQE-9, SG13009[pREP4], DNA purification columns, Ni^{2+}-NTA purification columns and resin, and Anti-His_6-RGS anitbody were purchased from Qiagen™(Valencia, CA). Genes for **A**, **B**, and $\mathbf{C_{10}}$ were obtained from Petka (*1*). Media components, including casein tryptone and yeast extract, were obtained from Amhersham Life Sciences. All other chemicals were purchased from Sigma, Fisher, or VWR.

Preparation of gene insert building blocks

Genes encoding **A, B,** or $\mathbf{C_{10}}$ were isolated by digesting pWAPL2A, pWAPL2B or pQE-9L1C plasmids (*1*), respectively, with *Spe*I and *Nhe*I restriction enzymes. The DNA was subsequently separated from the parent plasmid by gel electrophoresis through a 2 % (w/v) agarose gel, in which the insert bands, 156 bp for **A** or **B** and 305 bp for $\mathbf{C_{10}}$,were excised and the DNA was extracted from the agarose into ddH_20 using *QIAquick* gel extraction columns (Figure 3.5).

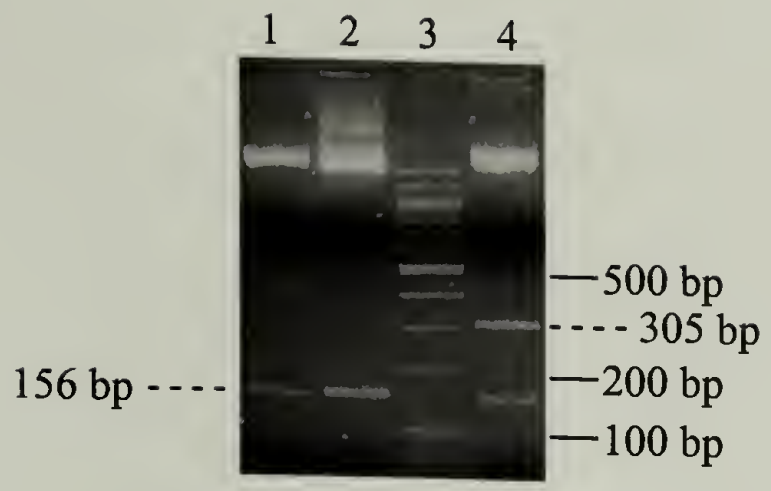

Figure 3.5 *Nhe*I/*Spe*I digested genes used as building blocks. Lane (1) **A** (2) **B**, (4) $\mathbf{C_{10}}$ DNA visualized with ethidium bromide staining on a TBE gel containing 2% agarose. 100 bp marker shown in lane 3 (0.5 μg).

Sequences for the gene inserts are provided in Figure 3.6. The lower band (~180 bp) in lane 4 of Figure 3.5 results from the digestion of a *Nhe*I site, which, in combination with the primary *Nhe*I/*Spe*I sites results in the fragmentation of the plasmid DNA into three sections.

(a)

*Nhe*I *Bst*EII

5’ CT AGC GGT GAC CTG GAA AAC GAA GTG GCC CAG
3’ G CCA CTG GAC CTT TTG CTT CAC CGG GTC

*Bgl*II

CTG GAA AGG GAA GTT AGA TCT CTG GAA GAT GAA GCG
GAC CTT TCC CTT CAA TCT AGA GAC CTT CTA CTT CGC

*Xho*I

GCT GAA CTG GAA CAA AAA GTC TCG AGA CTG AAA AAT
CGA CTT GAC CTT GTT TTT CAG AGC TCT GAC TTT TTA

*Bst*EII

GAA ATC GAA GAC CTG AAA GCC GAA ATT GGT GAC CAT
CTT TAG CTT CTG GAC TTT CGG CTT TAA CCA CTG GTA

*Xho*I *Spe*I

GTG GCG CCT CGA GAC A 3’
CAC CGC GGA GCT CTG TGA TCA 5’

(b)

*Nhe*I *Bst*EII

5’ CT AGC GGT GAC CTG AAA AAC AAA GTG GCC CAG
3’ G CCA CTG GAC TTT TTG TTT CAC CGG GTC

*Bgl*II

CTG AAA AGG AAA GTT AGA TCT CTG AAA GAT AAA GCG
GAC TTT TCC TTT CAA TCT AGA GAC TTT CTA TTT CGC

*Xho*I

GCT GAA CTG AAA CAA GAA GTC TCG AGA CTG GAA AAT
CGA CTT GAC TTT GTT CTT CAG AGC TCT GAC CTT TTA

*Bst*EII

GAA ATC GAA GAC CTG AAA GCC AAA ATT GGT GAC CAT
CTT TAG CTT CTG GAC TTT CGG TTT TAA CCA CTG GTA

*Xho*I *Spe*I

GTG GCG CCT CGA GAC A 3’
CAC CGC GGA GCT CTG TGA TCA 5’

Fig. 3.6 Continued next page

(c) Continued

*Nhe*I *Nru*I *Ban*I

5' CT AGC TAT CGC GAT CCG ATG GGT GCC GGC GCT
3' G ATA GCG CTA GGC TAC CCA CGG CCG CGA

GGT GCG GGC CCG GAA GGT GCA GGC GCT GGT GCG GGC
CCA CGC CCG GGC CTT CCA CGT CCG CGA CCA CGC CCG

*Ban*I

CCG GAA GGT GCC GGC GCT GGT GCG GGC CCG GAA GGT
GGC CTT CCA CGG CCG CGA CCA CGC CCG GGC CTT CCA

*Ban*I

GCA GGC GCT GGT GCG GGC CCG GAA GGT GCC GGC GCT
CGT CCG CGA CCA CGC CCG GGC CTT CCA CGG CCG CGA

GGT GCG GGC CCG GAA GGT GCA GGC GCT GGT GCG GGC
CCA CGC CCG GGC CTT CCA CGT CCG CGA CCA CGC CCG

*Ban*I

CCG GAA GGT GCC GGC GCT GGT GCG GGC CCG GAA GGT
GGC CTT CCA CGG CCG CGA CCA CGC CCG GGC CTT CCA

*Ban*I

GCA GGC GCT GGT GCG GGC CCG GAA GGT GCC GGC GCT
CGT CCG CGA CCA CGC CCG GGC CTT CCA CGG CCG CGA

GGT GCG GGC CCG GAA GGT GCA GGC GCT GGT GCG GGC
CCA CGC CCG GGC CTT CCA CGT CCG CGA CCA CGC CCG

*Ban*I *Sph*I *Spe*I

CCG GAA GGT GCC CGC ATG CCG A 3'
GGC CTT CCA CGG GCG TAC GGC TGA TC 5'

Figure 3.6 DNA sequences for (a) **A**, (b) **B**, and (c) $\mathbf{C_{10}}$ genes digested with *Nhe*I/ *Spe*I.

General procedure for transformation of DNA into competent cells

Plates containing no antibiotics were streaked from a frozen stock of cloning hosts, DH5αF' or XL1-Blue (Strategene); and expression host, SG13009 containing the

repressor plasmid pREP4, was streaked onto plates containing 50 μg/mL kanamycin (KAN). Four isolated colonies were grown to an OD_{600} of ~0.6-1.0 in 5 mL of Luria Broth (10 g/L casein, 5 g/L yeast extract, 5 g/L NaCl, adjusted to pH 7.4 with NaOH) with no antibiotics (DH5αF' or XL1-Blue) or 50 μg/mL kanamycin (KAN) (SG13009 [pREP4]). A flask containing 100 mL of 2xYT (16 g/L casein, 10 g/L yeast extract, 5 g/L NaCl) was inoculated with 2 mL of the culture and grown until the OD_{600} reached 0.45. Cells were collected in two 50 mL polypropylene tubes (Fisher Scientific) and incubated on ice for 15 minutes before centrifugation at 2500 rpm for 15 minutes at 4 °C. The supernatant was decanted and the cell pellet resuspended in 16L (for each 50 mL of culture) of TFB1(10 mM MES, 100 mM RbCl, 10 mM $CaCl_2 \cdot 2H_2O$, 50 mM $MnCl_2 \cdot 4H_2O$, adjusted to pH 5.8 with acetic acid). The suspension was incubated on ice for 15 minutes before centrifuging at 2500 rpm for 15 minutes at 4 °C. Pellets were resuspended in 2 mL of TFB2 (10 mM MOPS, 75 mM $CaCl_2 \cdot 2H_20$, 10 mM RbCl, 15% glycerol, pH 6.5) and incubated on ice for 15 minutes before aliquots of 50 or 200 μL were prepared for storage at –80 °C.

Thawed competent cells were divided into 50 μL aliquots, to which either 5 μL of ligation mixture or 0.3 μL of circular DNA was added, and then the mixture was incubated on ice for 30-45 minutes. Samples were transferred to a 42 °C sand bath for 90 seconds, incubated on ice for 5 minutes, then 250 μL of 2xYT medium was added and the samples were incubated at 37 °C on a rotating wheel for 1 hour. Transformation cultures were spread on plates (100-200 μL) containing the appropriate antibiotic for selection then incubated overnight at 37 °C.

Cloning of AC_xA and AC_xB genes in pUC-18

Plasmid pWAPL2A was prepared for ligation by digestion with *Spe*I and subsequent removal of 5'phosphate ends using calf intestinal alkaline phosphatase (CIP) to prevent self-ligation. A five fold molar excess of $\mathbf{C_{10}}$ insert to pWAPL2A vector was combined with T4 DNA ligase (20 Units/μL final concentration) in T4 DNA ligase buffer (50 mM tris-HCl pH 7.5, 10 mM $MgCl_2$, 10 mM DTT, 1 mM ATP, 25 μg/mL BSA) and incubated at 16 °C for 12-16 hours. DH5αF' competent cells were transformed with 3-5 μL of ligation mixture by heat shock before spreading on solid medium (2xYT with 15%(w/v) agar) containing Ampicillin (AMP) (200 μg/mL). Isolated colonies were grown to saturation overnight in 5 mL of 2xYT medium containing AMP (200 μg/mL); a 4 mL volume of each culture was centrifuged and the plasmid DNA was extracted from the cell pellet using QIAprep spin miniprep columns.

DNA isolation from clones

To check that the insert was correctly ligated into the plasmid DNA, restriction enzyme analysis was used to identify the size and orientation of the inserted gene. Two methods were used to isolate DNA to screen the recombinant sequences. Freshly transformed bacteria, with colonies 1-2 mm in diameter, were quickly screened using CloneChecker, GibcoBRL (Rockville, MD) restriction enzyme analysis with *Bam*H I to determine clones with single inserts.

Recombinant clones were digested with *Bam*HI enzyme (1 μL of 4 Units/μL) and 1 μL of 10x *Bam*HI buffer (1.5 M NaCl, 100mM tris-HCl, 100 mM $MgCl_2$, 10 mM DTT, pH 7.9, supplemented with 1 mg/mL BSA) as described using the CloneChecker system,

GibcoBRL (Rockville, MD). Before loading on a 1 % agarose TBE gel, 2 μL of Running Buffer, GibcoBRL, was added. DNA was resolved by electrophoresis and visualized by staining the gel post-electrophoresis with 0.5x TBE containing ethidium bromide (0.25 μg/mL ethidium bromide, 45 mM tris borate, 1 mM EDTA).

Suspended colonies screened for insert by the CloneChecker system, or isolated colonies from fresh transformations, were grown to saturation in 2xYT containing appropriate antibiotics. QIAquick spin miniprep columns were used to isolate plasmid DNA for futher restriction enzyme analysis or sequencing.

*Sph*I and *Hind*III restriction digests were used to verify the correct orientation for $\mathbf{C_{10}}$, and *Bgl*II and *Hind*III were used to check the orientation of **A** or **B** in pUC-18 recombinant plasmids. All inserts sizes were determined by digestion with *Bam*HI restriction enzyme.

Clones were sequenced by the DNA Sequencing Facility at Caltech using M13 primers. Although the sequencing reaction can provide information for 600-750 base pairs, shorter than the overall length of the prepared genes, the determined sequence was sufficient to confirm the correct sequence for the ligated area and the newly inserted gene.

Following the cloning strategy described in Figures 3.1 and 3.2, the recombinant genes were prepared in the pWAPL2 vector. Ligation reactions were run with a three to five molar excess of insert to vector.

After determining that the gene containing the insert in the correct orientation and with the correct number of inserts, the artificial gene was excised with *Bam*HI and the

DNA was gel purified. Plasmids were designated as pUC-18L2AC$_x$Aor pUC-18L2AC$_x$B, as denoted in Table 3.1.

Table 3.1 DNA digestion of recombinant genes in pUC-18 cloning plasmid

DNA	*Bam*H I digest	
	insert	vector
pUC-18L2AC$_{20}$A, pUC-18L2AC$_{20}$B	968	2647
pUC-18L2AC$_{30}$A, pUC-18L2AC$_{30}$B	1274	2647
pUC-18L2AC$_{40}$A, pUC-18L2AC$_{40}$B	1580	2647
pUC-18L2AC$_{50}$A, pUC-18L2AC$_{50}$A	1886	2647

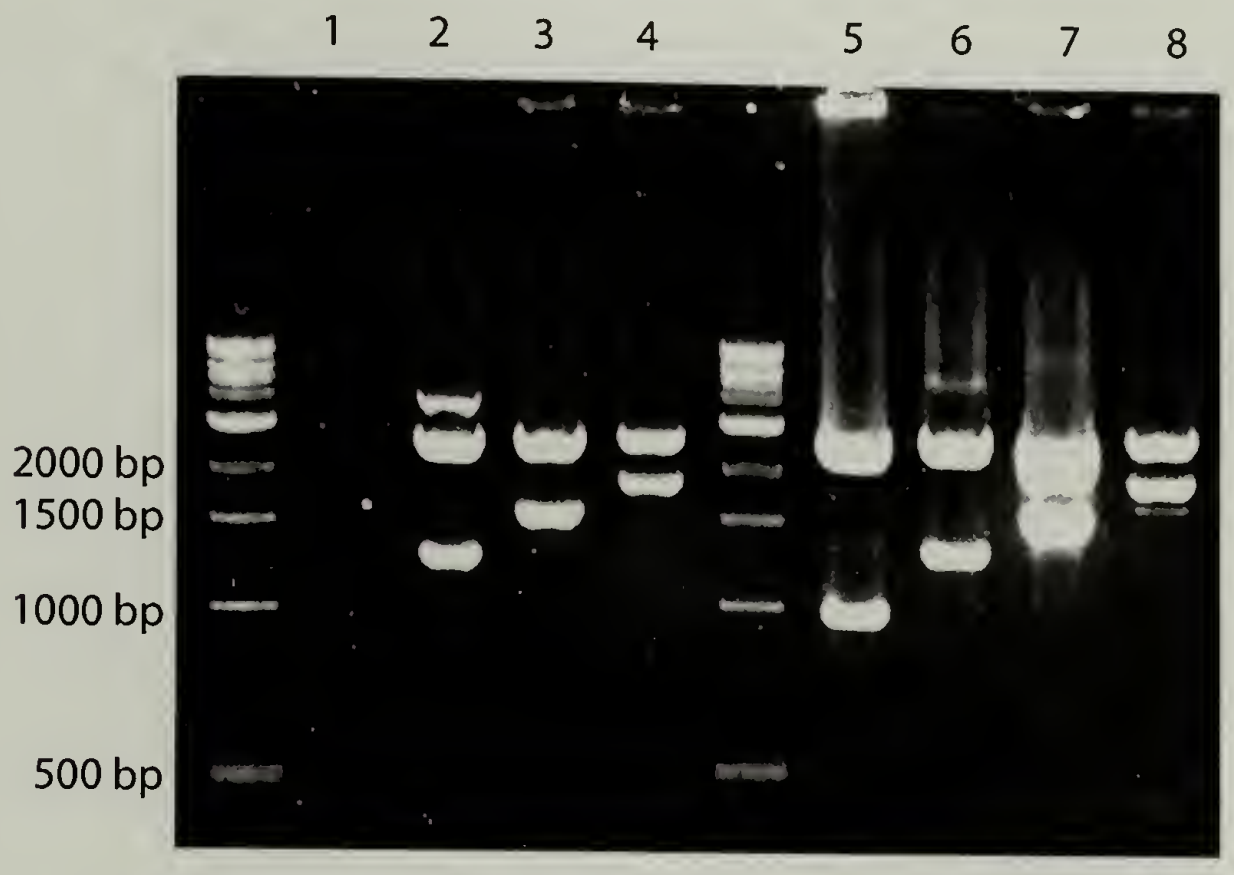

Figure 3.7 *Bam*HI digested recombinant DNA from pUC-18 cloning vector. (1) pUC-18L2AC$_{20}$A, (2) pUC-18L2AC$_{30}$A, (3) pUC-18L2AC$_{40}$A, (4) pUC-18L2AC$_{50}$A, (5) pUC-18L2AC$_{20}$B, (6) pUC-18L2AC$_{30}$B, (7) pUC-18L2AC$_{40}$B, (8) pUC-18L2AC$_{50}$B.

Figure 3.7 shows the resolved genes isolated by restriction enzyme digestion of the pUC-18 derived plasmids containing the synthesized gene. The expected sizes of the genes are shown in Table 3.1.

Cloning of AC_xA and AC_xB genes into pQE-9

Genes encoding AC_xAcys and AC_xBcys (x = 20,30,40,50) were transferred to the expression vector pQE-9. After checking insert size, using *Eco*RI and *Hind*III, and orientation, using *Nhe*I, the isolated pQE-9 recombinant plasmid was transformed into the expression host, SG13009 containing the pREP4 repressor plasmid (Qiagen™, Chatsworth, CA). The recombinant plasmids were named with pQE-9 as a prefix, denoting the original expression vector, with the target gene as a suffix (*i.e.* pQE-9L2AC_{20}A). Table 3.2 notes the names of the recombinant plasmids with the expected insert size determined by an *Eco*RI/*Hind*III digestion.

Figure 3.8 *Eco*RI/*Hind*III digested recombinant DNA from pQE-9 expression vector. (1) pQE-9L2AC_{20}A, (2) pQE-9L2AC_{30}A, (3) pQE-9L2AC_{40}A, (4) pQE-9L2AC_{50}A, (5) pQE-9L2AC_{20}B, (6) pQE-9L2AC_{30}B, (7) pQE-9L2AC_{40}B, (8) pQE-9L2AC_{50}B.

Table 3.2 *EcoRI/Hind*III DNA digestion of recombinant genes in pQE-9 expression plasmid

DNA	*Eco*RI/*Hind*III digest	
	insert	vector
pQE-9L2AC_{20}A, pQE-9L2AC_{20}B	1045	3363
pQE-9L2AC_{30}A, pQE-9L2AC_{30}B	1351	3363
pQE-9L2AC_{40}A, pQE-9L2AC_{40}B	1657	3363
pQE-9L2AC_{50}A, pQE-9L2AC_{50}B	1963	3363

Digested pQE-9 derived recombinant plasmids were resolved on a 1 %(w/v) agarose gel by electrophoresis in 0.5xTBE buffer, as shown in Figure 3.8.

3.2.3 Protein Expression and Purification

Recombinant plasmids with the gene of interest were transformed into *E. coli* strain SG13009 containing the repressor plasmid, pREP4. The pQE-9 plasmid appends a six Histadine sequence to the N-terminus of the protein, providing an efficient tag for protein purification using Ni^{2+}-NTA affinity chromatography. Cells with the recombinant gene of interest were grown in 2xYT medium [16 g/L casein hydrolysate (Amersham-Pharmacia), 10 g/L yeast extract, 5 g/L NaCl] containing antibiotics [200 μg/mL of AMP, 50 μg /mL of KAN] until the optical density measured at 600 nm reached 0.8-1. Isopropyl-β-thiogalactoside (IPTG), was then added to induce expression, and aliquots were removed from the culture before and after addition of IPTG to monitor protein expression by SDS-PAGE analysis.

Large scale protein expression was achieved by growth in 1 L of Terrific Broth medium (12 g/L casein hydrolysate (Amersham), 24 g/L yeast extract, 4 mL/L glycerol, 17 mM KH_2PO_4, 72 mM K_2HPO_4) until the optical density measured at 600 nm reached 0.8-1.0, upon which IPTG was added to a final concentration of 1mM to induce protein expression, and cell growth was continued for 4-5 hours. Cells were harvested by centrifugation at 10,000g for 7 minutes, then the pellet was resuspended in 6M guanidine hydrochloride, 10 mM tris HCl, pH 8.0 and frozen at –80 °C. After three freeze-thaw cycles, the resuspended pellet was sonicated until the viscosity of the solution was similar to that of 6M guanidine hydrochloride. Each of the target proteins remained soluble in the guanidine buffer, which allowed the cellular debris and insoluble proteins to be separated from the solution by centrifugation at 15,300g for 30 minutes.

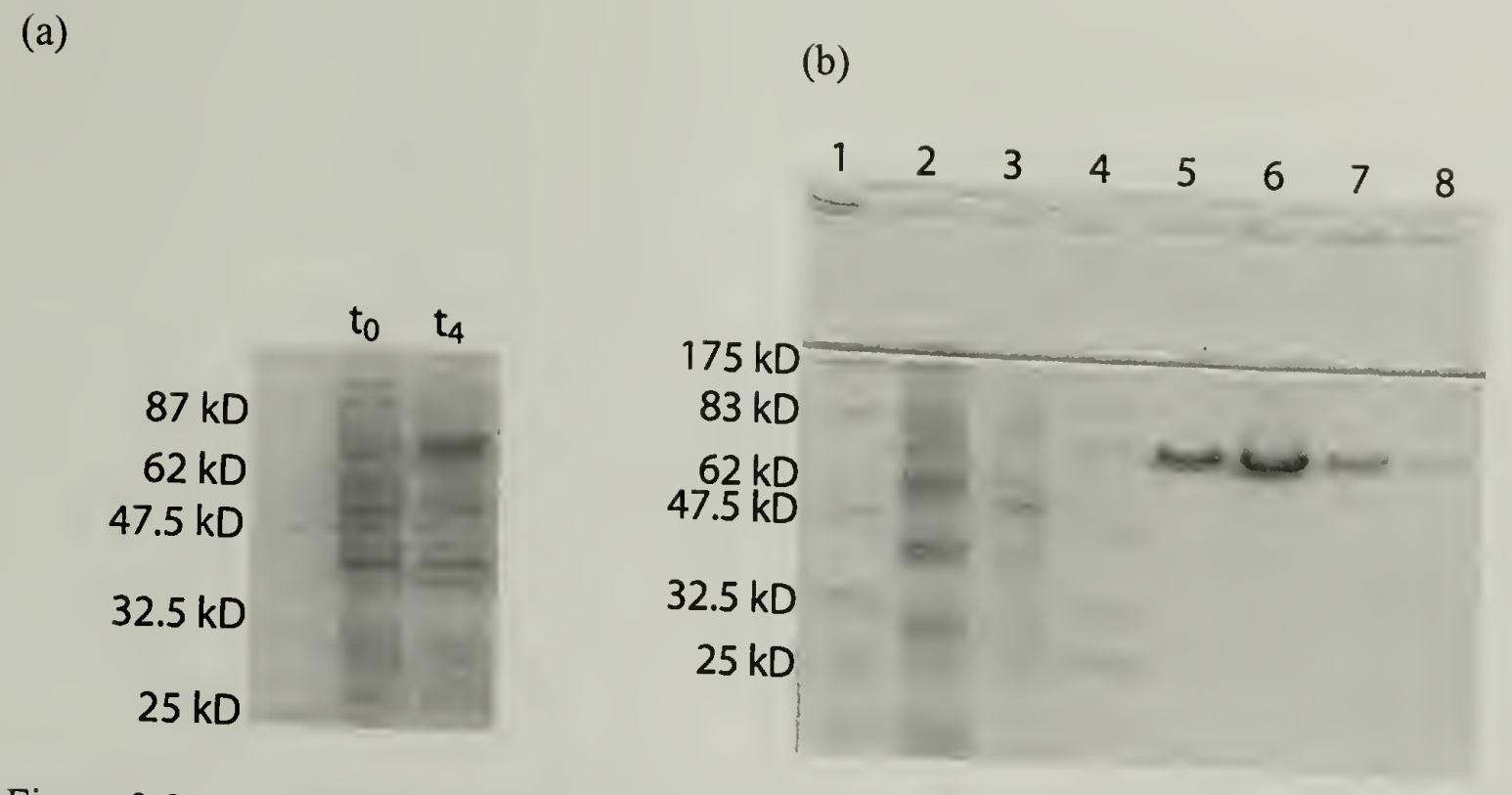

Figure 3.9 Tris/tricine PAGE analysis of (a) expression and (b) purification of AC_{30}Bcys. Molecular weight protein markers are listed in both (a) or (b). Cell lysates (t_0) before and (t_4) after induction of shake flask cultures of SG13009[pREP4] with pQE-9L2AC_{30}B shown in (a). Purification using Ni-NTA^{2+} affinity purification shown in (b): (2) flow through, (3) pH 8.0 8M Urea, (4) pH 6.3 8M Urea, (5) pH 5.9 8M Urea, (6) pH 4.5 8M Urea, 1st fraction, (7) pH 4.5 8M Urea, 2nd fraction, (8) pH 4.5 8M Urea, 3rd fraction.

The supernatant was applied to Ni^{2+}-NTA agarose (Qiagen^{TM}) and purified using a series of washes with 8M urea, 10 mM tris HCl, 1M NaCl. After initial purification of AC_{40}Acys and AC_{50}Acys a Ni^{2+}-NTA colum, the purity remained low. The eluted fractions were then brought to pH 8.0 and reapplied to the column for a second purification. Imidazole (10-15 mM) was added to a second pH 8.0 wash to remove non-specifically bound proteins from the column before elution of the protein with pH 6.3, 8M urea.

Proteins purified by Ni-NTA^{2+} chromatography were resolved on 10% (w/v) acrylamide gels buffered with Tris-tricine as shown in Figure 3.10.

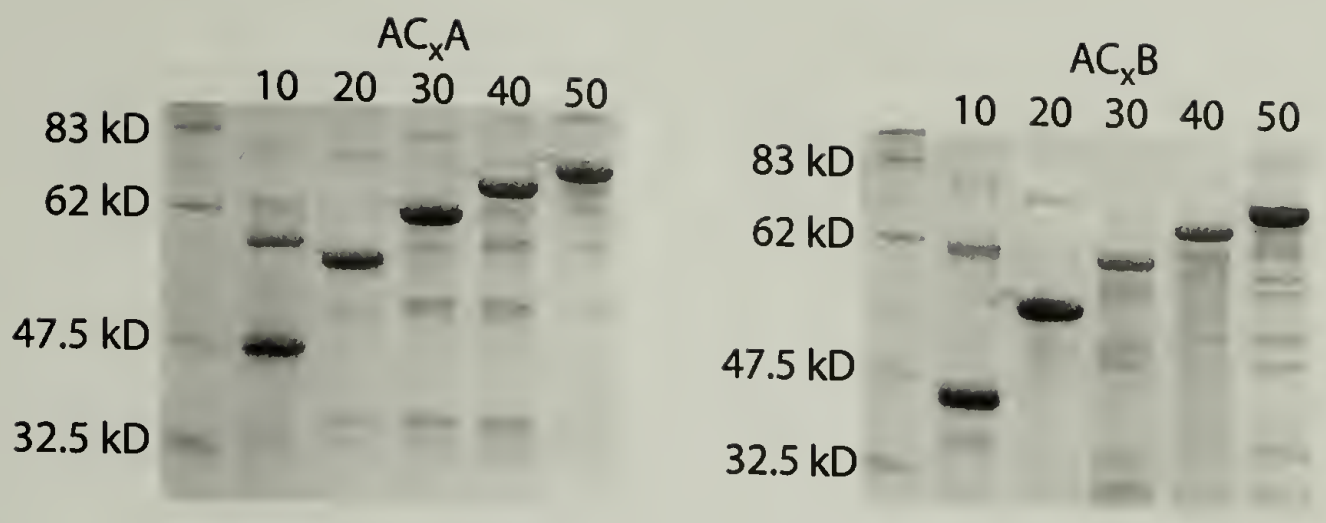

Figure 3.10 Tris-tricine PAGE analysis of AC_xAcys and AC_xBcys proteins purified by Ni-NTA^{2+} affinity chromatography. Lane markers indicate the number of repeats of midblock. (i.e. lane 10 in AC_xA gel is $AC_{10}Acys$, lane 30 in AC_xB gel indicates $AC_{30}Bcys$) Protein molecular weight makers are as shown.

Salts were removed by dialysis against 0.2 μm filtered ddH_20, or alternatively, by ultrafiltration using a stirred cell (Amicon) under pressure with N_2. After dialysis to exchange 8M urea to concentrations ≤ 0.5 M urea, the protein solutions were dialyzed against 10-50 mM ammonium acetate before final exchange against sterile ddH_20. The desalted protein solution was frozen at –20 °C for 4-8 hours, then transferred to –80 °C for at least 2 hours before lyophilization. Dry protein was stored at room temperature in a desiccator under vacuum.

Amino Acid Sequences for AC_xAcys and AC_xBcys proteins

The expected amino acid sequences are listed in Figure 3.11 for the eight newly synthesized proteins. The pQE-9 plasmid, encodes a N-terminal RGS-His_6 sequence upstream from the recombinant gene to provide a tag for purification using Ni^{2+}-NTA affinity chromatography.

(a) $AC_{20}Acys$

MRGSHHHHHHGSDDDDKWASGDLENEVAQLEREVRSLEDEAAELEQKVSRLK
NEIEDLKAEIGDHVAPRDTSYRDPMGAGAGAGPEGAGAGAGPEGAGAGAGPEG
AGAGAGPEGAGAGAGPEGAGAGAGPEGAGAGAGPEGAGAGAGPEGAGAGAGP
EGAGAGAGPEGARMPTSYRDPMGAGAGAGPEGAGAGAGPEGAGAGAGPEGAG
AGAGPEGAGAGAGPEGAGAGAGPEGAGAGAGPEGAGAGAGPEGAGAGAGPEG
AGAGAGPEGARMPTSGDLENEVAQLEREVRSLEDEAAELEQKVSRLKNEIEDLK
AEIGDHVAPRDTSMGGC

(b) $AC_{30}Acys$

MRGSHHHHHHGSDDDDKWASGDLENEVAQLEREVRSLEDEAAELEQKVSRLK
NEIEDLKAEIGDHVAPRDTSYRDPMGAGAGAGPEGAGAGAGPEGAGAGAGPEG
AGAGAGPEGAGAGAGPEGAGAGAGPEGAGAGAGPEGAGAGAGPEGAGAGAGP
EGAGAGAGPEGARMPTSYRDPMGAGAGAGPEGAGAGAGPEGAGAGAGPEGAG
AGAGPEGAGAGAGPEGAGAGAGPEGAGAGAGPEGAGAGAGPEGAGAGAGPEG
AGAGAGPEGARMPTSYRDPMGAGAGAGPEGAGAGAGPEGAGAGAGPEGAGA
GAGPEGAGAGAGPEGAGAGAGPEGAGAGAGPEGAGAGAGPEGAGAGAGPEGA
GAGAGPEGARMPTSYRDPMGAGAGAGPEGAGAGAGPEGAGAGAGPEGAGAG
AGPEGAGAGAGPEGAGAGAGPEGAGAGAGPEGAGAGAGPEGAGAGAGPEGAG
AGAGPEGARMPTSGDLENEVAQLEREVRSLEDEAAELEQKVSRLKNEIEDLKAEI
GDHVAPRDTSMGGC

(c) $AC_{40}Acys$

MRGSHHHHHHGSDDDDKWASGDLENEVAQLEREVRSLEDEAAELEQKVSRLK
NEIEDLKAEIGDHVAPRDTSYRDPMGAGAGAGPEGAGAGAGPEGAGAGAGPEG
AGAGAGPEGAGAGAGPEGAGAGAGPEGAGAGAGPEGAGAGAGPEGAGAGAGP
EGAGAGAGPEGARMPTSYRDPMGAGAGAGPEGAGAGAGPEGAGAGAGPEGAG
AGAGPEGAGAGAGPEGAGAGAGPEGAGAGAGPEGAGAGAGPEGAGAGAGPEG
AGAGAGPEGARMPTSYRDPMGAGAGAGPEGAGAGAGPEGAGAGAGPEGAGA
GAGPEGAGAGAGPEGAGAGAGPEGAGAGAGPEGAGAGAGPEGAGAGAGPEGA
GAGAGPEGARMPTSYRDPMGAGAGAGPEGAGAGAGPEGAGAGAGPEGAGAG
AGPEGAGAGAGPEGAGAGAGPEGAGAGAGPEGAGAGAGPEGAGAGAGPEGAG
AGAGPEGARMPTSGDLENEVAQLEREVRSLEDEAAELEQKVSRLKNEIEDLKAEI
GDHVAPRDTSMGGC

Fig. 3.11 Continued next page

(d) $AC_{50}Acys$

MRGSHHHHHHGSDDDDKWASGDLENEVAQLEREVRSLEDEAAELEQKVSRLK
NEIEDLKAEIGDHVAPRDTSYRDPMGAGAGAGPEGAGAGAGPEGAGAGAGPEG
AGAGAGPEGAGAGAGPEGAGAGAGPEGAGAGAGPEGAGAGAGPEGAGAGAGP
EGAGAGAGPEGARMPTSYRDPMGAGAGAGPEGAGAGAGPEGAGAGAGPEGAG
AGAGPEGAGAGAGPEGAGAGAGPEGAGAGAGPEGAGAGAGPEGAGAGAGPEG
AGAGAGPEGARMPTSYRDPMGAGAGAGPEGAGAGAGPEGAGAGAGPEGAGA
GAGPEGAGAGAGPEGAGAGAGPEGAGAGAGPEGAGAGAGPEGAGAGAGPEGA
GAGAGPEGARMPTSYRDPMGAGAGAGPEGAGAGAGPEGAGAGAGPEGAGAG
AGPEGAGAGAGPEGAGAGAGPEGAGAGAGPEGAGAGAGPEGAGAGAGPEGAG
AGAGPEGARMPTSYRDPMGAGAGAGPEGAGAGAGPEGAGAGAGPEGAGAGA
GPEGAGAGAGPEGAGAGAGPEGAGAGAGPEGAGAGAGPEGAGAGAGPEGAGA
GAGPEGARMPTSGDLENEVAQLEREVRSLEDEAAELEQKVSRLKNEIEDLKAEIG
DHVAPRDTSMGGC

(e) $AC_{20}Bcys$

MRGSHHHHHHGSDDDDKWASGDLENEVAQLEREVRSLEDEAAELEQKVSRLK
NEIEDLKAEIGDHVAPRDTSYRDPMGAGAGAGPEGAGAGAGPEGAGAGAGPEG
AGAGAGPEGAGAGAGPEGAGAGAGPEGAGAGAGPEGAGAGAGPEGAGAGAGP
EGAGAGAGPEGARMPTSYRDPMGAGAGAGPEGAGAGAGPEGAGAGAGPEGAG
AGAGPEGAGAGAGPEGAGAGAGPEGAGAGAGPEGAGAGAGPEGAGAGAGPEG
AGAGAGPEGARMPTSGDLKNKVAQLKRKVRSLKDKAAELKQEVSRLENEIEDL
KAKIGDHVAPRDTSMGGC

(f) $AC_{30}Bcys$

MRGSHHHHHHGSDDDDKWASGDLENEVAQLEREVRSLEDEAAELEQKVSRLK
NEIEDLKAEIGDHVAPRDTSYRDPMGAGAGAGPEGAGAGAGPEGAGAGAGPEG
AGAGAGPEGAGAGAGPEGAGAGAGPEGAGAGAGPEGAGAGAGPEGAGAGAGP
EGAGAGAGPEGARMPTSYRDPMGAGAGAGPEGAGAGAGPEGAGAGAGPEGAG
AGAGPEGAGAGAGPEGAGAGAGPEGAGAGAGPEGAGAGAGPEGAGAGAGPEG
AGAGAGPEGARMPTSYRDPMGAGAGAGPEGAGAGAGPEGAGAGAGPEGAGA
GAGPEGAGAGAGPEGAGAGAGPEGAGAGAGPEGAGAGAGPEGAGAGAGPEGA
GAGAGPEGARMPTSGDLKNKVAQLKRKVRSLKDKAAELKQEVSRLENEIEDLK
AKIGDHVAPRDTSMGGC

Fig. 3.11 Continued next page

(g) $AC_{40}Bcys$ Continued

MRGSHHHHHHGSDDDDKWASGDLENEVAQLEREVRSLEDEAAELEQKVSRLK
NEIEDLKAEIGDHVAPRDTSYRDPMGAGAGAGPEGAGAGAGPEGAGAGAGPEG
AGAGAGPEGAGAGAGPEGAGAGAGPEGAGAGAGPEGAGAGAGPEGAGAGAGP
EGAGAGAGPEGARMPTSYRDPMGAGAGAGPEGAGAGAGPEGAGAGAGPEGAG
AGAGPEGAGAGAGPEGAGAGAGPEGAGAGAGPEGAGAGAGPEGAGAGAGPEG
AGAGAGPEGARMPTSYRDPMGAGAGAGPEGAGAGAGPEGAGAGAGPEGAGA
GAGPEGAGAGAGPEGAGAGAGPEGAGAGAGPEGAGAGAGPEGAGAGAGPEGA
GAGAGPEGARMPTSYRDPMGAGAGAGPEGAGAGAGPEGAGAGAGPEGAGAG
AGPEGAGAGAGPEGAGAGAGPEGAGAGAGPEGAGAGAGPEGAGAGAGPEGAG
AGAGPEGARMPTSGDLKNKVAQLKRKVRSLKDKAAELKQEVSRLENEIEDLKA
KIGDHVAPRDTSMGGC

(h) $AC_{50}Bcys$

MRGSHHHHHHGSDDDDKWASGDLENEVAQLEREVRSLEDEAAELEQKVSRLK
NEIEDLKAEIGDHVAPRDTSYRDPMGAGAGAGPEGAGAGAGPEGAGAGAGPEG
AGAGAGPEGAGAGAGPEGAGAGAGPEGAGAGAGPEGAGAGAGPEGAGAGAGP
EGAGAGAGPEGARMPTSYRDPMGAGAGAGPEGAGAGAGPEGAGAGAGPEGAG
AGAGPEGAGAGAGPEGAGAGAGPEGAGAGAGPEGAGAGAGPEGAGAGAGPEG
AGAGAGPEGARMPTSYRDPMGAGAGAGPEGAGAGAGPEGAGAGAGPEGAGA
GAGPEGAGAGAGPEGAGAGAGPEGAGAGAGPEGAGAGAGPEGAGAGAGPEGA
GAGAGPEGARMPTSYRDPMGAGAGAGPEGAGAGAGPEGAGAGAGPEGAGAG
AGPEGAGAGAGPEGAGAGAGPEGAGAGAGPEGAGAGAGPEGAGAGAGPEGAG
AGAGPEGARMPTSYRDPMGAGAGAGPEGAGAGAGPEGAGAGAGPEGAGAGA
GPEGAGAGAGPEGAGAGAGPEGAGAGAGPEGAGAGAGPEGAGAGAGPEGAGA
GAGPEGARMPTSGDLKNKVAQLKRKVRSLKDKAAELKQEVSRLENEIEDLKAKI
GDHVAPRDTSMGGC

Figure 3.11 Protein sequences for (a) $AC_{20}Acys$, (b) $AC_{30}Acys$, (c) $AC_{40}Acys$, (d) $AC_{50}Acys$, (e) $AC_{20}Bcys$, (f) $AC_{30}Bcys$, (g) $AC_{40}Bcys$, (h) $AC_{50}Bcys$.

3.2.4 Characterization

3.2.4.1 Amino Acid Analysis

Amino acid analysis was performed by the Molecular Structure Facility at University of California, Davis. Lyophilized protein was transferred to a concentrated formic acid solution, then the protein was hydrolyzed with 6N HCl/0.1% phenol at 110 °C for 24 hours. After drying, the hydrolyzed protein was dissolved in buffer containing norleucine standard. Free amino acid concentrations were determined using a Beckman 6300Na citrate-based amino acid analyzer. Alternatively, some samples were run on a Li citrate-based analyzer. Results of amino acid analysis are shown in Tables 3.3-3.6.

Table 3.3 Amino acid analysis for AC_{20}Acys and AC_{30}Acys

Amino Acid		AC_{20}Acys		AC_{30}Acys	
		mol %(theor)	mol %(obs)	mol %(theor)	mol %(obs)
D	aspartic acid +				
N	asparagine	6.0	5.7	4.8	4.8
T	threonine	1.2	1.1	1.2	1.0
S	serine	3.3	3.2	2.8	2.6
E	glutamic acid +				
Q	glutamine	13.9	14.2	12.9	13.5
P	proline	7.8	8.0	8.8	8.7
G	glycine	27.1	25.2	30.2	29.3
A	alanine	22.0	24.4	24.0	25.4
V	valine	2.4	2.4	1.8	1.9
M	methionine	1.8	1.3	1.8	1.0
I	isoleucine	1.2	1.2	0.9	0.9
L	leucine	3.6	3.8	2.8	2.8
T	tyrosine	0.6	0.7	0.7	0.8
H	histadine	2.4	2.7	1.8	2.0
L	lysine	2.1	2.2	1.6	1.6
R	arginine	3.9	4.1	3.5	3.7

Table 3.4 Amino acid analysis for $AC_{40}Acys$ and $AC_{50}Acys$

Amino Acid	$AC_{40}Acys$		$AC_{50}Acys$	
	mol %(theor)	mol %(obs)	mol %(theor)	mol %(obs)
D aspartic acid + N asparagine	4.1	4.6	3.6	3.9
T threonine	1.1	1.2	1.1	1.1
S serine	2.4	2.3	2.2	2.0
E glutamic acid + Q glutamine	12.3	12.9	11.9	12.4
P proline	9.3	9.3	9.7	9.6
G glycine	32.1	31.2	33.4	32.3
A alanine	25.2	24.9	26	26.6
V valine	1.5	1.8	1.3	1.6
M methionine	1.9	1.2	1.9	1.3
I isoleucine	0.7	0.7	0.6	0.6
L leucine	2.2	2.3	1.9	1.9
T tyrosine	0.7	0.8	0.8	0.9
H histadine	1.5	1.8	1.3	1.3
L lysine	1.3	1.4	1.1	1.2
R arginine	3.2	3.5	3	3.2

Table 3.5 Amino acid analysis for AC_{20}Bcys and AC_{30}Bcys

Amino Acid		AC_{20}Bcys		AC_{30}Bcys	
		mol %(theor)	mol %(obs)	mol %(theor)	mol %(obs)
D	aspartic acid +				
N	asparagine	6.0	6.0	4.8	4.6
T	threonine	1.2	1.3	1.2	1.1
S	serine	3.3	3.3	2.8	2.5
E	glutamic acid +				
Q	glutamine	12.0	12.4	11.7	11.9
P	proline	8.1	7.8	8.8	8.9
G	glycine	27.1	24.5	30.2	29.8
A	alanine	21.7	23.7	24.0	25.7
V	valine	2.1	2.6	1.8	1.7
M	methionine	2.1	1.0	1.8	1.3
I	isoleucine	1.2	1.4	0.9	0.9
L	leucine	3.6	4.0	2.8	2.6
T	tyrosine	0.9	0.8	0.7	0.9
H	histadine	2.1	2.8	1.8	2.0
L	lysine	3.6	4.2	3	2.4
R	arginine	4.2	4.2	3.5	3.6

Table 3.6 Amino acid analysis for AC_{40}Bcys and AC_{50}Bcys

Amino Acid		AC_{40}Bcys		AC_{50}Bcys	
		mol %(theor)	mol %(obs)	mol %(theor)	mol %(obs)
D	aspartic acid +				
N	asparagine	4.1	4.7	3.6	4.1
T	threonine	1.1	1.2	1.1	1.3
S	serine	2.4	2.2	2.2	2.2
E	glutamic acid +				
Q	glutamine	11.1	12.0	10.9	11.8
P	proline	9.3	8.9	9.7	10.1
G	glycine	32.1	30.8	33.4	32.3
A	alanine	25.2	25.6	26.0	26.7
V	valine	1.5	1.9	1.3	1.7
M	methionine	1.9	1.1	1.9	0.1*
I	isoleucine	0.7	0.7	0.6	0.6
L	leucine	2.2	2.4	1.9	1.9
T	tyrosine	0.7	0.9	0.8	0.9
H	histadine	1.5	1.8	1.3	1.3
L	lysine	2.4	2.4	2.0	2.0
R	arginine	3.2	3.5	3.0	3.1

* Within limits of error.

Amino acid results indicate that the expected protein compositions were prepared. Molar percents of the individual amino acids fell within 2% of the expected values.

3.2.4.2 MALDI Mass Spectrometry

Protein molecular mass was determined using MALDI analysis. Purified, lyophilized protein was dissolved in ddH_2O to an approximate concentration of 100-200 mM, then 1 μL of the solution was combined with sinapinic acid matrix (0.1% TFA, 30% acetonitrile). Samples were spotted onto a target plate (Applied Biosystems, Foster City, CA) using 0.3 μL of protein in sinapinic acid matrix. Bovine serum albumin (BSA) (New England Biolabs) in sinapinic acid matrix, was used to externally calibrate the mass

spectrometer. A Voyager-DE Pro Biospectrometry Workstation (Applied Biosystems, Foster City, CA) was used to collect spectra for each protein. The table below lists the average mass obtained for the M+ ion, for five samples, with the exception of $AC_{40}Acys$, in which two samples were taken. The expected mass was determined by analysis of the amino acid sequences listed in Figure 3.10 using Sherpa 4.0 lite, a freeware program available at http://www.hairyfatguy.com/Sherpa/. For large peptides (molecular masses ≥ 2500 Da) or proteins, the natural abundance of ^{13}C becomes significant in calculating the expected mass. Although the natural abundance of ^{13}C is 1.10%, as the number of carbons in each molecule increases, there is a higher probability that each chain has at least one ^{13}C among all of the carbons in the chain. Whereas the most abundant species of a small peptide is characterized by the monoisotopic mass—calculated using only the mass of the most abundant species for each element—the most abundant isotope for proteins becomes an average of the various isotopic variants of the protein (*3*). MALDI MS results of the target proteins are summarized in Table 3.7.

Table 3.7 MALDI MS summary for AC_xAcys, x = {20,30,40,50} and AC_xBcys, x = {20,30,40,50}

Protein	expected M+ (Da)	observed M+ (Da)	relative error (%)
$AC_{20}Acys$	30,493	30,441 ± 15	0.17
$AC_{30}Acys$	38,534	38,437 ± 30	0.25
$AC_{40}Acys$	46,574	46,612 ± 4	0.16
$AC_{50}Acys$	54,614	54,412 ± 42	0.37
$AC_{20}Bcys$	30,488	30,425 ± 41	0.21
$AC_{30}Bcys$	38,528	38,683 ± 43	0.40
$AC_{40}Bcys$	46,568	46,535 ± 38	0.07
$AC_{50}Bcys$	54,609	54,469 ± 10	0.26

3.2.4.3 Circular Dichroism Spectroscopy

Lyophilized, purified proteins were dissolved in ddH_2O to achieve stock concentrations between 100 and 200 mM. In some cases, 1N NaOH was added to clarify the solution, ensuring that the protein was completely solubilized. Theoretical extinction coefficients were determined based on the number of tryptophan or tyrosine residues in the protein (*4, 5*). Wavelength scans of solutions containing an estimated protein concentration between 20-50 μM were taken at 25 °C from 300 to 260 nm with a Carey UV-vis spectrophotometer. Based on the extinction coefficient and the absorbance at 280 nm, the concentration was calculated using Beer's law:

$$A=\varepsilon cl,$$

where A is the measured absorbance, ε is the extinction coefficient, l is the cell path length in cm, and c is the concentration of the solution in M. Table 3.8 shows the expected extinction coefficients for each protein. The $\mathbf{C_{10}}$ block contains one tyrosine, thus the expected extinction coefficient increases with increasing midblock length.

Table 3.8 Extinction coefficients for AC_xAcys and AC_xBcys proteins

Protein	ε_{280} ($M^{-1}cm^{-1}$)	Protein	ε_{280} ($M^{-1}cm^{-1}$)
$AC_{10}Acys$	6970	$AC_{10}Bcys$	6970
$AC_{20}Acys$	8250	$AC_{20}Bcys$	8250
$AC_{30}Acys$	9530	$AC_{30}Bcys$	9530
$AC_{40}Acys$	10810	$AC_{40}Bcys$	10810
$AC_{50}Acys$	12090	$AC_{50}Bcys$	12090

Circular dichroism measurements were recorded using an AVIV 62DS spectropolarimeter (Lakewood, NJ), calibrated with an aqueous solution of (1S)-(+)-(10)-camphorsulfonic acid. Wavelength scans were taken at 25 °C from 250 to 195 nm, every 1 nm, averaged over 4 seconds, with 1nm bandwidth. Three spectra were recorded and averaged for each wavelength scan. The data presented in Figures 3.11 and 3.12 represent the average of two separate measurements of the same protein preparation.

Protein solutions were prepared by dilution of the stock solution to a final concentration of 5 μM, in phosphate buffered saline (PBS), adjusted to pH 7.4 with 1N HCl.

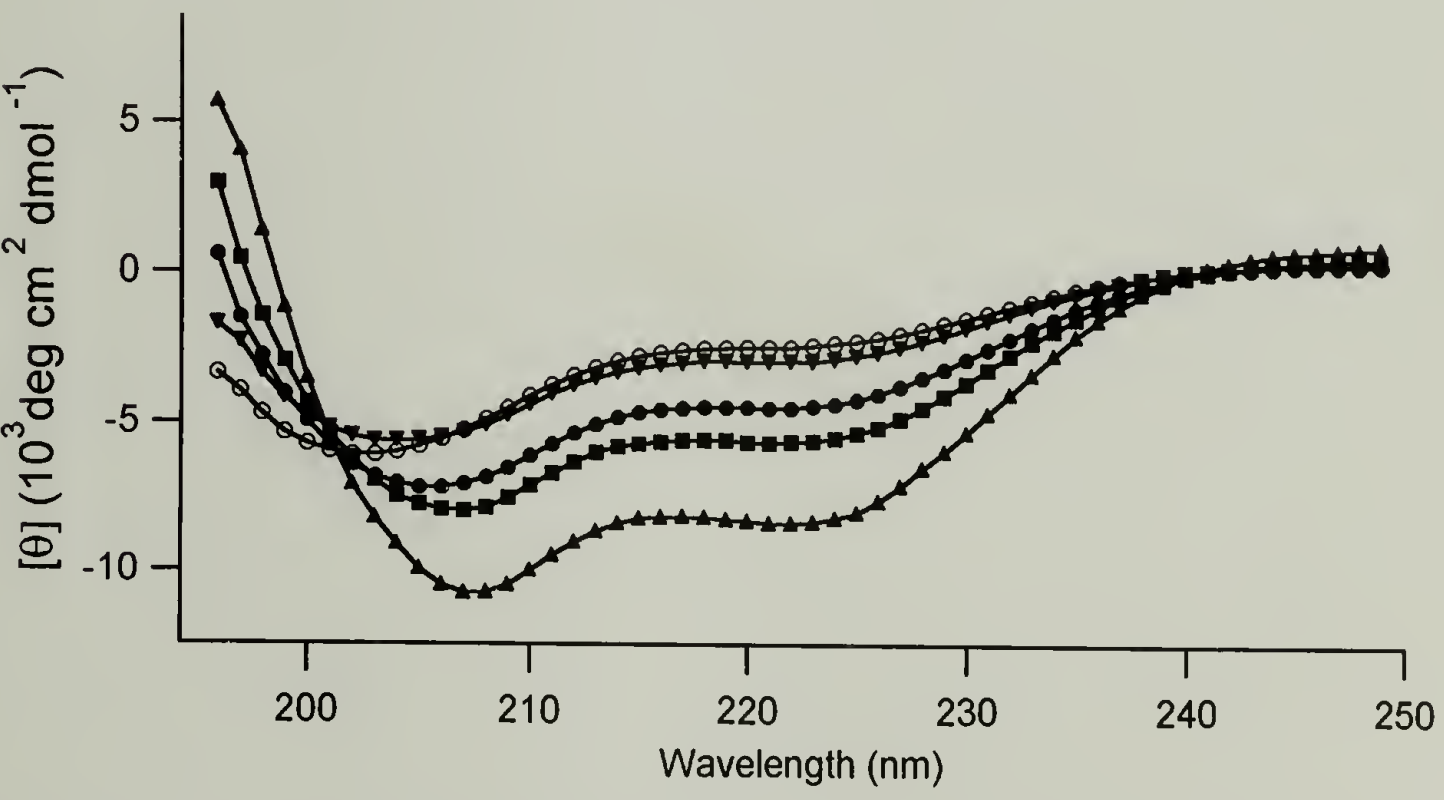

Figure 3.12 Circular dichroism for AC_xAcys proteins at 5 μM in PBS (10 mM phosphate, 150 mM NaCl), pH 7.4, $AC_{10}Acys$ (▲), $AC_{20}Acys$ (■), $AC_{30}Acys$ (●), $AC_{40}Acys$ (▼), $AC_{50}Acys$ (○).

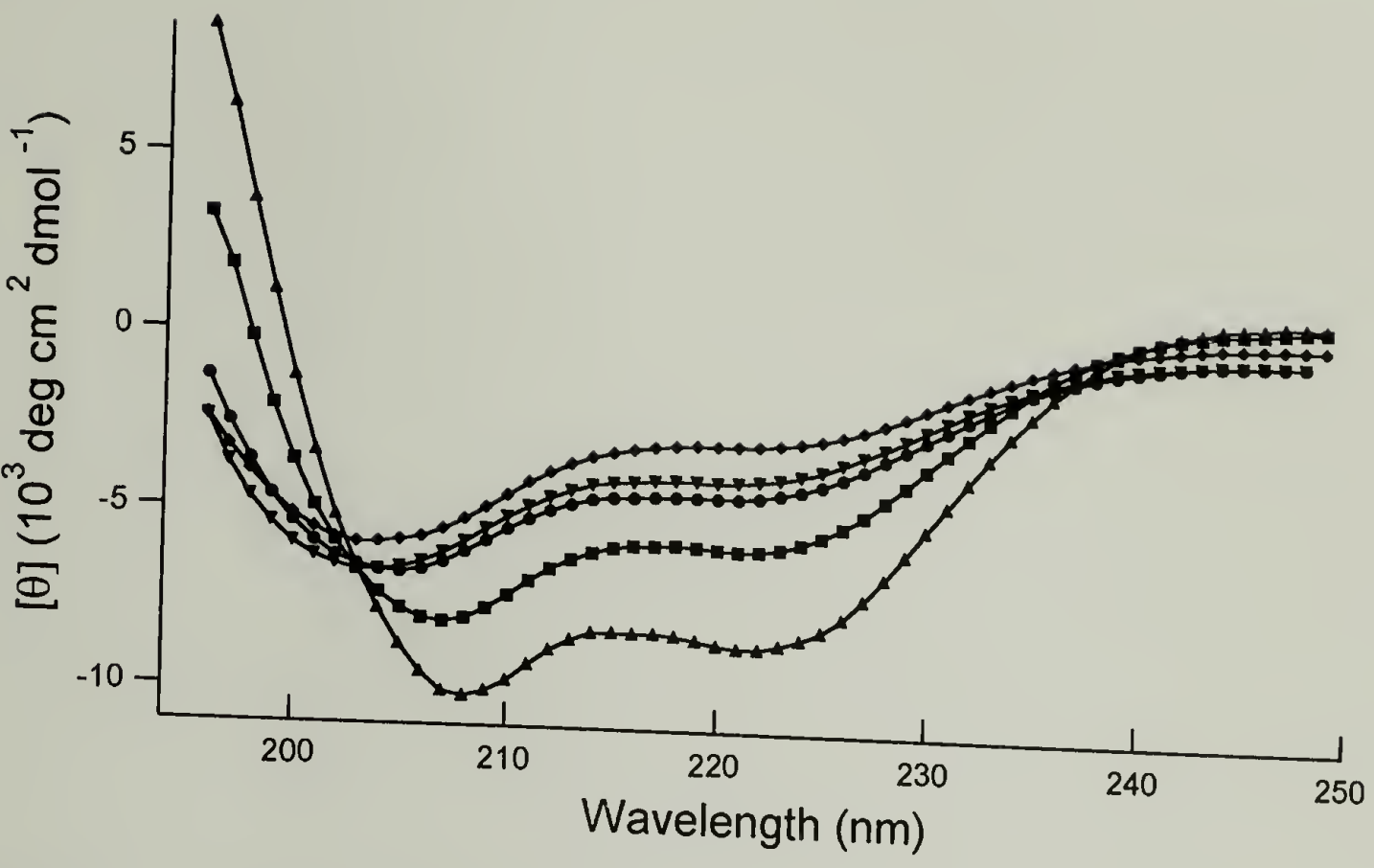

Figure 3.13 Circular dichroism for AC_xBcys proteins at 5 μM in PBS (10 mM phosphate, 150 mM NaCl), pH 7.4, $AC_{10}Bcys$ (▲), $AC_{20}Bcys$ (■), $AC_{30}Bcys$ (●), $AC_{40}Bcys$ (▼), $AC_{50}Bcys$ (◆).

3.3 Discussion

Eight proteins were designed at the DNA level and prepared using recombinant DNA technology. The proteins were expressed in low cell density cultures with induction by IPTG. All genes were prepared in the pQE-9 expression vector, which uses the T5 promotor. Proteins were isolated by Ni^{2+}-NTA chromatography and resolved by electrophoresis on a Tris-tricine acrylamide gel.

Previously (*2, 6*), proteins containing the polyelectrolyte sequence, $[(AG)_3PEG]_x$ were observed to migrate more slowly than naturally occurring proteins of similar molecular weight. The surfactant, SDS, presumably binds to the protein, creating a highly charged, rod-like complex, which migrates through the acrylamide sieving matrix at rate determined by its molecular mass. In the case of the non-natural sequence,

$[(AG)_3PEG]_x$, we suggest that SDS does not effectively bind, causing the migration to be anomalously slow.

The presence of protein bands at lower molecular weight than the target protein in Figure 3.10, may be attributed to inefficient translation, to genetic instability, or to degradation. It is likely that the proteins are of the similar composition as the target proteins, as evidenced by amino acid analysis (Tables 3.3-3.6). The reported molar percentages for each amino acid fall within 2 % of the expected values, which would not preclude the presence of a mixture of target protein with fragmented chains of similar composition. The use of Ni^{2+}-NTA affinity chromatography is not effective to isolate the full length proteins from the shorter fragments, however, further purification by HPLC or size exclusion chromatography could be used when necessary.

Mass spectrometry was used to confirm the expression of the full length target proteins. Results reported in Table 3.7 show that the observed masses were within 1% of the expected average mass. Protein dialysis was found to affect the resolution of the spectra. The reported results were observed for samples dialyzed against 10-50 mM ammonium acetate before a final exchange against ddH_2O. Presence of excess sodium ions will drastically broaden the observed signals. Ammonium ions can exchange the sodium ions associated with the protein during dialysis, but low concentrations of ammonium may be tolerated by MALDI-TOF. As a result, the spectra are better resolved and more accurate.

Secondary structure for each protein was characterized by circular dichroism. Figures 3.11 and 3.12 illustrate the decreasing amount of helicity, as indicated by double minima at 222 and 208 nm, as a function of the increasing midblock length. For

AC_{10}Acys and AC_{10}Bcys, the minima at 222 and 208 nm are observed at a molar ellipticity around –9,000 deg cm^2 $dmol^{-1}$. The value of the molar ellipticity at 222 nm for both molecules indicates that their helical fraction is similar. As the midblock length increases in both the AC_xAcys (Figure 3.11) and AC_xBcys (Figure 3.12) proteins, the double minimum at 208 nm and 222 nm is less apparent; this change indicates proteins with longer midblock domains are characteristic of a lower helical fraction as compared to AC_{10}Acys or AC_{10}Bcys (*7, 8*). The main contribution of the random coil spectra is negative absorbance around 195 nm (*9*). Comparing the AC_xAcys or AC_xBcys proteins, one can observe the shift in the minimum at 208 nm to a less negative value centered at lower wavelength as the midblock length increases. This result indicates the greater fraction of random coil, as anticipated.

In conclusion, recombinant DNA techniques were used to prepare eight new proteins which are characterized by leucine zipper end-blocks flanking a polyelectrolyte midblock that adopts a random coil conformation. The proteins were biosynthetically prepared and purified under denaturing conditions using metal affinity chromatography. Amino acid analysis and MALDI-TOF spectrometry were used to confirm the identity of the target proteins, and CD spectroscopy was used to verify that the secondary structure of the individual blocks was maintained.

3.4 References

1. W. A. Petka, Ph.D. dissertation, University of Massachusetts, Amherst (1997).

2. K. P. McGrath, M. J. Fournier, T. L. Mason, D. A. Tirrell, *J. Am. Chem. Soc.* **114**, 727-733 (1992).

3. S. A. Carr, R. S. Annan, in *Current Protocols in Molecular Biology*. (John Wiley & Sons, Inc., 1997) pp. 10.21.1-10.21-27.

4. S. C. Gill, *Anal. Biochem.* **189**, 283-283 (1990).

5. S. C. Gill, P. H. Vonhippel, *Anal. Biochem.* **182**, 319-326 (1989).

6. W. A. Petka, J. L. Harden, K. P. McGrath, D. Wirtz, D. A. Tirrell, *Science* **281**, 389-392 (1998).

7. Y.-H. Chen, J. T. Yang, K. H. Chau, *Biochemistry-US* **13**, 3350-3359 (1974).

8. M. C. Manning, *J. Pharmaceut. Biomed.* **7**, 1103-1119 (1989).

9. A. J. Adler, N. J. Greenfield, G. D. Fasman, *Method. Enzymol.* **27**, 675-735 (1973).

CHAPTER 4

DISSOLUTION OF TRIBLOCK PROTEIN HYDROGELS BY ADDITION OF LEUCINE ZIPPER BLOCKS

4.1 Introduction

Associative telechelic polymers are a class of water-soluble molecules characterized by the ability to form temporary networks (*1-3*). The associative polymers (AP) are designed with a water soluble midblock, typically poly(ethylene oxide) or a polyelectrolyte, capped on both ends with a short hydrophobe. When dissolved in water, the hydrophobic end blocks associate in micelles, exposing the water soluble midblock to the solvent while shielding the interior from the aqueous environment. The micro-phase separation of the hydrophobes leads to increased viscosities or gelation in the vicinity of the overlap concentration, where micelles are close enough for individual chains to bridge neighboring hydrophobic micelle interiors.

Thuresson and co-workers (*4*) compared the rheology in solutions of associating diblock and triblock copolymers in water to illustrate the network formation from triblock architectures. At high concentrations, the triblock copolymer can either form a loop, where the hydrophobic ends on one chain are in the same micelle interior, or form a bridge, connecting two micelles together. In contrast, the diblock copolymer has only one hydrophobe on each chain; thus, there is only the possibility to form individual micelles. As a result, the increase in viscosity as a function of concentration was highest for the triblock and lowest for the diblock, with mixtures of the two architectures falling between the two extremes, depending on the concentration of each component.

The triblock copolymer prepared by Yu and co-workers relied on the association of syndiotactic poly(methyl methacrylate) (sPMMA)to lead to the formation of a network (*5*). In a solution of o-xylene, triblock copolymers of sPMMA-polybutadiene (PBD)-sPMMA were solubilized, then heated to 80 °C and quenched to below 35 °C to induce folding of the sPMMA endblocks. The microphase separated domains of folded sPMMA served as crosslinks, while the PBD was solubilized by the o-xylene.

These systems contain elements which can be compared to the triblock protein hydrogels, in that the triblock is necessary to form the network, and assumes that the clusters contain hydrophobes from a minimum of three independent, elastically effective chains, and the junction points result from the secondary structure of the end blocks.

Atrp addition to $AC_{10}Acys$:

It is thought that the physical crosslinks in triblock protein hydrogels can be attributed to the association of the helical end blocks on different chains, with the random coil midblock connecting and solubilizing these aggregates to produce a network, similar to that described for associating polymers. The stabilization of aggregates in triblock protein hydrogels, such as $AC_{10}Acys$, differ from those associating polymers because it is presumed that the secondary structure of the end blocks determine their tendency to aggregate into dimers or higher order structures. This hypothesis is examined here by a competition experiment in which individual end blocks are combined with triblocks under conditions where the end blocks are assumed to be folded into the secondary structure, the leucine zipper, which promotes aggregation. The rheological properties are

measured by single particle tracking, and the secondary structure is monitored by circular dichroism.

A monofunctional end block was prepared by modification of the gene encoding Acys to impart a C-terminal tryptophan in the place of the cysteine. It was anticipated that the addition of Atrp to AC_{10}Acys, would displace 'A' end blocks from the AC_{10}Acys that were elastically effective, thus disrupting the network. The helical blocks (Atrp) were expected to dimerize with helical domains on the triblock copolymers, as the leucine zipper domains on both proteins are identical. With increasing concentrations of Atrp, aggregates of the coiled coil domains may contain only one end block from AC_{10}Acys, surrounded by Atrp. Dissociation of the gel by this mechanism supports the hypothesis that the gelation mechanism is controlled by the helical domain association. Single particle tracking was used probe the viscoelasticity of the mixtures. It was observed that at concentrations where AC_{10}Acys forms a gel, the addition of Atrp can frustrate the formation of the network.

4.2 Experimental Work

4.2.1 Synthesis and Characterization of Atrp

4.2.1.1 Genetic Strategy to Prepare Atrp

Preparation of DNA for insertion of A into pWAP-L1

The cloning strategy for Atrp is outlined in figures 4.1 and 4.2. The cloning vector, pWAP-L1 (*6*), a modified pUC-18 (*Pharmacia*™) plasmid, was linearized by digestion with *Bst*E*II*, a unique site located in the 27 base pair gene, L1. Calf Intestinal Alkaline Phosphatase, (CIP), was used to remove 5' phosphates from the linear vector to prevent self-ligation. A 126 base pair insert encoding the acidic leucine zipper domain, **A**, was prepared by digestion of pWAP-L2A (*6*) at *Bst*E*II*. The dephophorylated, linearized pWAPL1 and the *Bst*E*II* digested **A** gene were gel purified and extracted into ddH_2O. DNA was extracted from the agarose gel into 10 mM tris, pH 8.5 using QIAEX II gel extraction system according to the procedure outlined by *Qiagen*™ (Valencia, CA). Ligation mixtures containing 2 μL of plasmid, 2 μL, 5 μL, or 10 μL of insert, 1 μL of T4 DNA ligase (20 Units), 1.5 μL of 10X T4 DNA ligase buffer (500 mM Tris-HCl, 100 mM $MgCl_2$, 100 mM DTT, 1 mM ATP, 250 μg/mL BSA, pH 7.5), and ddH_20 to bring the total volume to 15 μL were incubated overnight at 16 °C. DH5αF' competent cells were transformed with 3-5 μL of ligation mixture.

(a)

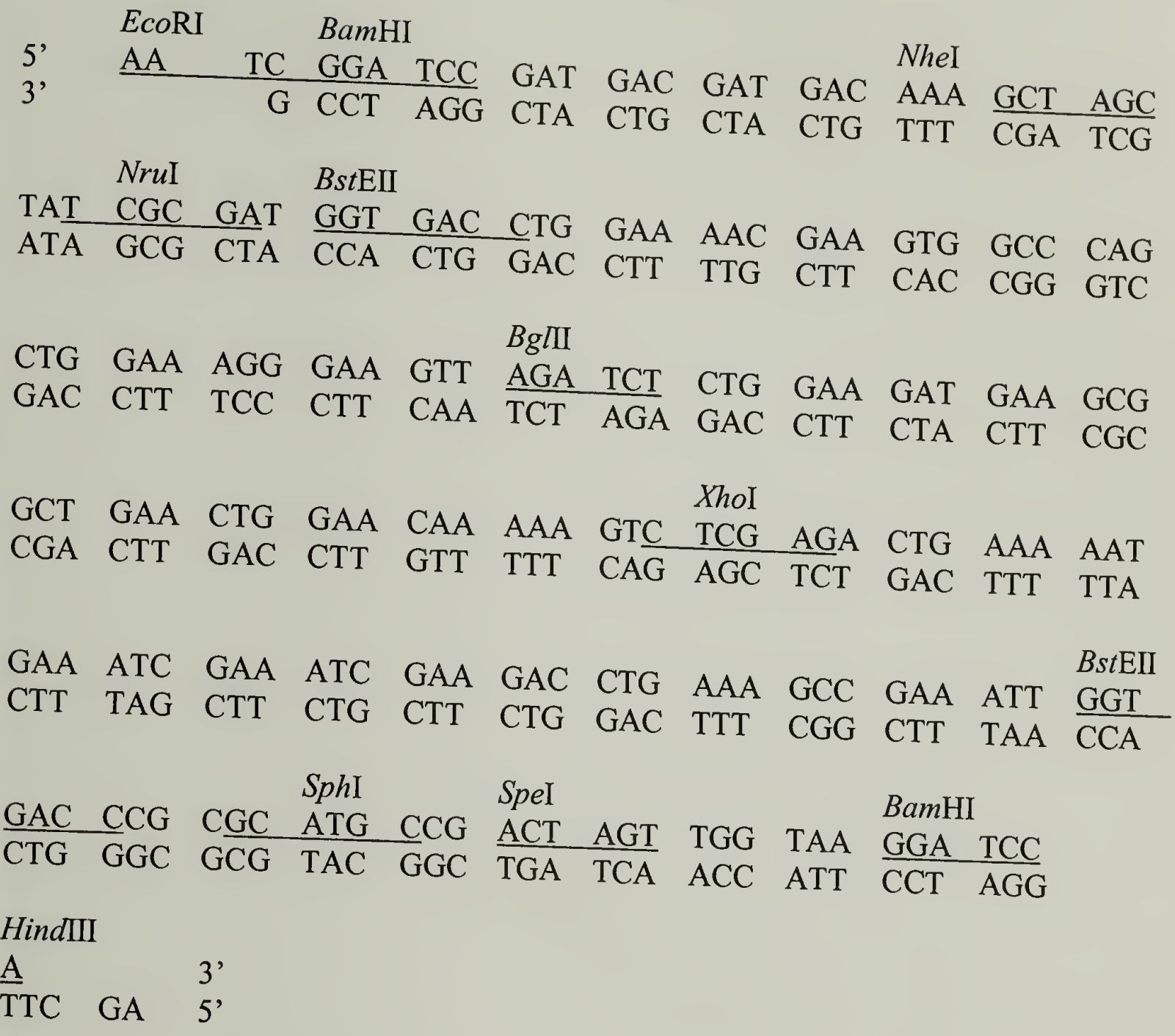

Figure 4.1 DNA sequences of coding (5'-3') and non-coding (3'-5') strands for Atrp incorporated into the pUC-18 cloning vector. Restriction sites used for cloning or screening are underlined and indicates a nucleotide deletion.

The mixtures were screened by spreading 150 μL of the mixture on a 2xYT agar plate containing 200 μg/mL AMP. Colonies were found on plates from ligation mixtures containing 2 μL, 5 μL, or 10 μL of A1. The ligation mixture containing only linear pWAP-L1 resulted in only three distinct colonies. Insertion of the DNA encoding the acid helix into linearized pWAP-L1 was indicated by the number of colonies which resulted from ligations with A1 and pWAP-L1. The absence of colonies from a self-

ligation of pWAP-L1 indicates that self-ligation did not occur at a high frequency as a result of a successful dephosphorylation reaction.

General mini-prep procedure for DNA isolation from a single colony

A sterile test tube containing 5 mL of 2xYT medium with appropriate antibiotics for selection of the desired vector (200 μg/mL AMP for pUC-18; 200 μg/mL AMP and 50 μg/mL KAN for pQE-9) was inoculated with a single colony. Cultures were grown on a rotating wheel overnight at 37 °C. Cells were harvested from 3 mL of culture by centrifugation at 13,000 rpm for 1 minute. The pellet was resuspended in 200 μL of sterile GTE buffer (50 mM glucose, 25 mM tris-HCl, pH 8.0, 1 mM EDTA) by repeated pipetting. Cell lysis was achieved by adding 200 μL of a solution containing 1% SDS/0.2 M NaOH and mixing by inversion of the microfuge tube 2-5 times. Chromosomal DNA was precipitated upon addition of 200 μL of neutralizing solution (3 M NaOAc, brought to pH 4.8 with glacial acetic acid) and incubation on ice for five minutes. Samples were centrifuged at 13,000 rpm for 10 minutes at 4 °C; the supernatant was transferred to a sterile microfuge tube containing 2 μL of RNase (10 mg/mL). After incubation at 37 °C for 30 minutes (or alternatively, at 50 °C for 10 minutes), 500 μL of phenol/chloroform (50:50 mixture of chloroform with phenol saturated with Tris HCl) was added and samples were vortexed. Following centrifugation at 13,000 rpm, the aqueous (upper) layer was transferred to a sterile microfuge tube containing 500 μL of isopropyl alcohol, used to precipitate DNA from solution. Samples were incubated on ice for 20 minutes before spinning at 13,000 rpm for 30 minutes to pellet the DNA. The supernatant was removed, and 50 μL of PEG8000 solution (25 % PEG8000, 2.5 M NaCl) and 100 μL of

sterile ddH_2O were added before vortexing and incubation at –20 °C for 30 minutes. Purified DNA was sedimented by centrifugation at 13,000 rpm at 4 °C. The pellet was resuspended in ddH_20 (for sequencing reactions) or 10 mM tris, pH 8.5 (for long term storage).

Screening of pUC-18L1A

DNA was purified according to the mini-prep procedure described earlier (*7*) from sixteen isolated colonies from the three plates containing pUC-18L1A. Insertion of A1 in the correct orientation was examined by digestion at the *Hind*III and *Bgl*II sites. The digestion mixture were prepared using 5 µL of purified DNA, 2 µL NEBuffer 2 (50 mM NaCl, 10 mM Tris-HCL, 10 mM $MgCl_2$, 1 mM dithiothreitol, pH 7.9), 1 µL *Hind*III enzyme, 1 µL *Bgl*II enzyme, and 11 µL of sterile ddH_2O. Digestion mixtures were incubated overnight at 37 °C, then 2 µL of 6x Running Buffer III (0.25 %(w/v) bromophenol blue, 0.25 %(w/v) xylene cyanol FF, 30 %(v/v) glycerol) was added before loading samples on a 2% Agarose gel containing 0.25 µg/mL ethidium bromide. DNA was resolved by electrophoresis in 0.5 TBE buffer (45 mM tris borate, 1 mM EDTA, pH 8.3) at 75 V and subsequently visualized under UV light.

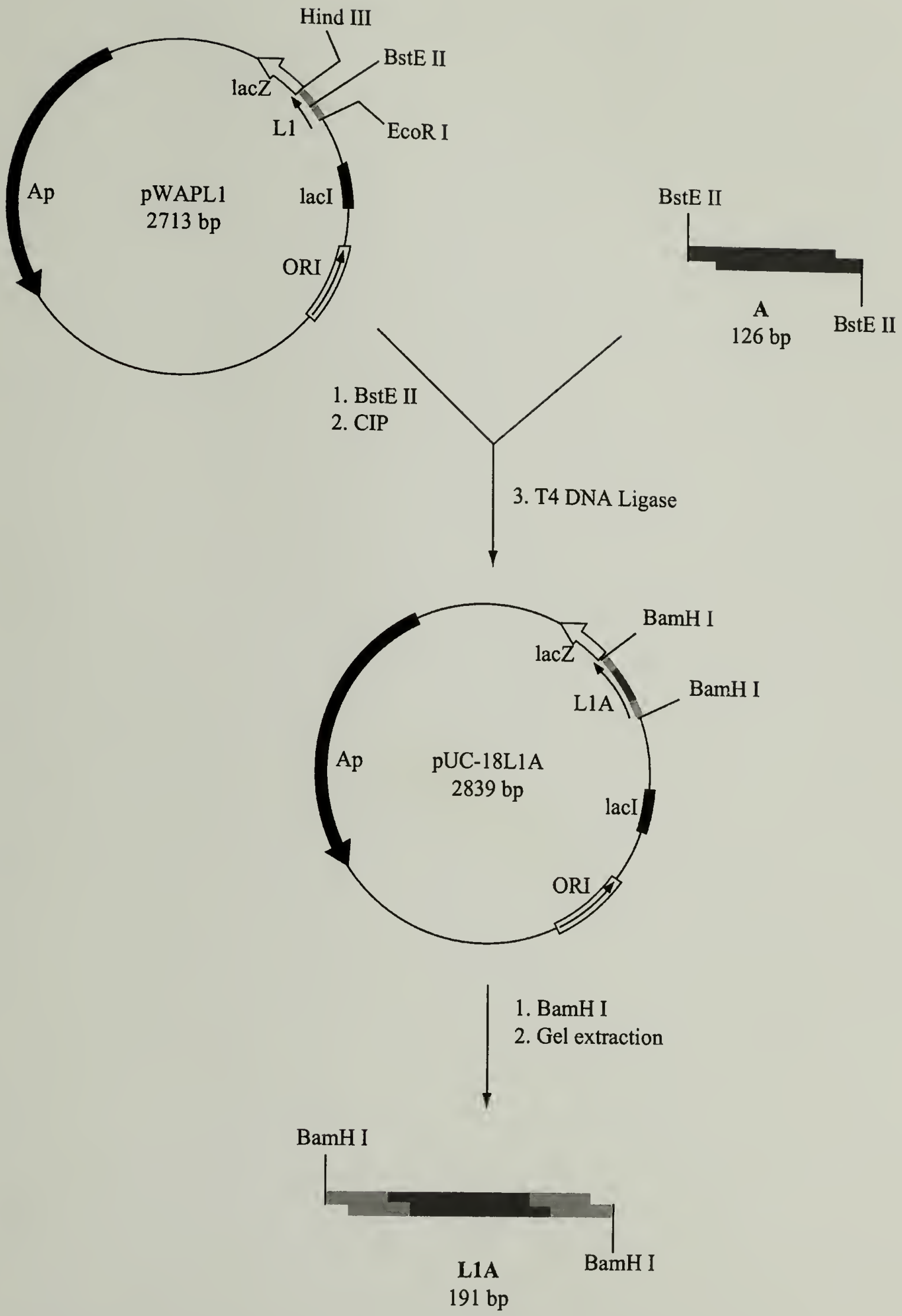

Figure 4.2 Genetic strategy to prepare L1A gene encoding Atrp protein.

The *Bgl*II site is absent in pUC-18 but present in A1; the *Hind*III site is retained if the linker was inserted in the correct orientation. Double digestion using these two enzymes results in two linear fragments, since each restriction site occurs only once in pWAP-L1. The correct orientation of the insert is indicated by the presence of a 114 base pair fragment which results from a digestion at the *Hind*III and *Bgl*II sites, while a 72 base pair fragment would be observed for insertion in the wrong orientation. Incidentally, *Bst*EII is a non-palandromic restriction site, meaning that the 5' and 3' overhangs are not identical. As a result, the insert can only ligate in one orientation.

Plasmids of pUC-18L1A were also screened to determine the size of the plasmid inserted. Through the process of cloning, no additional *Bam*HI sites are introduced, ensuring that only two sites are present in the vector that are located outside the site of ligation. By digesting the purified plasmid at *Bam*HI restriction sites, it was determined that insertion of only one repeat occurred in all of the screened colonies.

Ligation of L1A gene into pQE-9 expression vector

The expression vector, pQE-9 L1C, was digested with *Bam*HI overnight, and the ends were dephosphorylated with CIP as previously described. The linearized pQE-9 was purified from the L1C insert on a 1% agarose gel and extracted into ddH_2O using the QIAEX II gel extraction kit. Ligation mixtures were prepared using three different ratios of L1A insert to the linearized pQE-9, with a control mixture containing only the dephosphorylated pQE-9 in the ligation mixture. The samples were incubated at 16 °C overnight, then transformed into competent cells prepared from the SG13009 cells containing pREP-4 repressor plasmid. The pREP-4 plasmid imparts kanamycin

resistance, while the pQE-9 vector imparts ampicillin resistance. Agar plates containing both antibiotics were spread with 50μL of transformed cells prepared from each of the ligation mixtures. Colonies were isolated and screened for the monomer insertion in the correct orientation.

Eighteen colonies were grown overnight in 2xYT media containing AMP (200 μg/mL) and KAN (50 μg/mL). The DNA was isolated by the miniprep protocol described previously (*7*). Monomer insertion of L1A was determined by digestion at *EcoR*I and *Hind*III sites; both are unique to pQE-9 and are outside the site for insertion. Monomer insert was indicated by a 268 bp fragment resulting from digestion and resolved on a 2% agarose gel—observed in 13 of the 18 minipreps. To screen for correct orientation of the monomer insert, DNA from the 13 minipreps was digested with *Eco*RI and *Spe*I. Resolution of the resulting fragment on a 2% agarose gel indicated nine of the minipreps contained monomer insert in the correct orientation. Two of the colonies were used to prepare frozen stocks of the pQE-9 L1A cells.

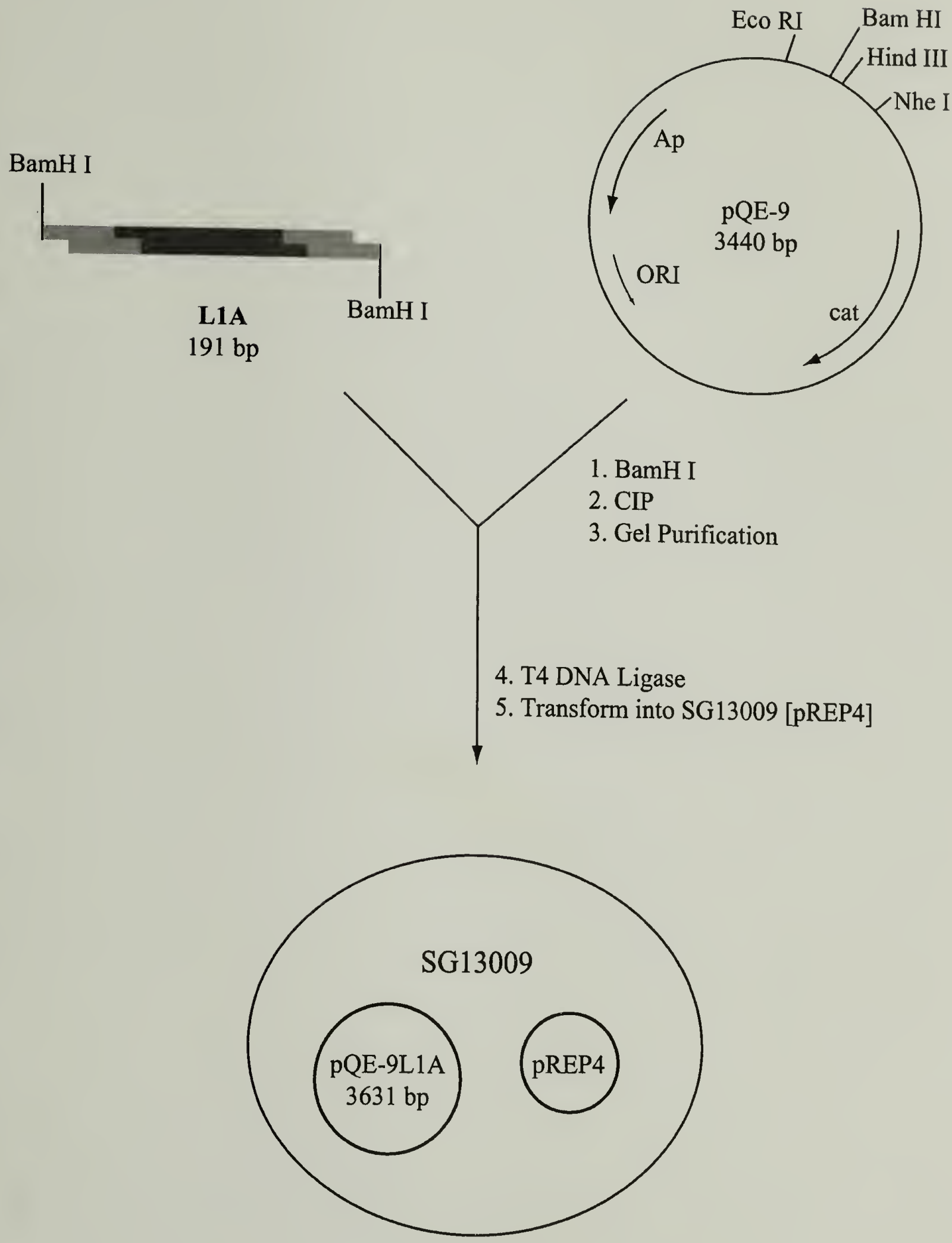

Figure 4.3 Strategy to prepare SG13009 [pREP4] cell for expression of Atrp.

4.2.1.2 Protein Synthesis and Characterization of Atrp

The expression protocol for Atrp generally follows that described by *Qiagen*™ under native conditions. Figure 4.4 illustrates (a) shake flask expression and (b) Ni-NTA^{2+} affinity chromatography purification under native conditions of Atrp.

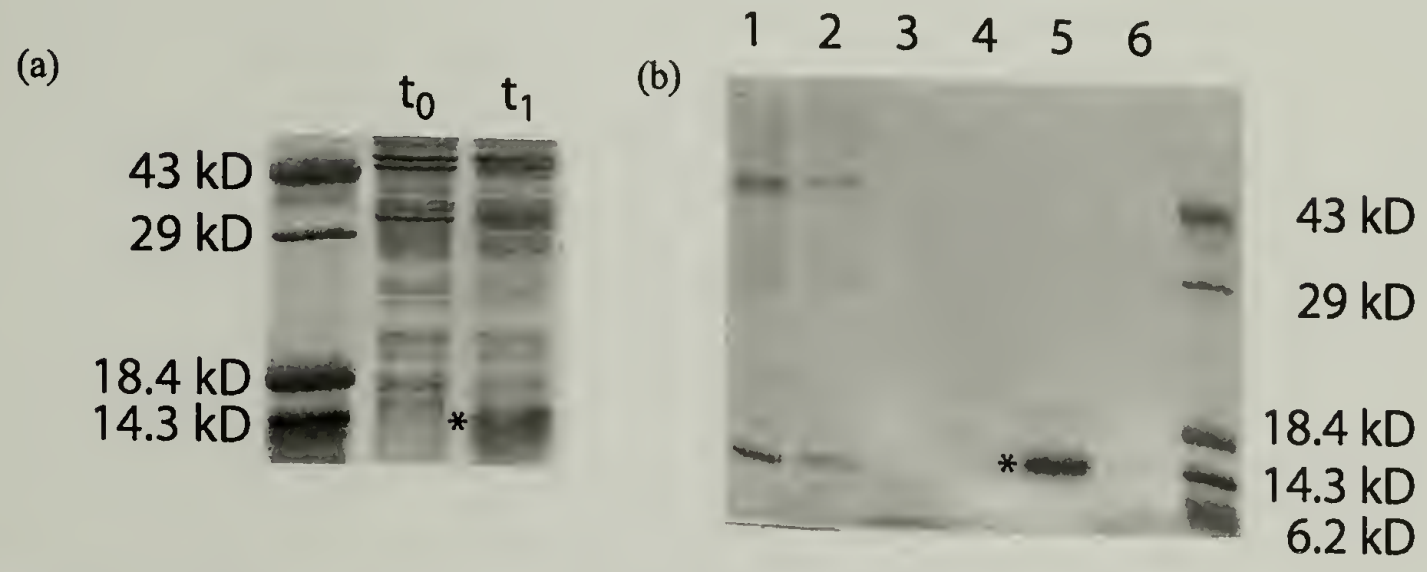

Figure 4.4 SDS-PAGE analysis for (a) protein expression and (b) purification of Atrp. Protein molecular weight standards are indicated. Uninduced cell lysate (t_0), cell lysate 4 hours after protein induction with 1 mM IPTG (t_1).

The expected amino acid sequence—73 amino acids—of Atrp is shown in Figure 4.5, with the heptad repeat grouped and the **a** and **d** positions shown in bold.

MRGSHHHHHHGSDDDDKASYR-Helix-IGDPRMPTSW

Helix: **D**GDLENE **V**AQLERE **V**RSLEDE **A**AELEQK **V**SRLKNE **I**EDLKAE

Figure 4.5 Amino acid sequence for Atrp. Amino acid abbreviations are: A, alanine; D, aspartic acid; E, glutamic acid; G, glycine; H, histadine; I, isoleucine; M, methionine; N, asparagine; P, proline; Q, glutamine; R, arginine; S, serine; T, threonine; V, valine; and W, tryptophan. Residues which occupy **a** and **d** positions are in bold.

Table 4.1 Amino acid analysis for Atrp

Amino Acid		mol %(theor)	mol %(obs)
D	aspartic acid + N asparagine	15.1	15.4
T	threonine	1.4	1.6
S	serine	8.2	7.0
E	glutamic acid + Q glutamine	17.8	17.2
P	proline	2.7	3.0
G	glycine	5.5	5.9
A	alanine	6.9	7.2
V	valine	4.1	4.4
M	methionine	2.7	2.3
I	isoleucine	2.7	2.5
L	leucine	8.2	9.1
Y	tyrosine	1.4	1.4
H	histadine	8.2	8.2
L	lysine	5.5	5.8
R	arginine	8.2	9.1

Amino acid analysis, shown in table 4.1, was performed by Cheryl Cote (University of Massachusetts, Amherst). Purified Atrp protein was hydrolyzed by treatment with 6N HCl, which does not allow for detection of tryptophan, due to its destruction under strong acidic conditions. Compositional analysis shows that the individual amino acids are observed at molar percentages that lie within 1.2% of the expected values.

4.2.2 CD Characterization of Atrp and $AC_{10}Acys$

Circular dichroism measurements were recorded using an AVIV 62DS spectropolarimeter (Lakewood, NJ), calibrated with an aqueous solution of (1S)-(+)-(10)-camphorsulfonic acid. Wavelength scans were taken at 25 °C from 250 to 195 nm, every 1 nm, averaged over 4 seconds, with 1nm bandwidth. Three repeats were averaged, and the final data are presented as the average for two samples.

Protein stock solutions were prepared by dissolving lyophilized protein into sterile ddH_20 at a concentration of 100 or 200 mM. NaOH (8N) was added in 1 μL increments to AC_{10}Acys, Atrp or Acys stock solutions until a clarified solution was observed, whereas 6N HCl was used to bring the BC_{10}Bcys protein into solution at 200 mM. Concentrations were determined by the method described in Chapter 3 (*8, 9*), where the extinction coefficients of Acys and Atrp are 5690 ($M^{-1}cm^{-1}$) and 6970 ($M^{-1}cm^{-1}$), respectively (*10*). Protein solutions were prepared by dilution of the stock solution to a final concentration of 5 μM, in phosphate buffered saline (PBS), adjusted to pH 7.4 with 1N HCl.

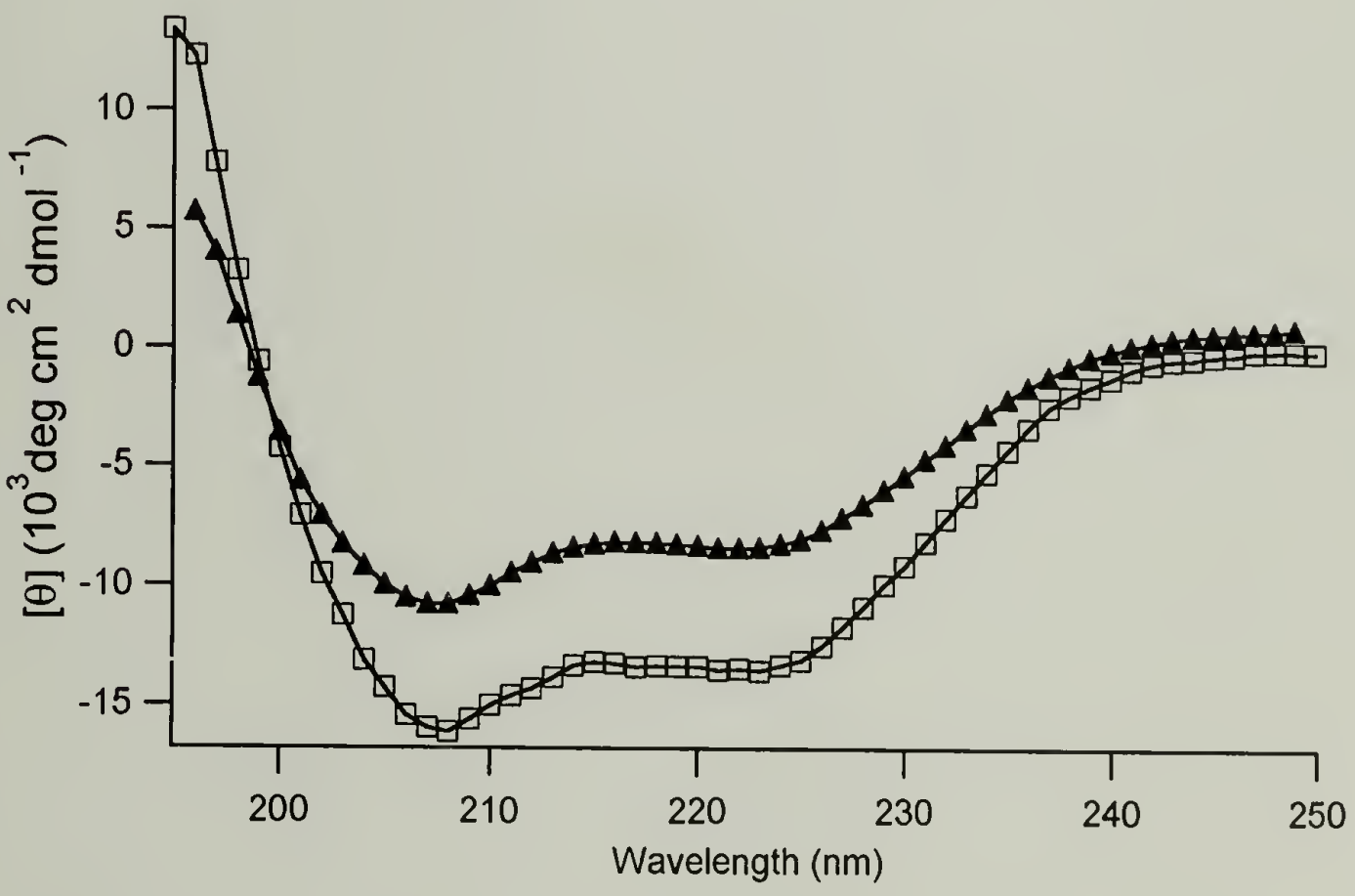

Figure 4.6 Circular dichroism for AC_{10}Acys (▲) and Atrp (□) at 5 μM in PBS (10 mM phosphate, 150 mM NaCl), pH 7.4.

4.2.3 $AC_{10}Acys$ Dissolution by Atrp

Sample preparation

A concentrated (4.46 mM, ~ pH 11) stock solution of $AC_{10}Acys$ was prepared and aliquoted (10 μL) into sterile microfuge tubes. To each sample, 5x tris (500 mM tris HCl, pH 8.5), 0.56 μm beads (2 %(w/v)), and concentrated Atrp were added before adding 2N NaOH to achieve pH 8.5. Before preparing all samples, one aliquot was used to determine the amount of 2N NaOH needed to bring the pH to 8.5. After each sample was brought to volume with ddH_2O (0.06 %(w/v) NaN_3 to prevent bacterial growth), the pH was checked using a pH meter (Isofet).

The Brownian motion of the fluorescent beads in each sample was recorded by video microscopy, following the techniques described in Chapter 2. Mean squared displacement as a function of time was determined after analysis in IDL following methods described by Crocker and Grier (*11*). Figures 4.7 and 4.8 illustrate the change in viscosity resulting from the addition of Atrp to $AC_{10}Acys$ at 2.23 mM or 1.78 mM.

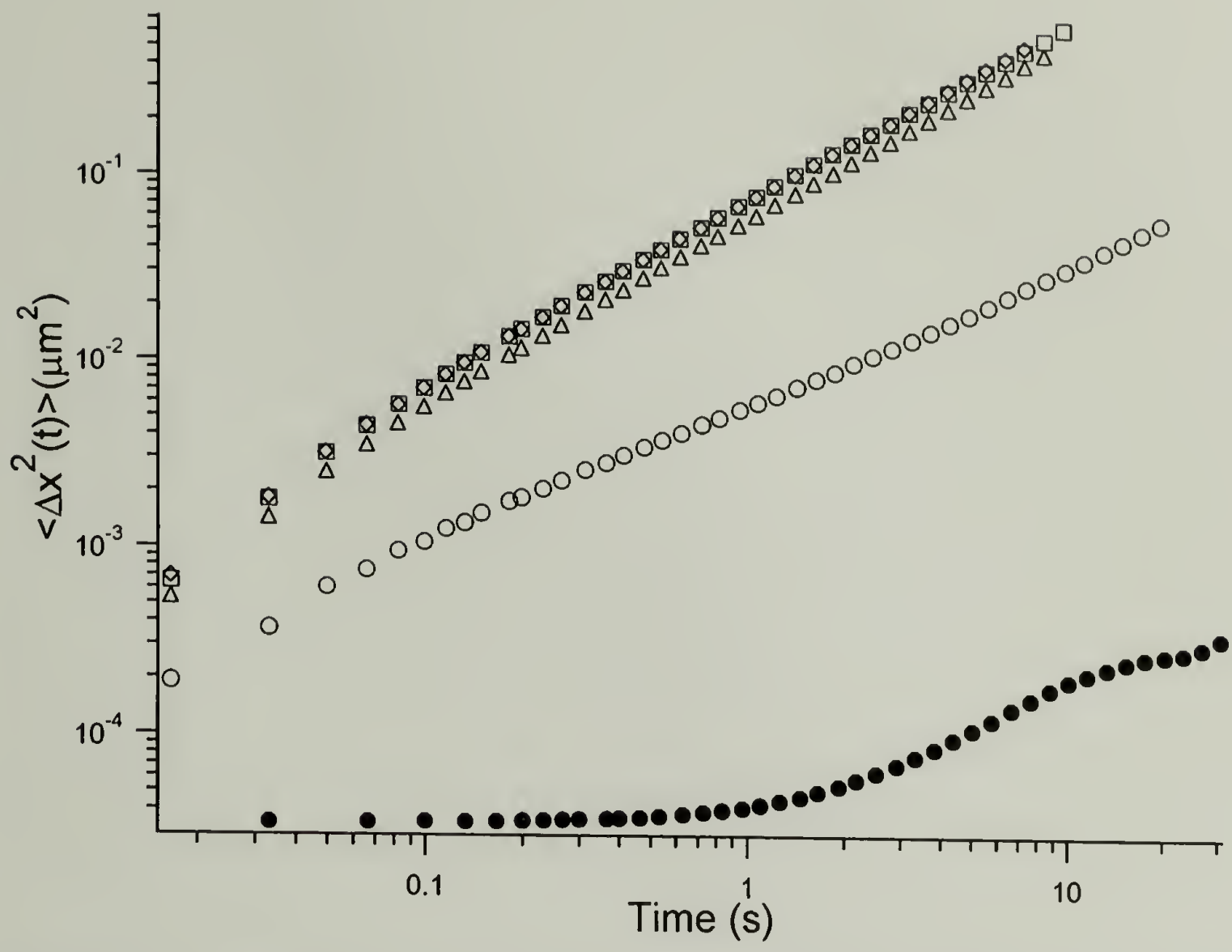

Figure 4.7 Dissolution of 2.23 mM AC_{10}Acys gel by Atrp addition. 0 mM Atrp(●), 1.11 mM Atrp (○), 2.23 mM Atrp (□), 3.34 mM Atrp(◇), 4.46 mM Atrp (△). Samples were buffered with 100 mM tris HCl, pH 8.5 and contain fluorescent beads 0.2 %(w/v).

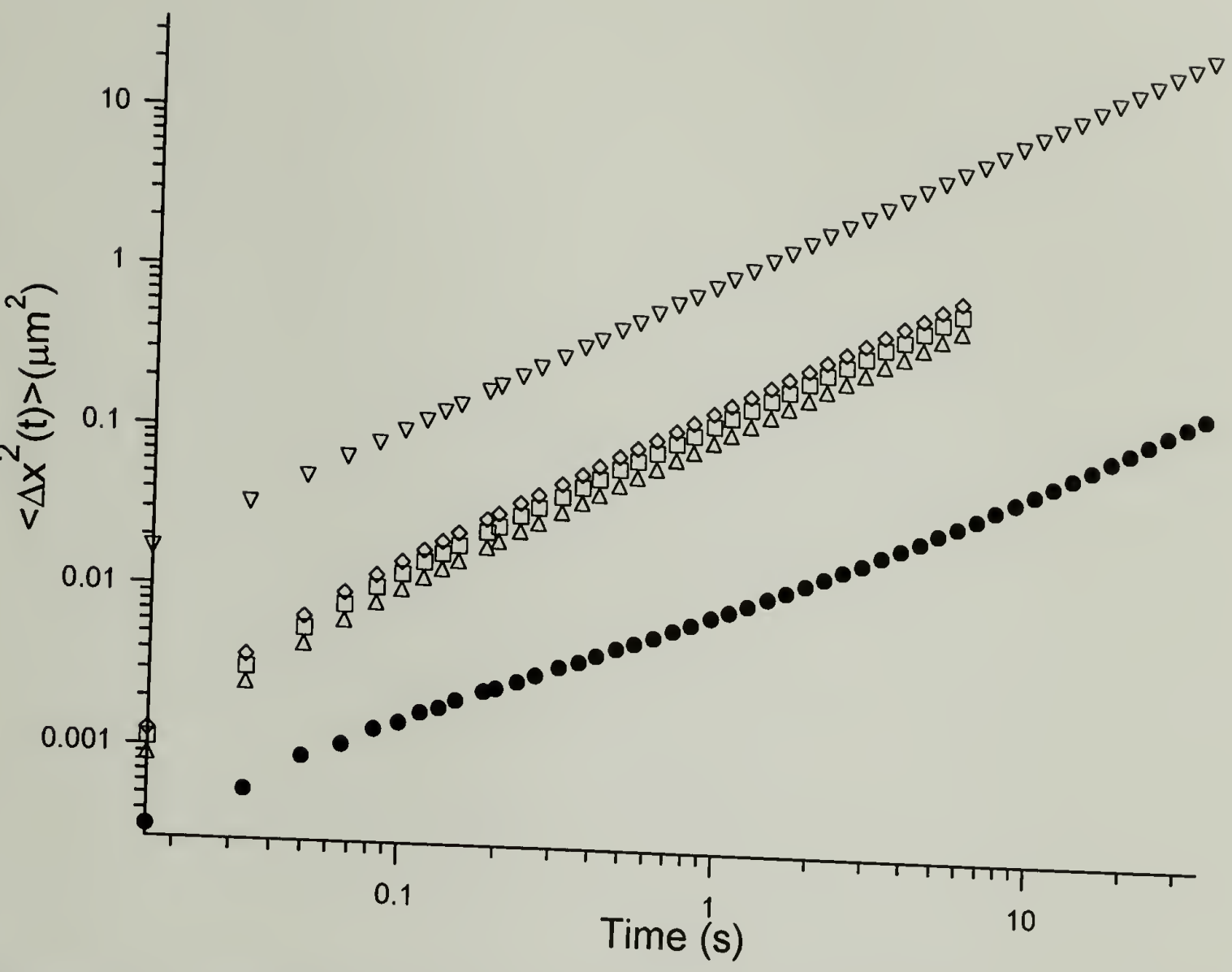

Figure 4.8 Mean square displacement vs. time for 1.78 mM AC_{10}Acys with 0 mM (●), 0.89 mM (□), 1.78 mM (△), 3.57 mM (◇), or 5.35 mM Atrp (▽). Samples were buffered with 100 mM tris HCl, and contain fluorescent beads 0.2 %(w/v).

4.3 Discussion

Circular dichroism spectra for AC_{10}Acys and Atrp display double minima at 222 and 208 nm, indicating helical secondary structure under the conditions probed by single particle tracking (Figure 4.6). The AC_{10}Acys protein has reduced minima at 222 and 208 nm compared to Atrp, due to the presence of the random coil domain, C_{10}, resulting in a decrease in the overall helicity of the protein.

The Atrp protein contains the same leucine zipper domain as the A block in AC_{10}Acys, so it is expected to aggregate into dimers or higher order aggregates under the

same conditions as those observed for $AC_{10}Acys$. Based on the similar behavior for the acidic leucine zipper, whether in the context of a triblock or alone, the isolated leucine zipper blocks can be used to exchange network junction points in a $AC_{10}Acys$ hydrogel.

Atrp represents a monofunctional end block, since it can only associate through the folding of the leucine zipper domain. In contrast, Acys can be considered a difunctional end block—physical crosslinking occurs through the coiled-coil motif, and chemical crosslinking occurs through disulfide bonds from the terminal cysteine residues. Addition of Acys to $AC_{10}Acys$ gels could change the mechanical properties if disulfide bonding is present. Essentially, the molecular weight between crosslinks would be decreased, and the strength of the gel would increase.

A 2.23mM $AC_{10}Acys$ sample shows a plateau in the mean squared displacement (MSD) vs time, indicating that the bead motion is restricted for times less than a few seconds (Figure 4.7). The increase in MSD at longer times indicate that the junction points can associate and dissociate on the time scale of the experiment. Figure 4.8 shows a sample of $AC_{10}Acys$, which was a viscoelastic fluid before the addition of Atrp. There is little difference among samples containing 0.89 mM, 1.78 mM, or 3.57 mM Atrp. The addition of Atrp, however, results in a decrease in the viscosity, as indicated by the increase in the intercept value. On a log-log plot, a slope of unity indicates that the MSD increases linearly with time and the medium is purely viscous. All samples shown in figure 4.8 appear to have more viscous than elastic character.

Atrp addition to $AC_{10}Acys$ hydrogels resulted in dissolution of the elastic network observed for 2.23 mM $AC_{10}Acys$ samples. Atrp and the acidic leucine zipper endblocks on $AC_{10}Acys$ are expected to fold under the same conditions. Junction points, made up

of folded acidic leucine zippers, are displaced by Atrp. The addition of Atrp at a concentration of 1.11 mM, or a 1:4 molar ratio of Atrp to A in $AC_{10}Acys$ (there are two moles of A in the triblock), causes the bead motion to be unrestricted over the time examined during the experiment. Viscous solutions are characterized by increasing MSD over time, as illustrated with the addition of Atrp. As the ratio of Atrp to $AC_{10}Acys$ increases, the viscosity decreases. This experiment demonstrates the role of the leucine zipper domain in network formation.

4.4 References

1. T. Annable, R. Buscall, R. Ettelaie, D. Whittlestone, *J. Rheol.* **37**, 695-726 (1993).

2. T. Annable, R. Buscall, R. Ettelaie, *Colloid Surface A* **112**, 97-116 (1996).

3. F. Tanaka, *Prog. Theor. Phys. Supp.* **126**, 257-260 (1997).

4. K. Thuresson *et al.*, *J. Phys. Chem. B* **103**, 1425-1436 (1999).

5. J. M. Yu, R. Jerome, P. Teyssie, *Polymer* **38**, 347-354 (1997).

6. W. A. Petka, Ph.D. dissertation, University of Massachusetts, Amherst (1997).

7. T. Maniatis, E. F. Fritsch, J. Sambrook, *Molecular cloning: A laboratory manual* (Cold Spring Harbor Laboratory Press, New York, 1989).

8. S. C. Gill, P. H. Vonhippel, *Anal. Biochem.* **182**, 319-326 (1989).

9. S. C. Gill, *Anal. Biochem.* **189**, 283-283 (1990).

10. R. D. Appel, A. Bairoch, D. F. Hochstrasser, *Trends Biochem. Sci.* **19**, 258-260 (1994).

11. J. C. Crocker, D. G. Grier, *J. Colloid Interf. Sci.* **179**, 298-310 (1996).

CHAPTER 5

ELECTROSTATIC EFFECTS IN TRIBLOCK HYDROGELS

5.1 Introduction

Polymeric materials have traditionally been used for biomedical applications because of their desirable mechanical properties. Dacron or Teflon can be sewn into a new blood vessel, poly(methyl methacrylate) can be shaped to fit around the eye as contact lenses, and polyurethane can provide both elasticity and strength for an artificial heart (*1-3*). Although these materials have served their purpose as adequate mechanical replacements, their eventual failure is often a result of adverse cellular interactions and immune rejection. For this reason, polymers are modified to include desirable chemical and biological components that more closely mimic the natural material the artificial one is designed to replace. This may include decorating a synthetic polymer with cell-adhesion sites (*4, 5*), synthesizing biodegradable implants (*6, 7*), or designing new materials from natural protein sequences to recreate physiologically relevant mechanical and cellular behavior (*8, 9*).

Synthetic hydrogels are often found as scaffolds for tissue replacement due to their ability to maintain hydration similar to natural tissues, while affording control over chemical structure to modify mechanical properties. In addition, chemical modification allows one to incorporate biologically active species into the matrix, further mimicking physiological conditions (*2, 3, 10*). These chemical modifications have led to the creation of stimuli-responsive hydrogels. Some examples of "intelligent" materials

include those that change shape in a magnetic field (*11*), or change volume in response to a specific protein (*12, 13*).

Petka et al. designed protein gels that transition between a gel and solution based on the pH or temperature. Protein-based hydrogels (*14, 15*) and synthetic-protein hybrid materials (*16, 17*) rely on protein folding to produce physical crosslinks to hold the hydrogel together. Under physiological conditions, the leucine zipper end groups, designated **A** in the protein $AC_{10}Acys$, form oligomeric bundles that cross-link the network of molecules. The midblock, **C**, does not have regular secondary structure, but serves to hydrate the helical bundles to form the hydrogel. At high pH, the leucine zipper domains dissociate and the gel dissolves. Here we examine the influence of protein electrostatics on the bulk mechanical properties of the hydrogel by varying the protein charge with genetic engineering.

Materials such as those described here could serve as a transitional matrix that could immobilize live cells for the treatment of auto immune diseases such as type I diabetes. Hydrogels have been used to create an artificial pancreas, with limited success (*18, 19 and references therein*). Type I diabetes occurs when the body's own immune system destroys the functioning islet of Langerhans cells within the pancreas. These cells control the body's metabolism by producing insulin in response to increases in blood glucose levels. Patients with type I diabetes must administer insulin after meals, when glucose levels rise—to substitute the body's natural response by a controlled one. If one could replace unhealthy cells with functioning islets, however, insulin could be delivered at the appropriate time, in the appropriate amount. Encapsulated islets that are implanted into the body can serve as a self regulating insulin pump—an artificial pancreas. By

implanting islet cells, a self-regulating insulin replacement can be achieved. Implantation, however, requires that the cells are protected from the immune system in order to survive. Such an encapsulating material requires permeability to small molecules like glucose, but not to larger cellular species or immune cells that would attack the islets. In order to conform to the shape of the implanted region and promote the cell viability, it is desirable to form this protective barrier in-situ.

The thermal and pH reversibility of $AC_{10}Acys$ hydrogels, demonstrated by Petka (*15*) illustrates the possibility to fulfill these objectives. Gelation in these protein solutions occurs due to association of the 'A' leucine zipper domains between protein molecules, occurring spontaneously at physiological conditions. The high pH or high temperature required to overcome the 'A' block interactions to maintain $AC_{10}Acys$ as a solution, however, may result in denaturation of therapeutic proteins, decreased activity of enzymes or decreased viability of cells incorporated into $AC_{10}Acys$. An alternative method to trigger gelation is to alter the electrostatic interactions that lead to gelation, by adopting a combination of two oppositely charged protein solutions which alone are unable to form an elastic network, but combined will comprise a hydrogel.

To examine this concept, two triblock proteins with oppositely charged leucine zipper domains were prepared according to the techniques outlined in Chapter 3. In these proteins, the majority (9 of 12) of the residues in the positions flanking the hydrophobic face of the coiled coil, the **e** and **g** positions, are occupied by glutamic acid or lysine. The domain rich in glutamic acid, 'A', may be thought of as an acidic block, whereas the domain containing lysine, 'B', is a basic block. Heterodimeric leucine zipper peptides have been previously examined and shown to associate preferentially in comparison to

their homodimeric alternative (*20-22*). The concentration of acidic or basic amino acids in the **e** and **g** positions defined the propensity to form a heterodimer rather than a homodimer. The interaction of oppositely charged residues across the hydrophobic interface is thought to stabilize the heterodimer by charge neutralization or by formation of salt-bridges (*23, 24*).

Triblock proteins $AC_{10}Acys$ and $BC_{10}Bcys$, where cys indicates a cysteine at the C-terminus, were synthesized from *E. coli* and purified by Ni-NTA^{2+} chromatography (described generally in Chapter 3). In the artificial protein, 'A' and 'B' represent the acidic and basic leucine zipper domains, and 'C' is the polyelectrolyte spacer [$(AG)_3PEG$]. Diffusing wave spectroscopy was used to characterize $AC_{10}Acys$ as a hydrogel under physiological pH and temperature (*15*); the rheological properties of $BC_{10}Bcys$, however, have not been reported (*25*). The difference in charge between the 'A' and 'B' end blocks is illustrated in the helical wheel representation (Figure 5.1).

(a)

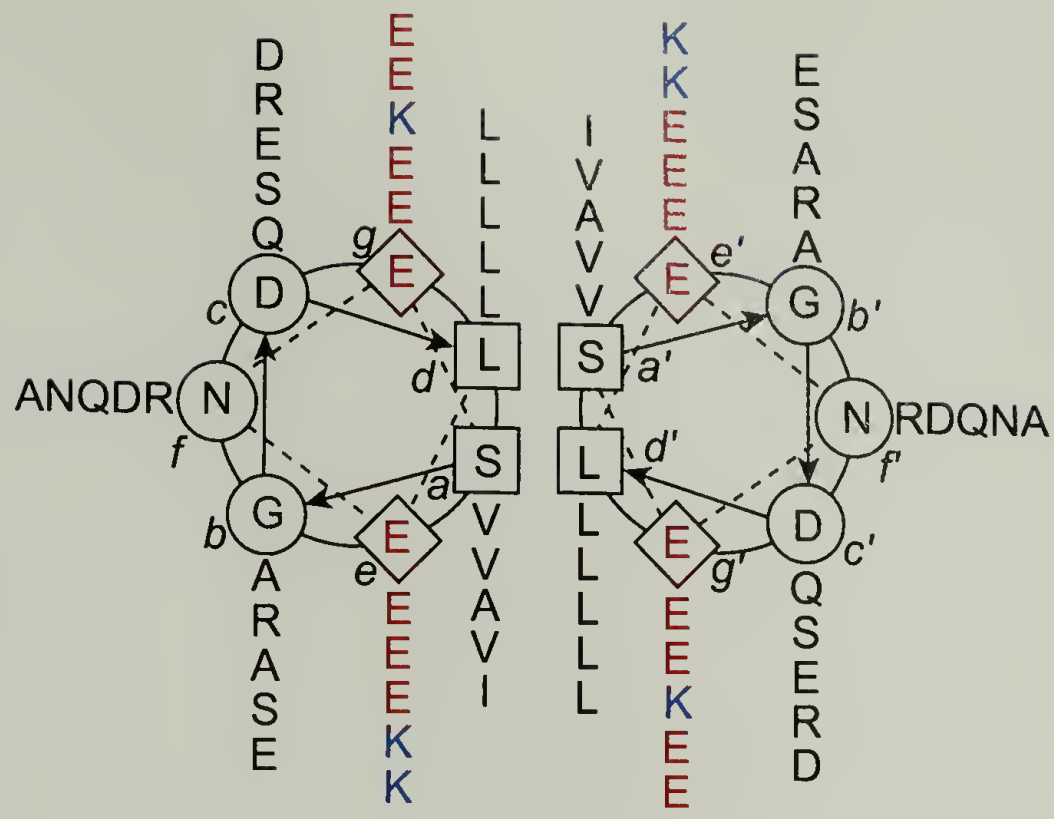

(b)

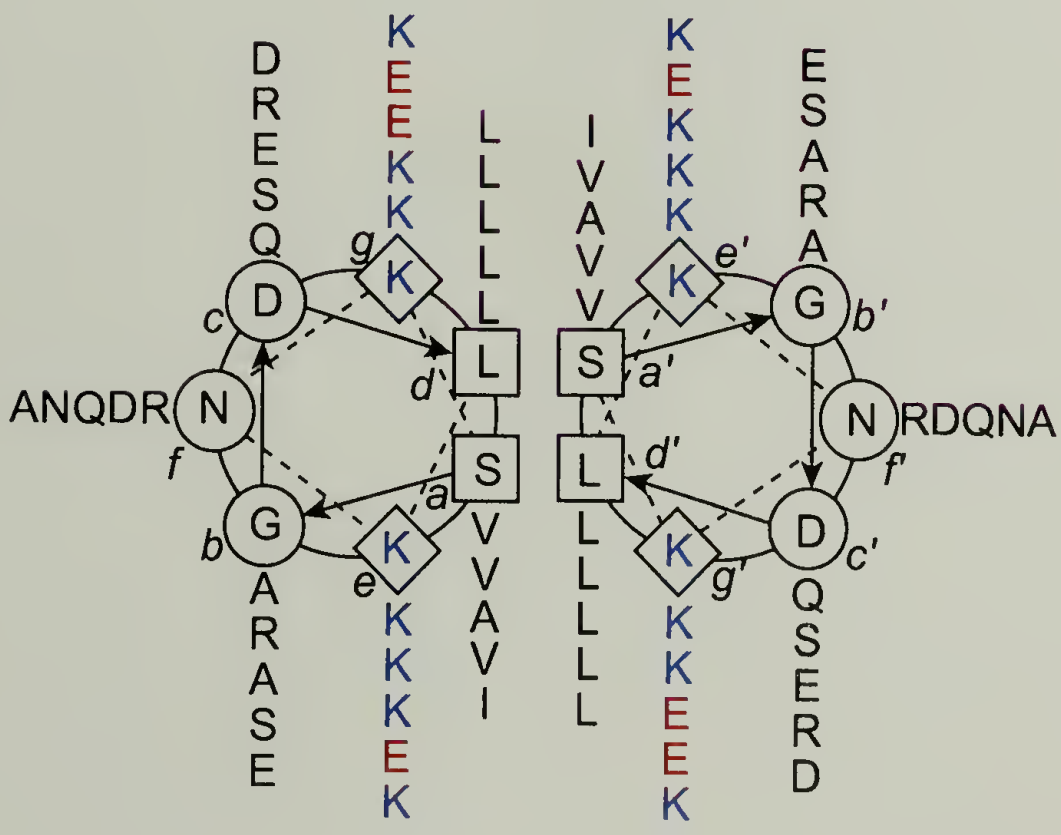

Figure 5.1 Helical wheel representation for (a) parallel A-A coiled coil and (b) parallel B-B coiled coil, where the charged flanking residues are shown in color.

The concept of combining two oppositely charged leucine zipper domains was previously demonstrated with a chimeric protein, $AC_{10}Bcys$ (*26*). Under conditions where $AC_{10}Acys$ formed a viscous solution (high pH), the alternative protein, $AC_{10}Bcys$, (containing one acidic and one basic leucine zipper domain) was a stiff gel. The sequence of $AC_{10}Acys$ and $AC_{10}Bcys$ differs by fewer than 15 residues among the 232 amino acids that define the entire protein. Although the compositional difference between the two proteins is small, the bulk behavior shows marked changes. The position of the glutamic acid or lysine along the hydrophobic interface has a large influence on the folding of the leucine zipper. This demonstrates the advantage afforded by the using the leucine zipper motif—secondary structure is predetermined by the primary sequence, allowing the precise placement of amino acids to induce molecular interactions.

The secondary structure of the 'A' and 'B' blocks as a function of pH was determined by circular dichroism. The helicity, which indicates whether the leucine zipper is folded, may be estimated by the molar ellipticity measured at 222 nm. When a leucine zipper is folded, the molar ellipticity is a minimum. As the protein unfolds this minimum diminishes. From the difference between $[\theta]_{222}$ when the protein is folded or unfolded, the relative fraction of folded molecules can be estimated. The melting temperature, Tm, is defined as the temperature at which half of the molecules are unfolded.

Previous studies (*27*) of acidic and basic leucine zipper domains alone, denoted A1 and B1, respectively were shown to have increased stability when mixed, as compared to that observed for the individual homodimers. When A1 and B1 were combined at equal

concentrations, the molar ellipticity $[\theta]_{222}$ indicated that the proteins remained largely helical even up to 95 °C between pH 8.1 – 10.1. Additionally, A1-B1 solutions required larger amounts of urea to denature the coiled coil formation compared to the homodimer counterparts (A1-A1 and B1-B1). The melting temperature of A1 increased with decreasing pH, while the analogous basic protein, B1, showed the opposite dependence of melting temperature on pH—T_m increased with increasing pH.

Since mixtures of A1 and B1 leucine zippers were shown to have increased Tm, as compared to that observed for the individual homodimers, it is hypothesized that the same behavior may be observed for triblocks containing the same leucine zipper domains. If the heterodimer, A-B, is favored over the formation of either homodimer, A-A or B-B, then the one would expect aggregates of A with B would also form in a solution containing $AC_{10}Acys$ and $BC_{10}Bcys$. This chapter describes the preparation of hydrogels by the combination of two triblock proteins, $AC_{10}Acys$ and $BC_{10}Bcys$, with opposite charges.

5.2 Experimental Work

5.2.1 $AC_{10}Acys$ vs. $BC_{10}Bcys$

Proteins $AC_{10}Acys$ and $BC_{10}Bcys$ were combined in an equimolar concentration over a range of pH and overall protein concentrations to examine the effect of heterodimer formation on the bulk viscoelastic behavior. The sequences of $AC_{10}Acys$ and $BC_{10}Bcys$ vary only in the **e** and **g** positions of the leucine zipper end blocks.

Initially, Atrp or Acys was added to a BC_{10}Bcys solution to determine if the addition of acidic end blocks to a basic triblock solution would induce gelation.

(a) **A:** SGDL**E**N**E** VAQL**E**R**E** VRSL**E**D**E** AAEL**E**Q**K** VSRL**K**N**E** IEDL**K**A**E**

(b) **B:** DGDL**K**N**K** VAQL**K**R**K** VRSL**K**D**K** AAEL**K**Q**E** VSRL**E**N**E** IEDL**K**A**K**

(c) AC_{10}Acys:

MRGSHHHHHHGSDDDDKWASGDLENEVAQLEREVRSLEDEAAELEQKVSRLK
NEIEDLKAEIGDHVAPRDTSYRDPMGAGAGAGPEGAGAGAGPEGAGAGAGPEG
AGAGAGPEGAGAGAGPEGAGAGAGPEGAGAGAGPEGAGAGAGPEGAGAGAGP
EGAGAGAGPEGARMPTSGDLENEVAQLEREVRSLEDEAAELEQKVSRLKNEIED
LKAEIGDHVAPRDTSMGGC

(d) BC_{10}Bcys

MRGSHHHHHHGSDDDDKWASGDLKNKVAQLKRKVRSLKDKAAELKQEVSRLE
NEIEDLKAKIGDHVAPRDTSYRDPMGAGAGAGPEGAGAGAGPEGAGAGAGPEG
AGAGAGPEGAGAGAGPEGAGAGAGPEGAGAGAGPEGAGAGAGPEGAGAGAGP
EGAGAGAGPEGARMPTSGDLKNKVAQLKRKVRSLKDKAAELKQEVSRLENEIE
DLKAKIGDHVAPRDTSMGGC

Figure 5.2 Sequences of (a) A, acidic, and (b) B, basic leucine zipper domain, and (c) AC_{10}Acys and (b) BC_{10}Bcys proteins. The residues occupying the **e** and **g** positions as shown in (a) and (b) are bolded and underlined. The entire sequence of the triblock proteins (c) and (d) illustrate the context of the two different leucine zipper domains.

5.2.1.1 CD Characterization

BC_{10}Bcys, Atrp, and Acys preparation:

Protein stock solutions were prepared by dissolving lyophilized protein into sterile ddH_20 at a concentration of 100 or 200 mM. NaOH (8N) was added in 1 μL increments to AC_{10}Acys, Atrp or Acys stock solutions until a clarified solution was observed, whereas 6N HCl was used to bring the BC_{10}Bcys protein into solution at 200 mM.

Concentrations were determined by the method described in chapter 3 (*28, 29*), where the extinction coefficients (*30*) of Acys and Atrp are 5690 ($M^{-1}cm^{-1}$) and 6970 ($M^{-1}cm^{-1}$), respectively. Protein solutions were prepared by dilution of the stock solution to a final concentration of 5 μM, in phosphate buffered saline (PBS), adjusted to pH 7.4 with 1N HCl.

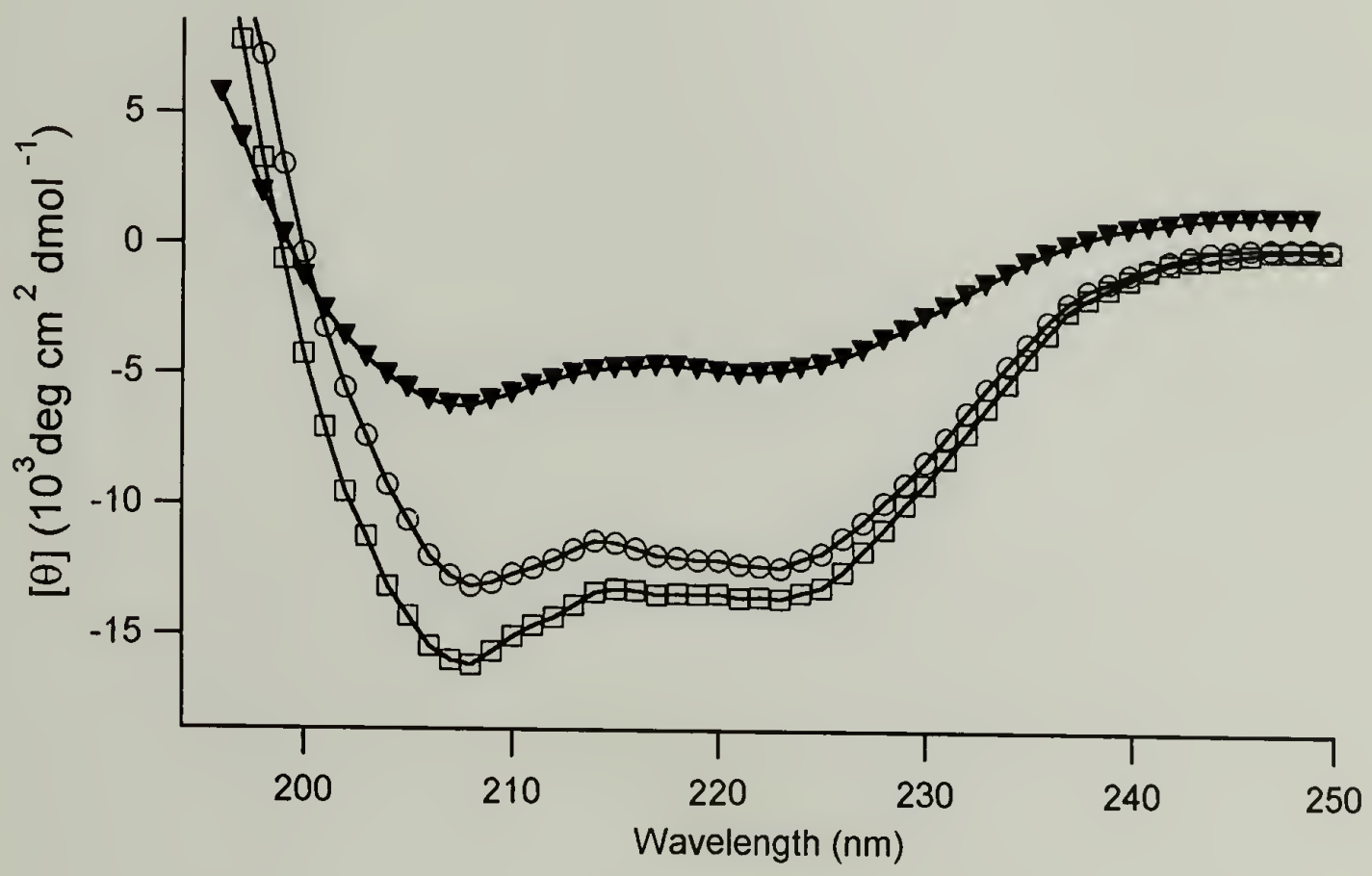

Figure 5.3 Circular dichroism for $BC_{10}Bcys$ (▼), Acys (○) and Atrp (□) at 5 μM in PBS (10 mM phosphate, 150 mM NaCl), pH 7.4.

$AC_{10}Acys$, $BC_{10}Bcys$, $AC_{10}Bcys$ and $AC_{10}Acys/BC_{10}Bcys$ equimolar mixture preparation

The secondary structure of the triblock proteins was characterized using circular dichroism. Protein stock solutions were prepared by dissolving lyophilized protein into sterile ddH_20 at a concentration of 100 or 200 mM. The exact concentration was determined by UV analysis and the estimation of the extinction coefficient based on the number of tryptophan and tyrosine residues in each protein sequence (*28, 29*). The stock solution was diluted to 20-40 μM in 8M guanidine hydrochloride (HCl), buffered with

0.2 mM potassium phosphate, pH 8.0 (8M guanidine HCl was used to ensure the protein was completely denatured). Protein solutions were prepared for CD analysis by diluting stock solutions to a final concentration of 5 μM, in PBS (10mM sodium phosphate, 150 mM NaCl, pH 7.4). The equimolar mixture was prepared by mixing the $AC_{10}Acys$ and $BC_{10}Bcys$ stock solutions to achieve individual concentrations of 2.5 μM for each protein, in PBS.

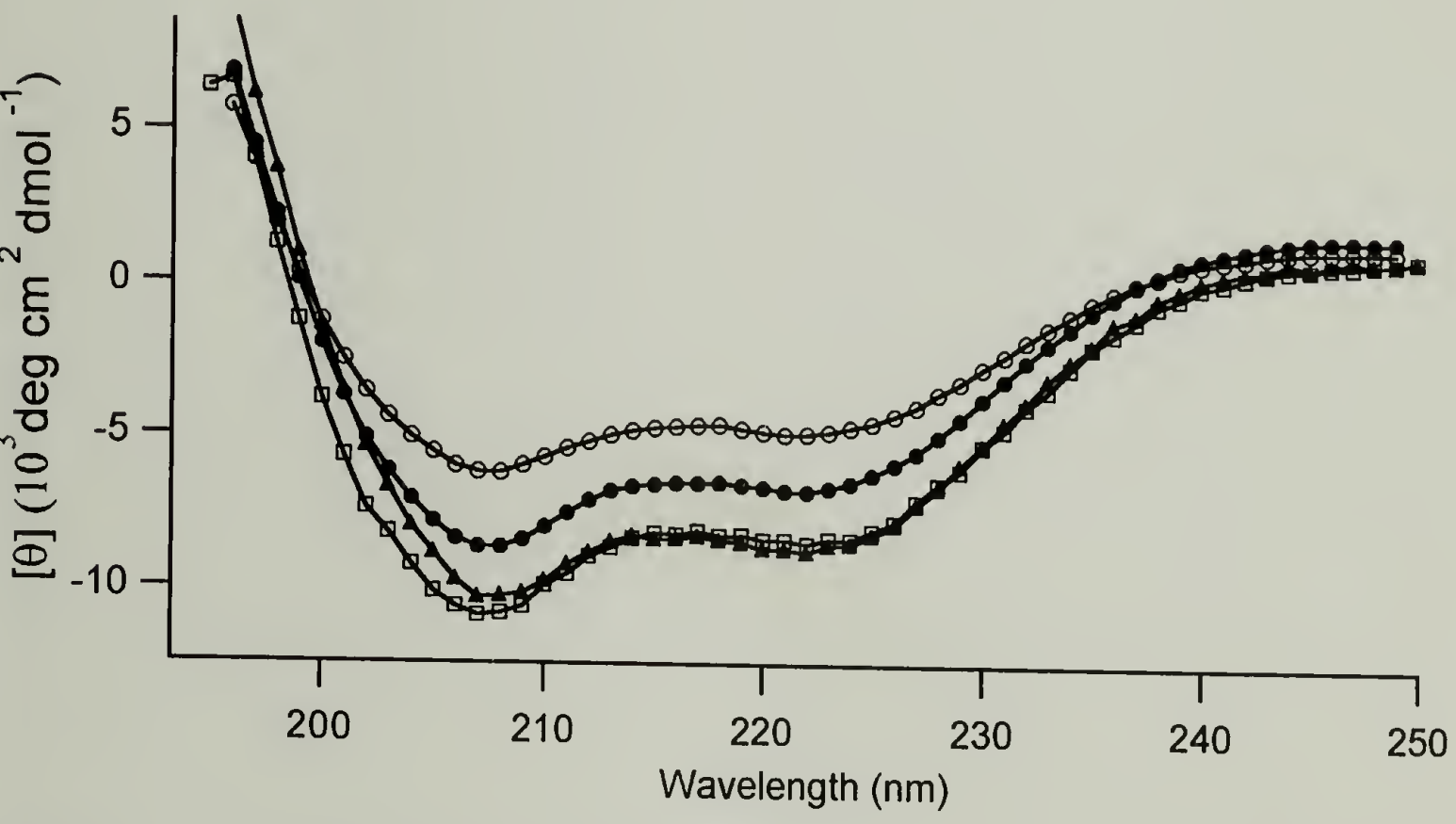

Figure 5.4 Circular dichroism for 5 μM $AC_{10}Bcys$(▲), $AC_{10}Acys$(□), $BC_{10}Bcys$(○), and 2.5 μM $AC_{10}Acys$ with 2.5 μM $BC_{10}Bcys$ (●) in PBS (10 mM phosphate, 150 mM NaCl), pH 7.4.

5.2.1.2 Atrp Addition to $BC_{10}Bcys$

In contrast to the dissolution of an elastic gel, as described for Atrp addtion to $AC_{10}Acys$ (Chapter 5), it is also desirable to induce gelation by the addition of a second component. Based on the idea that leucine zipper domains control the network formation

by the aggregation of end blocks from different chains, it was theorized that the addition of Atrp or Acys would increase the likelihood of $BC_{10}Bcys$ forming a hydrogel network. Attempts to form a hydrogel from $BC_{10}Bcys$ alone proved unsuccessful, even at concentrations double that required to form an elastic gel using $AC_{10}Acys$.

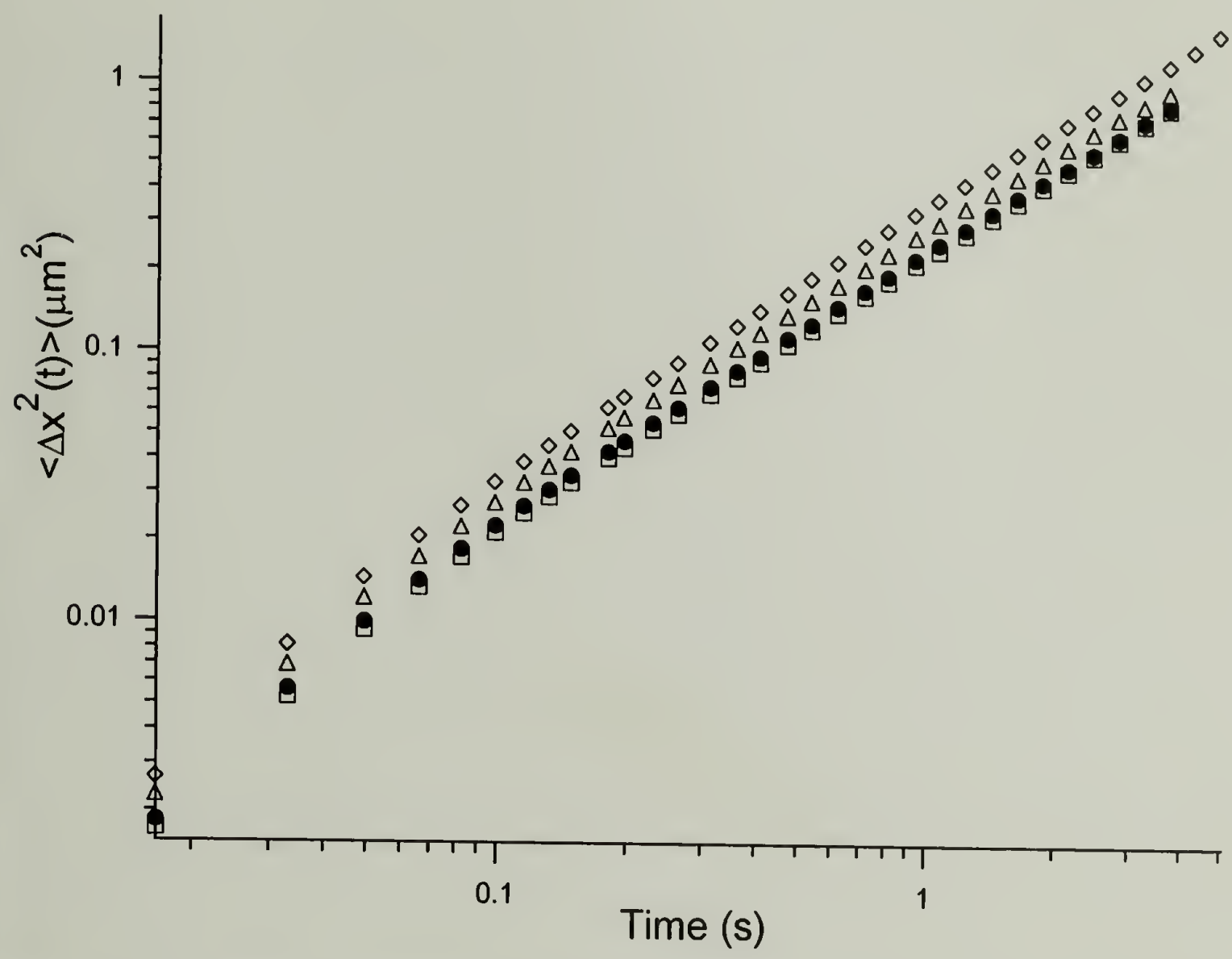

Figure 5.5 Mean square displacement vs. time for 1.78 mM $BC_{10}Bcys$ with 0 mM (●), 1.11 mM (○), 2.23 mM (□), 3.34 mM (◇), or 4.46 mM Atrp (△). Samples were buffered with 100 mM tris HCl, and contain 0.2 %(w/v) fluorescent beads.

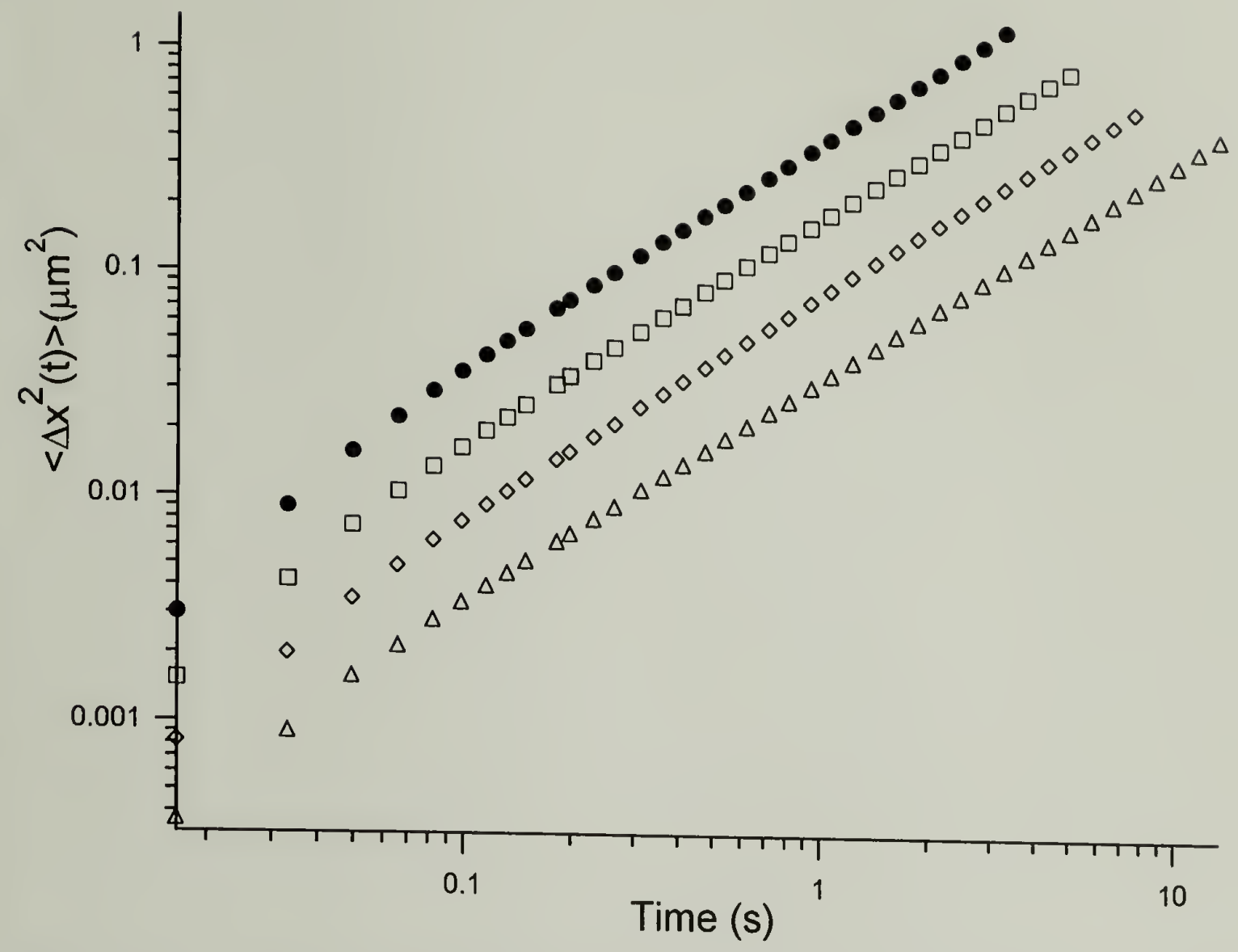

Figure 5.6 Mean square displacement vs. time for 1.34 mM $BC_{10}Bcys$ with 0 mM (●), 0.67 mM (□), 1.34 mM (◇), or 2.67 mM Acys(△). Samples were buffered with 100 mM tris HCl, and contain 0.2 %(w/v) fluorescent beads.

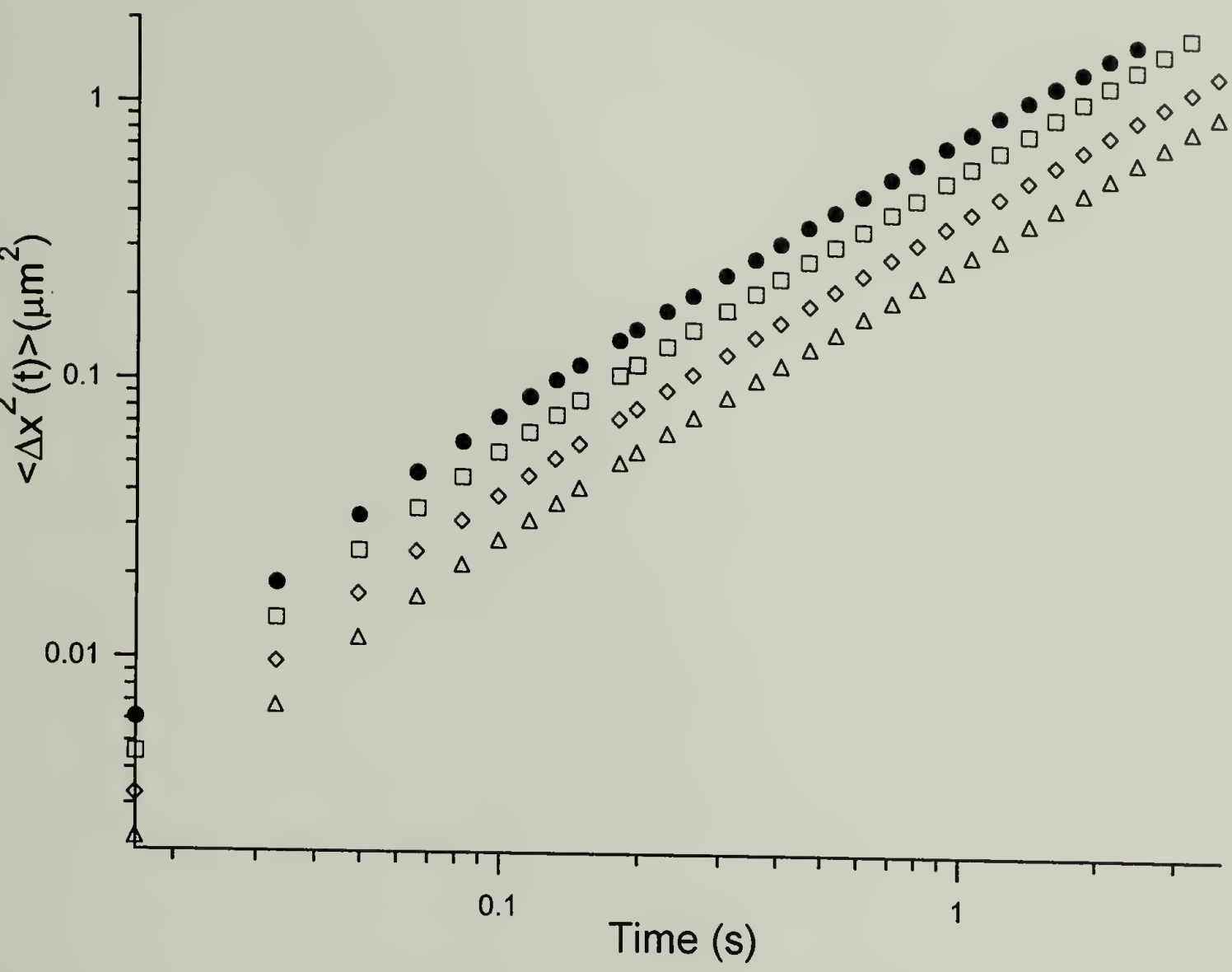

Figure 5.7 Mean square displacement vs. time for 2.23 mM $BC_{10}Bcys$ with 0 mM (●), 1.11 mM (□), 1.67 mM (◇), or 2.23 mM Acys(△). Samples were buffered with 100 mM tris HCl, and contain 0.2 %(w/v) fluorescent beads.

5.2.1.3 Combined Gelation Behavior

Sample preparation

A concentrated solution of $BC_{10}Bcys$ was prepared by dissolving 13.8 mg of lyophilized protein in 23 μL of 500 mM tris, 92 μL of ddH_2O containing 0.06%(w/v) NaN_3; 3 μL of 2N HCl was added to help solubilize the protein. This stock solution was used to prepare samples containing a final concentration of $BC_{10}Bcys$ at 1.78 mM, buffered with 100 mM trisHCl, and 0.2%(w/v) 0.56 μm fluorescent beads.

An $AC_{10}Acys$ stock solution was prepared by addition of 47 μL of 500 mM tris and 153 μL of ddH_2O containing 0.06%(w/v) NaN_3 to 23.5 mg of lyophilized protein. Base (8 μL of 8N NaOH) was added to solubilize the protein and lower the viscosity of the solution before bringing the solution to 4.46 μM $AC_{10}Acys$ by adding 20 μL of ddH_2O containing 0.06%(w/v) NaN_3.

The stock solutions were brought to 1.78 mM protein by diluting either $AC_{10}Acys$ or $BC_{10}Bcys$ stock solutions to a final volume of 25 μL containing 100 mM tris HCl, and 0.14% (w/v) 0.56 μm fluorescent beads (Molecular Probes). An equimolar (1.78 mM) solution of the two proteins was prepared by adding fluorescent beads and 500 mM tris HCl to an aliquot of $BC_{10}Bcys$. After mixing, $AC_{10}Acys$ was added before bringing the pH to 8.5 or 7.4. The appropriate amount of HCl or NaOH needed to bring the protein solutions to the correct pH was determined by preparing a sample with the equivalent amounts of protein, fluorescent beads and 100 mM tris HCl and adding acid or base until the desired pH was achieved. Based on these amounts, HCl or NaOH was added to each aliquot before bringing the sample to volume with ddH_2O.

The Brownian motion of the fluorescent beads in each sample was recorded by video microscopy, following the techniques described in Chapter 2. Mean square displacement as a function of time was determined after analysis in IDL following methods described by Crocker and Grier (*31*). Figures 5.4 and 5.5 illustrate the difference between solutions containing $AC_{10}Acys$ or $BC_{10}Bcys$ at 1.78 mM, pH 8.5 or 7.4 compared to the preparation of an equimolar mixture at the same concentration.

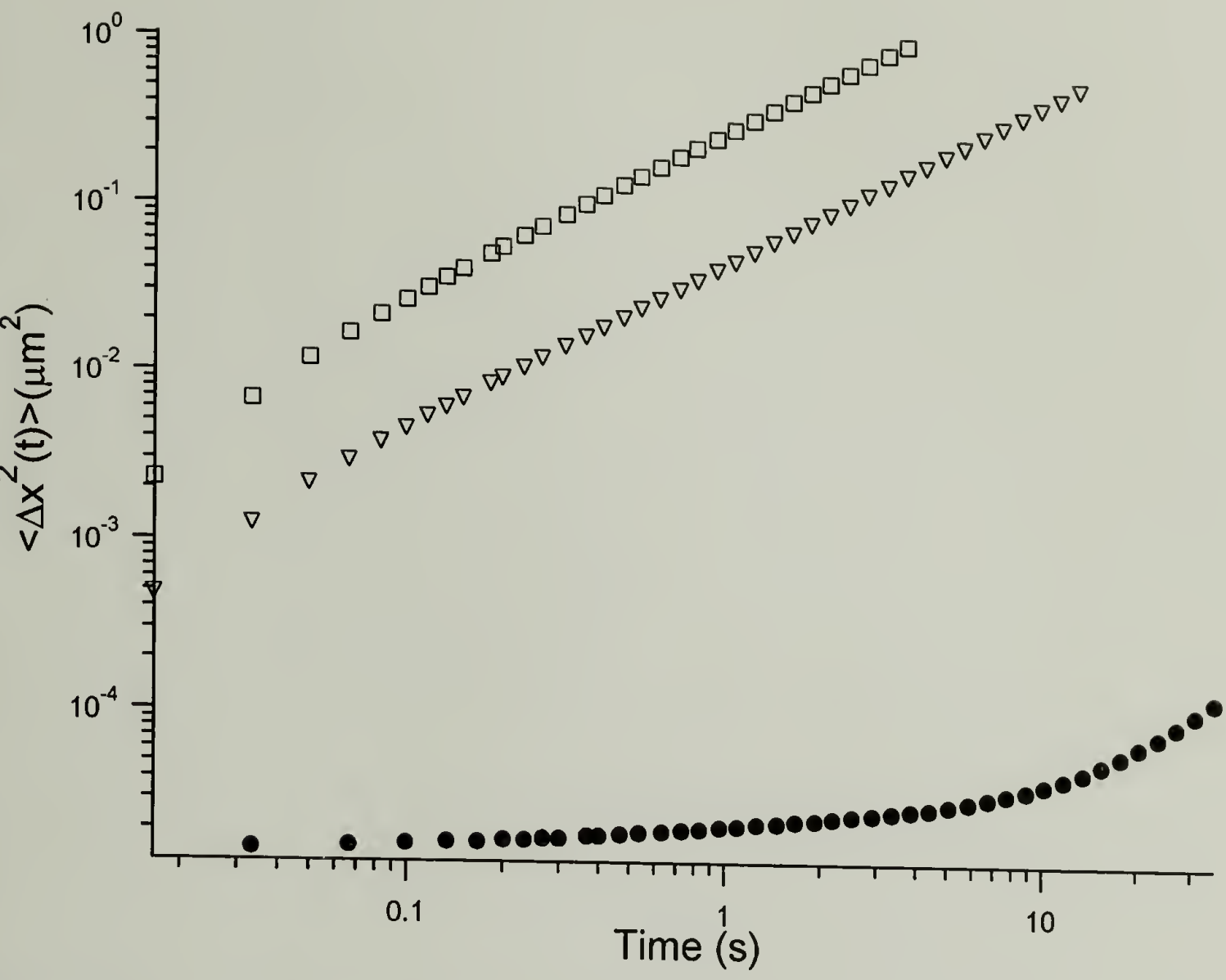

Figure 5.8 Mean square displacement vs. time for $AC_{10}Acys$ (▽), $BC_{10}Bcys$ (□), or $AC_{10}Acys$ with $BC_{10}Bcys$ (●), at pH 7.4, 1.78 mM total protein concentration. Samples were buffered with 100 mM tris HCl and contain 0.2 %(w/v) fluorescent beads.

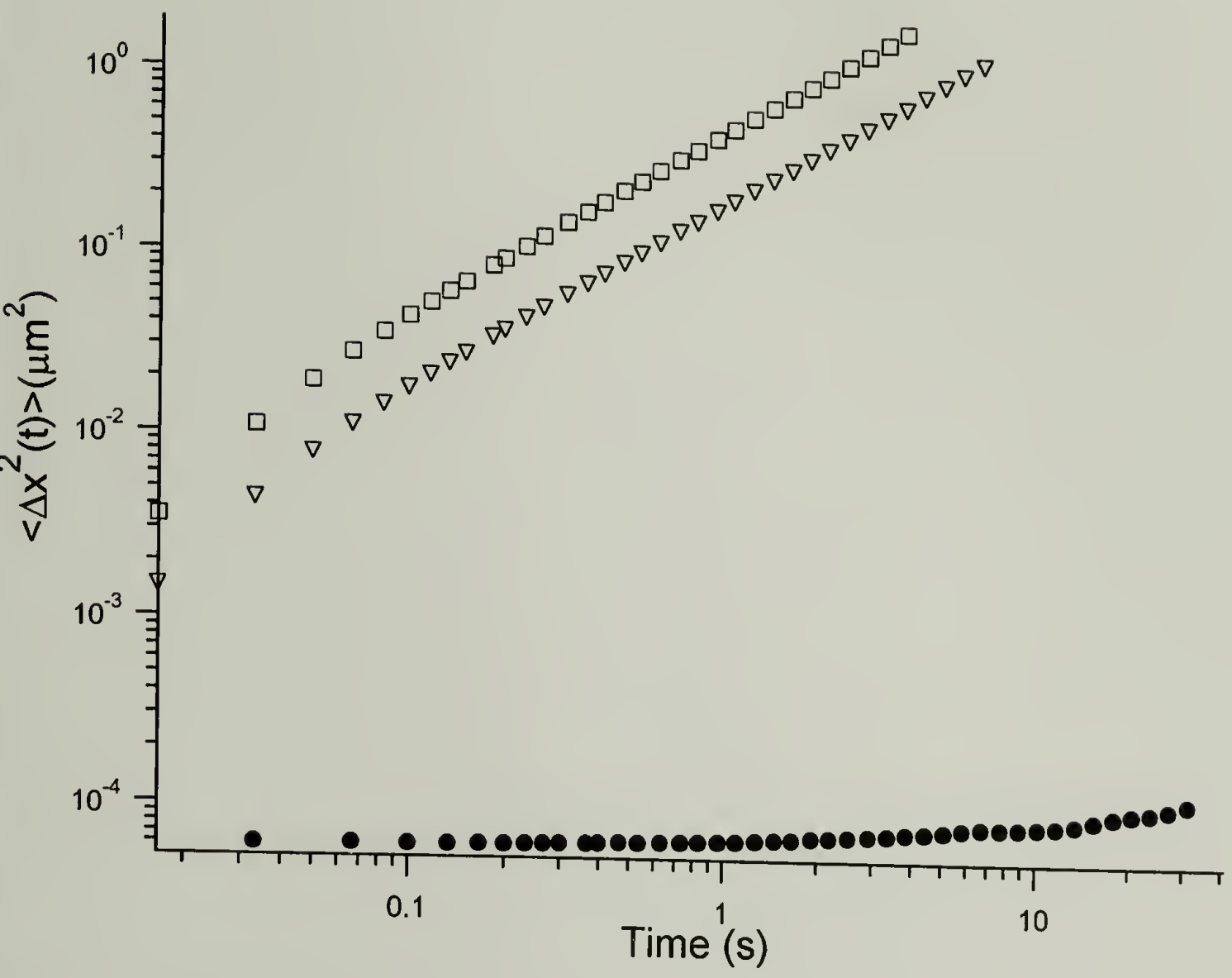

Figure 5.9 Mean square displacement vs. time for $AC_{10}Acys$ (▽), $BC_{10}Bcys$ (□), or $AC_{10}Acys$ with $BC_{10}Bcys$ (●), at pH 8.5, 1.78 mM total protein concentration. Samples were buffered with 100 mM tris HCl and contain 0.2 %(w/v) fluorescent beads.

5.2.1.4 Concentration Dependence of Gelation Behavior

Sample Preparation

Concentrated solutions of $AC_{10}Acys$ and $BC_{10}Bcys$ were prepared at 4.23 mM and 2.38 mM, respectively. To keep the $AC_{10}Acys$ stock solution from gelling, the pH was increased above pH 11. The stock solutions were aliquoted (2.9 μL of $AC_{10}Acys$ and 5 μL of $BC_{10}Bcys$) into sterile microfuge tubes. To each sample, 5x tris HCl (500 mM tris HCl, pH 8.5) and 0.56 μm beads (2.0 %(w/v)) were added before adding 0.5N

HCl or 1N NaOH to bring the pH to the appropriate value shown in Figure 5.6. After each sample was brought to volume with ddH_2O (0.06 %(w/v) NaN_3 to prevent bacterial growth), the pH was checked using a ISFET pH meter (Shindengen Electric Manufacturing Co, LTD, Tokyo, Japan).

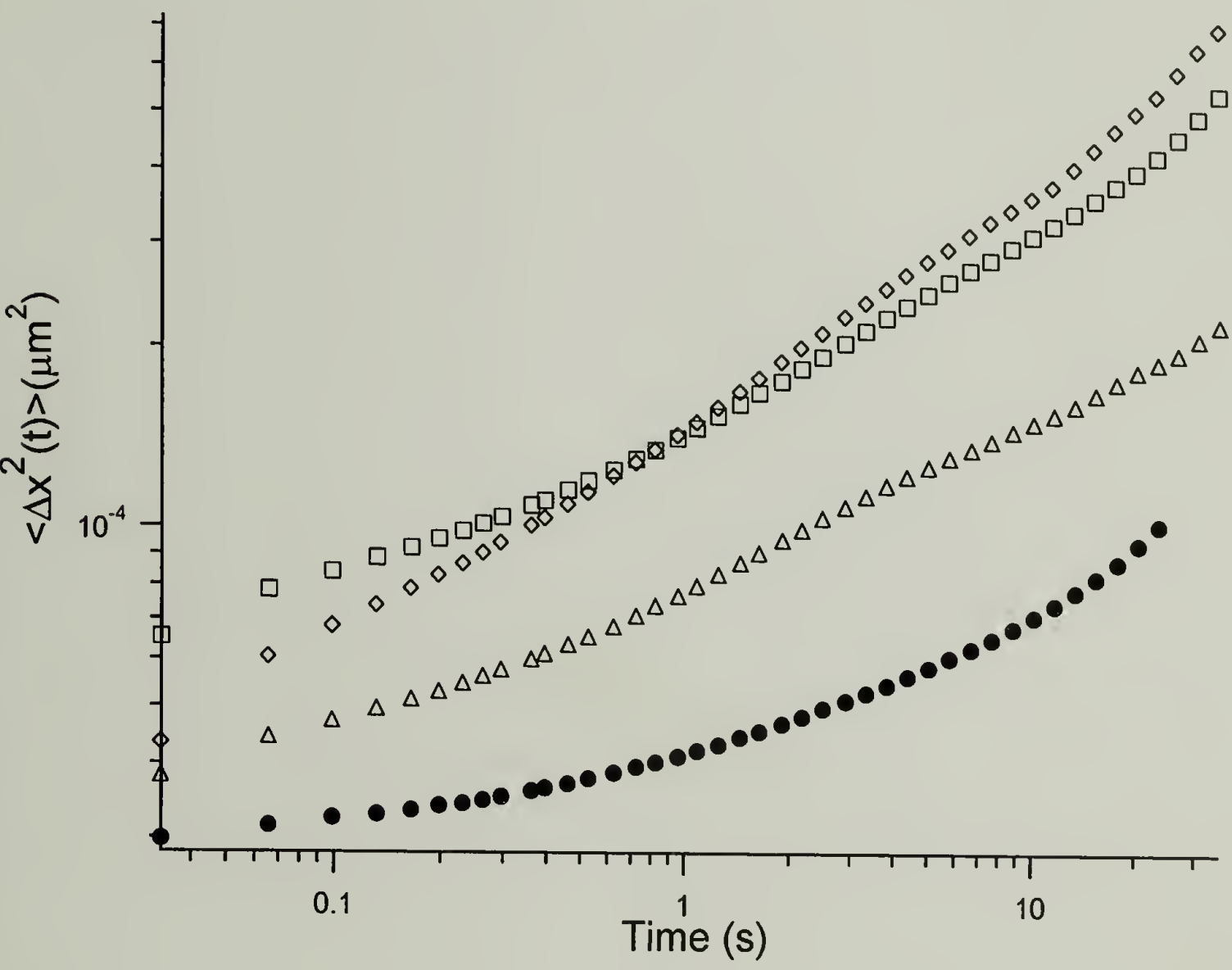

Figure 5.10 Mean square displacement vs. time for equimolar mixture of $AC_{10}Acys$ with $BC_{10}Bcys$, 1.34 mM total protein concentration. pH 8.6 (●), pH 8.8 (□), pH 9.0 (◇), pH 9.1 (△). Samples were buffered with 100 mM tris HCl, and contain 0.13 %(w/v) fluorescent beads.

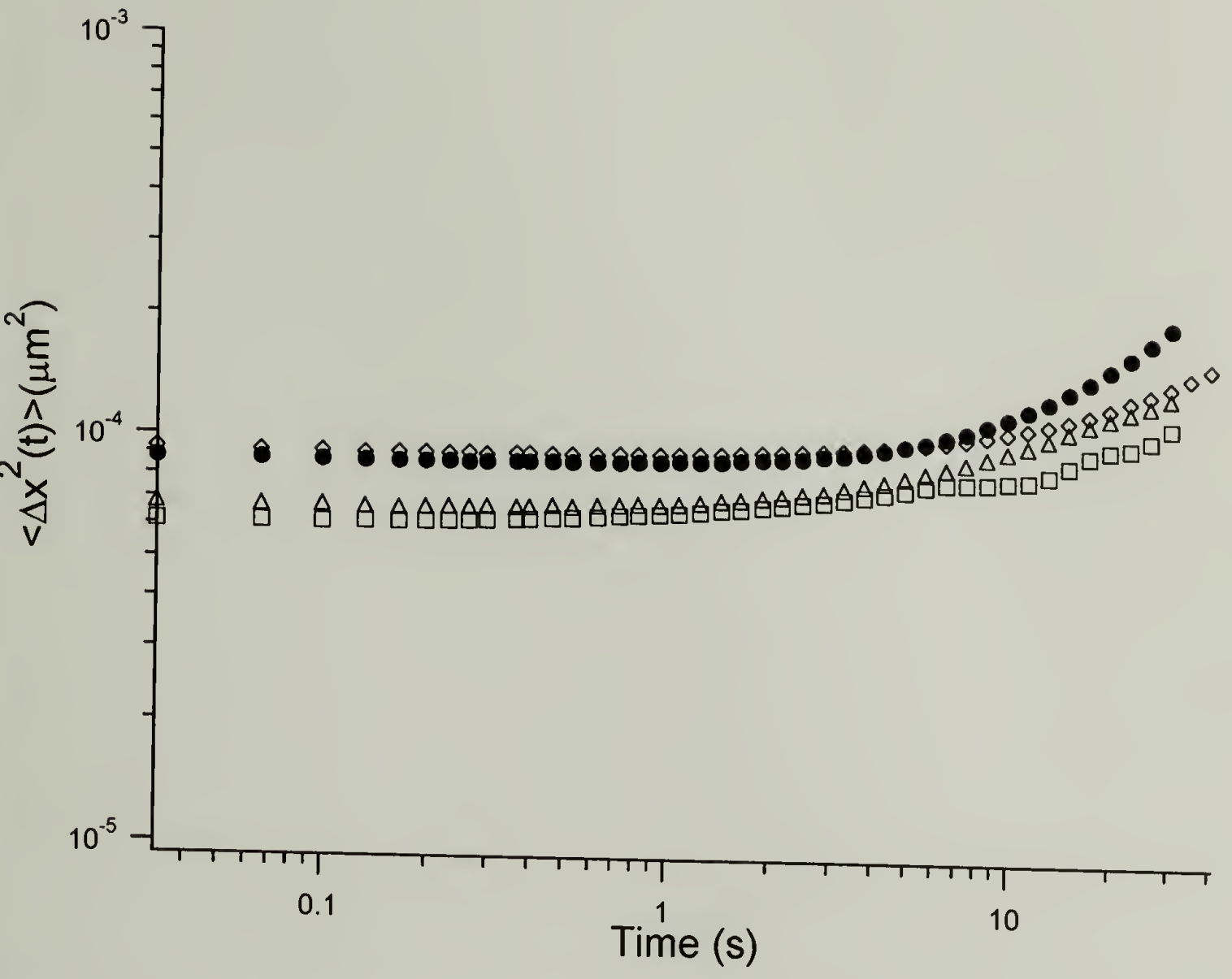

Figure 5.11 Mean square displacement vs. time for equimolar mixture of $AC_{10}Acys$ with $BC_{10}Bcys$, 1.78 mM. pH 8.1 (●), pH 8.4 (□), pH 9.2 (◇), pH 9.8 (△). Samples were buffered with 100 mM tris HCl, and contain 0.13 %(w/v) fluorescent beads.

5.3 Discussion

Circular dichroism spectra (Figure 5.2) for each of the proteins, Acys, Atrp, and $BC_{10}Bcys$ display double minima at 222 and 208 nm, indicating helical secondary structure, with less prominent minima observed for $BC_{10}Bcys$ as compared to Acys or Atrp, due to the presence of the random coil domain, C_{10}. The circular dichroism measurements indicate that $AC_{10}Acys$ and $AC_{10}Bcys$ have larger fractions of helicity as compared to $BC_{10}Bcys$ and equimolar mixtures of $AC_{10}Acys$ with $BC_{10}Bcys$. It was anticipated that the percent helicity of the $AC_{10}Bcys$ would be similar to that of an

equimolar mixture of $AC_{10}Acys$ with $BC_{10}Bcys$. Instead, the CD spectrum for $AC_{10}Acys$ with $BC_{10}Bcys$ appears to be a linear addition of the spectra for the individual proteins.

Two types of individual end blocks, Acys or Atrp, were added to $BC_{10}Bcys$. Both chemical and physical crosslinks can be formed using Acys—a disulfide bond may connect the C-termini of two proteins chemically, or physical bond may form when the proteins fold into the coiled coil motif. Although the $AC_{10}Acys$ protein forms a gel at 2.23 mM, the $BC_{10}Bcys$ protein does not form an elastic network. With the addition of acidic leucine zipper blocks, Atrp or Acys, the viscosity of the $BC_{10}Bcys$ does not change. Acys has the ability to form physical aggregates as well as covalent linkages through the C-terminal cysteine residue, however, under the conditions examined, a hydrogel could not be formed. In order for leucine zipper aggregates to serve as junction points, the aggregate must connect at least three chains. The addition of the A block, in the context of Atrp or Acys, could not induce formation of a gel in a $BC_{10}Bcys$ solution, however, one would expect that mixtures of $AC_{10}Acys$ with $BC_{10}Bcys$ might be sufficient to induce gelation. In the same way, Acys has the identical putative leucine zipper sequence as $AC_{10}Acys$, so is also anticipated to fold under the same conditions as $AC_{10}Acys$ and Atrp. The CD spectra shown in Figure 4.6 indicates that the helical content for Atrp is higher than that observed for Acys. Both Acys and Atrp have a higher helical content than the triblocks, $AC_{10}Acys$ and $BC_{10}Bcys$, as would be expected due to the presence of the midblock, which adopts a random coil conformation. The difference between the helicity in Acys compared to Atrp was not anticipated, however, both show higher helical content than the triblocks, which illustrates that the secondary structure is largely helical under the same conditions as that observed for the triblocks.

The observed double minima at 208 and 222 nm indicate that both acidic and basic triblock proteins are folded at pH 7.4. At concentrations below 2.23 mM, $AC_{10}Acys$ does not form an elastic gel, likely due to the number of molecules that form intramolecular loops rather than crosslinks that contribute to network formation. Similarly, although $BC_{10}Bcys$ is folded under physiological conditions, the protein can only form a viscous liquid. Figures 5.4 and 5.5 show that $AC_{10}Acys$ and $BC_{10}Bcys$ are viscous solutions at 1.78 mM, pH 7.4 and 8.5, indicated by constantly increasing MSD vs. time. A plateau in the MSD vs. time indicated that an elastic network was formed for the mixture of the two protein solutions.

The individual components, $AC_{10}Acys$ and $BC_{10}Bcys$, were analyzed using particle tracking analysis at 1.78 mM concentrations, pH 7.4 and 8.5. Under these conditions, solutions remained viscous. Upon combination, however, an elastic gel was observed.

Mixing of $AC_{10}Acys$ and $BC_{10}Bcys$ solutions results in drastic changes in macroscopic properties of the bulk material, however, the secondary structure remains unchanged. The resulting hydrogel formation may be attributed to the transition between intramolecular loops and network contributing bridges. Although both acid and basic leucine zippers display helical secondary structure, their propensity to form an intramolecular loop rather than an intermolecular bridge is affected by the molecular spacer $[(AG)_3PEG]_{10}$, or effectively, the length between the reactive ends.

Jacobson and Stockmayer (*32, 33*) related the number of rings in a polycondensation reaction to the degree of polymerization by, $R_n \sim Vn^{-5/2}$, where R_n is the number of *n*-mer rings in a volume, V. By this relation, the number of rings will increase

with volume, but small species, or low degrees of polymerization, will comprise most of R_n. The weight fraction of rings is found to increase linearly with dilution, up to critical dilution, beyond which only rings are observed. At 1.78 mM, $AC_{10}Acys$ and $BC_{10}Bcys$ may be near critical dilution, leading to a majority of rings, or loops. Upon mixing, heterodimers are favored to form over homodimers, thus decreasing the intramolecular rings, according to the Jacobson-Stockmayer theory. As a result, more chains are elastically effective causing the viscous solution to transition to an elastic gel (Figure 5.12).

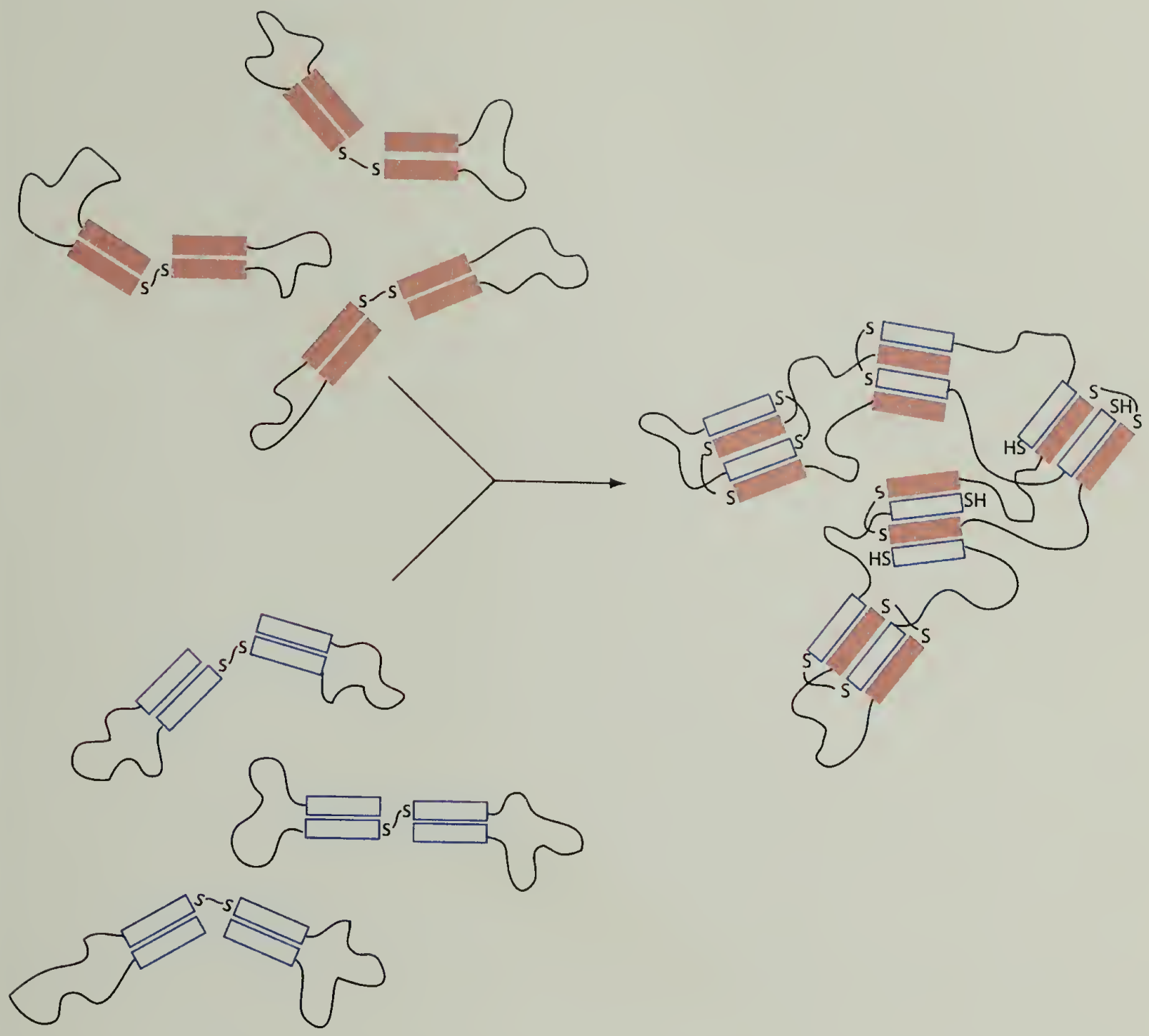

Figure 5.12 Schematic showing combination of folded AC_{10}Acys and BC_{10}Bcys solutions to form an AC_{10}Acys/BC_{10}Bcys network. The preference to form a heterodimer between acidic, A, and basic, B, blocks shifts the equilibrium from loops to bridges, causing the network formation.

The elastic gel is maintained at 1.78mM for pH 7.4 – 9.8, indicating that the material may be useful under physiological conditions as well as over a broader pH range. A viscoelastic material is observed at slightly lower concentrations of 1.34 mM total protein, as indicated in figure 5.6. The MSD increases with time, a signature of

viscous behavior, but the increase is not constant, as would be expected for a purely viscous solution.

The utility of this system may be most apparent for the encapsulation of cells for transplantation or generating artificial organs. In one example of islet cell encapsulation (*19*), the cells are co-injected into a hexadecane solution by using a two syringe apparatus. The cell suspension is directed through the center syringe, which is surrounded by a solution of poly(ethylene glycol) mixed with poly(2-hydroxyethyl methacrylate-co-methyl methacrylate) (poly(HEMA-co-MMA)). Co-injection of the two solutions into hexadecane causes precipitation of poly(HEMA-co-MMA) and extraction of the poly(ethylene glycol). Microparticles of cells encapsulated in poly(ethylene glycol) can be collected and washed before implantation.

1. Using the same type of apparatus to prepare microcapsules, a similar encapsulation technique could be applied to the $AC_{10}Acys$ and $BC_{10}Bcys$ system. The cells could be suspended in one protein solution and injected from the center nozzle, which would be surrounded by the oppositely charged protein solution. Upon injection into an aqueous solution, or directly into the body, the mixture would form an elastic gel.

5.4 References

1. B. D. Ratner, A. S. Hoffman, F. J. Schoen, J. E. Lemons, Eds., *Biomaterials science: An introduction to materials in medicine* (Academic Press, Inc., San Diego, CA, 1996).

2. N. Angelova, D. Hunkeler, *TIBTech.* **17**, 409-421 (1999).

3. S. E. Sakiyama-Elbert, J. A. Hubbell, *Annu. Rev. Mater. Res.* **31**, 183-201 (2001).

4. D. L. Hern, J. A. Hubbell, *J. Biomed. Mater. Res.*, 266-276 (1998).

5. J. A. Hubbell, *Bio-Technol.* **13**, 565-576 (1995).

6. R. Langer, J. P. Vacanti, *Science* **260**, 920-926 (1993).

7. B. Jeong, Y. H. Bae, D. S. Lee, S. W. Kim, *Nature* **388**, 860-862 (1997).

8. K. DiZio, D. A. Tirrell, *Macromolecules* **36**, 1553-1558 (2003).

9. E. R. Welsh, D. A. Tirrell, *Biomacromolecules* **1**, 23-30 (2000).

10. J. A. Hubbell, *Curr. Opin. Biotech.* **10**, 123-129 (1999).

11. M. Zrinyi, *Trends Polym. Sci.* **5**, 280-285 (1997).

12. T. Mayata, M. Asami, T. Uragami, *Nature* **399**, 766-769 (1999).

13. C. M. Hassan, I. Francis J. Doyle, N. A. Peppas, *Macromolecules* **30**, 6166-6173 (1997).

14. A. P. Nowak *et al.*, *Nature* **417**, 424-428 (2002).

15. W. A. Petka, J. L. Harden, K. P. McGrath, D. Wirtz, D. A. Tirrell, *Science* **281**, 389-392 (1998).

16. C. Wang, J. Kopecek, R. J. Stewart, *Biomacromolecules* **2**, 912-920 (2001).

17. C. Wang, R. J. Stewart, J. Kopecek, *Nature* **397**, 417-420 (1999).

18. M. V. Sefton, W. T. K. Stevenson, in *Advances in Polymer Science* N. A. Peppas, R. S. Langer, Eds. (Springer-Verlag, New York, 1993), vol. 107, pp. 145-197.

19. H. Iwata, in *Gels Handbook* Y. Osada, K. Kajiwara, Eds. (Academic Press, San Diego, 2001), vol. 3, pp. 248-260.

20. E. K. O'Shea, R. Rutkowski, P. S. Kim, *Science* **243**, 538-542 (1989).

21. E. K. O'Shea, K. J. Lumb, P. S. Kim, *Curr. Biol.* **3**, 658-667 (1993).

22. H. Wendt *et al.*, *Biochemistry-US* **36**, 204-213 (1997).

23. K. J. Lumb, P. S. Kim, *Science* **268**, 436-438 (1995).

24. P. Lavigne *et al.*, *J. Mol. Biol.* **254**, 505-520 (1995).

25. W. A. Petka, Ph.D. dissertation, University of Massachusetts, Amherst (1997).

26. W. A. Petka, J. L. Harden, J. K. Sakata, D. A. Tirrell, *Mat. Res. Soc. Symp.* **550**, 23-28 (1999).

27. K. P. McGrath *et al.*, *J. Bioact. Compat. Pol.* **15**, 334-356 (2000).

28. S. C. Gill, *Anal. Biochem.* **189**, 283-283 (1990).

29. S. C. Gill, P. H. Vonhippel, *Anal. Biochem.* **182**, 319-326 (1989).

30. R. D. Appel, A. Bairoch, D. F. Hochstrasser, *Trends Biochem. Sci.* **19**, 258-260 (1994).

31. J. C. Crocker, D. G. Grier, *J. Colloid Interf. Sci.* **179**, 298-310 (1996).

32. H. Jacobson, W. H. Stockmayer, *J. Chem. Phys.* **18**, 1600-1606 (1950).

33. H. Jacobson, C. O. Beckmann, W. H. Stockmayer, *J. Chem. Phys.* **18**, 1607-1612 (1950).

CHAPTER 6

EFFECT OF MIDBLOCK LENGTH ON GELATION FOR TRIBLOCK HYDROGELS

6.1 Introduction

The previous chapter detailed a strategy for controlling the electrostatic interactions between protein triblock polymers to influence gelation properties. This chapter investigates how the length of the polyelectrolyte midblock, 'C' affects gelation in a family of triblock proteins, AC_xAcys, where an acidic leucine zipper comprises the 'A' end blocks. The midblock domain can be characterized by a random coil secondary structure (*1*), and the gelation of $AC_{10}Acys$ (*2*) has been attributed to the aggregation of the leucine zipper end blocks, corroborated by the results in former chapters. A series of proteins, AC_xAcys (x = 20, 30, 40, 50) were prepared by recombinant DNA technology expressed by *E. coli*, and purified by Ni^{2+}-NTA affinity chromatography. Changing the length of the midblock was presumed to change viscoelastic properties of the resulting hydrogel without affecting the folding of leucine zipper end blocks. In particular, the gel point was anticipated to decrease with increasing midblock length, while the hydrogel was expected to persist over the same pH range as observed for $AC_{10}Acys$.

Transition from a viscous liquid to an elastic solid has been studied by rheology for chemical and physical gels (*3*). The gel point, or liquid to solid transition, has been determined as the point where tan δ, or G''/G', is frequency independent for thermoreversible triblock copolymers (*4, 5*). Yu and coworkers studied the gelation of

syndiotactic poly(methyl methacrylate)(sPMMA)-polybutadiene(PBD)-sPMMA triblock copolymers as a function of the midblock character (substituting hydrogenated PBD for the PBD midblock) or composition (varying the %syndiotacticPMMA or the PMMA molecular weight). At the gel point, the shear storage modulus, G'(ω), and the shear loss modulus, G"(ω), scale with the angular frequency, ω:

$$G'(\omega) \sim G''(\omega) \sim \omega^{\Delta}, \tag{1}$$

where Δ is the scaling exponent. For differences in midblock character, or length, or in endblock composition, Δ was found to be in the 0.65 – 0.75 range (*4, 5*), however, the gelation time was dependent on midblock length, concentration, and composition.

This work describes the determination of gel point by single particle tracking (SPT). Schnurr *et al.* measured viscoelasticity in soft materials using a non-invasive technique similar to SPT (*6*). Both methods rely on the thermal fluctuation of sub-micron tracer particles to determine the viscous and elastic response of the medium. Schnurr studied the properties of F-actin and poly(acrylamide) gels using interferometry. The scaling behavior was determined for F-actin, and the plateau moduli were measured for poly(acrylamide) gels of concentrations less than 5% (w/v). This technique requires that probe particles be larger than the mesh size of the network, and it provides measurements over a large, high frequency range.

Singe particle tracking also affords the ability to probe samples in a non-invasive and passive way; however, high frequency measurements available with laser interferometry or light scattering (*7, 8*) are limited by video acquisition rate, which is on the order of miliseconds. For triblock proteins of the general structure, AC_xAcys, however, this frequency range is sufficient to examine the onset of gelation. The

transition from a liquid to a solid is defined by the emergence of a plateau in the mean square displacement (MSD) of fluorescent particles suspended in the medium. When the particles are freely diffusing, the MSD increases constantly as a function of time, whereas the particle motion is restricted in an elastic medium, resulting in a plateau in the MSD over time. This definition is used to determine the onset of gelation.

Chemically and physically crosslinked gels differ in that physical crosslinks are non-covalent junction points that have the ability to diffuse freely on some time scale. In the case of $AC_{10}Acys$, this relaxation time appears in the MSD as a viscous onset (MSD increasing linearly with time) at a frequency on the order of seconds to tens of seconds around pH 8.0, 2.23 mM (*9*). On this time scale, the junction points are thought to freely exchange, thus displaying viscous character at longer times. For chemically crosslinked networks, the plateau extends to the longest measured frequency of the experiment and presumably out to infinitely long time (*10*).

SPT was used to determine gelation of AC_xAcys proteins, where x = (20, 30, 40, 50), as a function of concentration around pH 8.5, 25 °C. Hydrogels were then prepared at various pH and at concentrations where each protein was observed to form an elastic network, as evidenced by a plateau in the MSD vs. time.

6.2 Experimental Work

6.2.1 AC_xAcys Gelation

6.2.1.1 Concentration Dependence

Lyophilized $AC_{20}Acys$ protein, 22.1 mg, was resuspended in 201 μL of 100 mM tris HCl, pH 7.5 by vortexing until a clear, viscous solution was achieved. The stock solution was divided into 10 μL aliquots delivered to sterile microfuge tubes. Initially, one aliquot was prepared with 0.18%(w/v) 0.56 μm fluorescent microspheres (Molecular Probes, Eugene, OR), then brought to 1.64 mM with 100 mM tris HCl. The pH was measured using an ISFET pH meter (Shindengen Electric Manufacturing Co, LTD, Tokyo, Japan), and 2N NaOH was added to achieve a final pH of 8.3. Based on this first sample, the same amount of 2N NaOH was added to the subsequent aliquots to achieve pH 8.3. The final concentrations of protein in each sample varied from 1.64 mM to 2.23 mM, with 0.18 %(w/v) 0.56 μm fluorescent microspheres and buffered with 100 mM tris HCl.

All protein samples were prepared in an analogous manner to that described for $AC_{20}Acys$. Stock solutions were prepared at 2.6 – 2.8 mM for $AC_{30}Acys$, $AC_{40}Acys$, and $AC_{50}Acys$. Although the $AC_{20}Acys$ samples were prepared at pH 8.3, the remaining proteins were examined at pH 8.5. The difference in pH was made so that the longer coils could be compared to results on gelation from $AC_{10}Acys$ (*2, 9*). In the interest of time, the $AC_{20}Acys$ was not re-examined at pH 8.5.

Upon preparation of protein hydrogels containing 0.5 μm microspheres, the solutions were placed in a grease chamber, ca. 1-2 mm thick, sealed between a microscope slide and a No. 1 ½ coverslip. Samples were annealed at 50 °C for 10 minutes to promote leucine zipper exchange, and increase the likelihood of intermolecular aggregation over intramolecular coiled coil formation. Single particle tracking procedures described earlier were followed to obtain the MSD vs. time data shown in Figures 6.1 – 6.4.

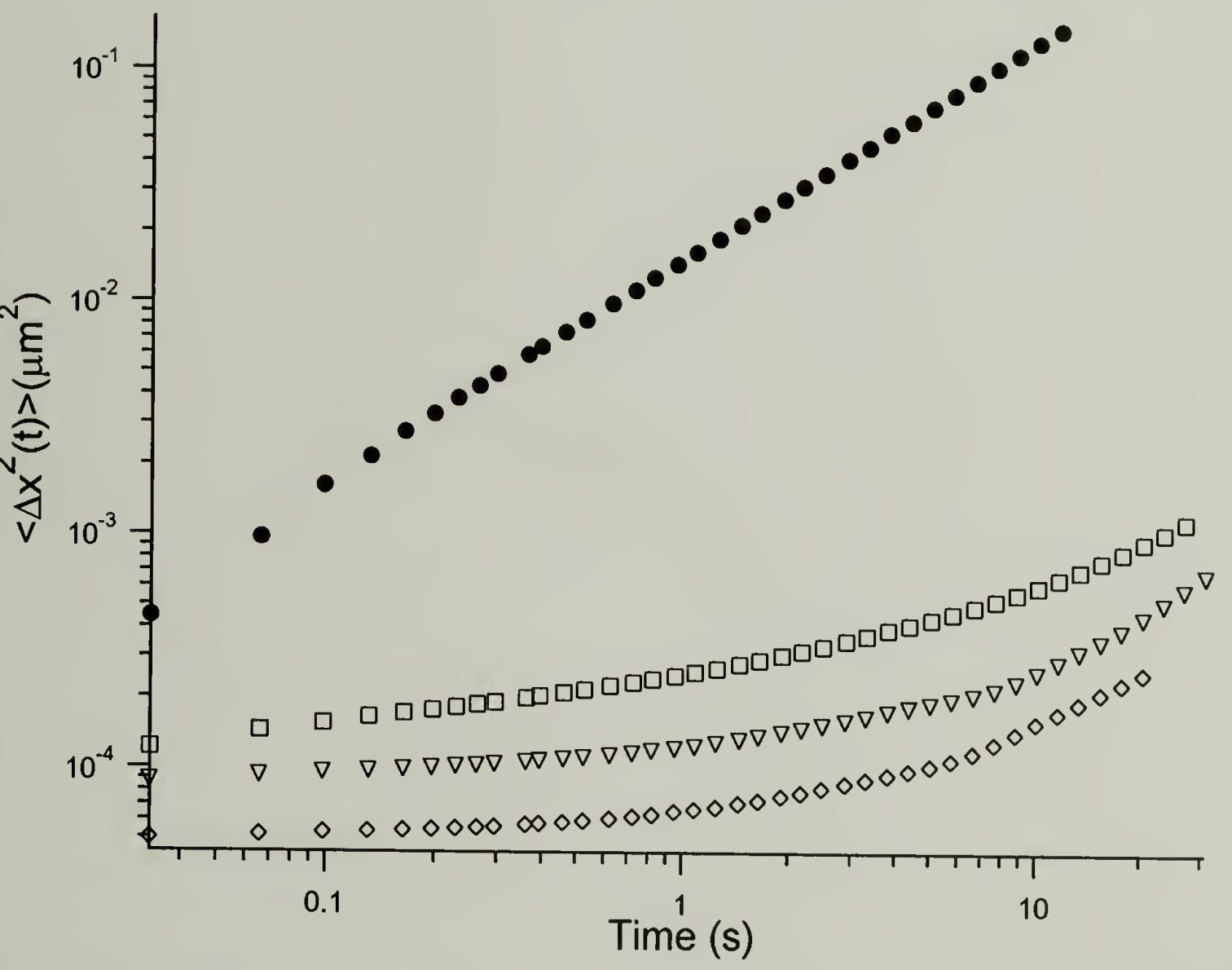

Figure 6.1 Mean square displacement vs. time for $AC_{20}Acys$, pH 8.3, 100mM tris HCl, 25 °C at 1.64 mM (●), 1.80 mM (□), 1.97 mM (▽), and 2.23 mM (◇).

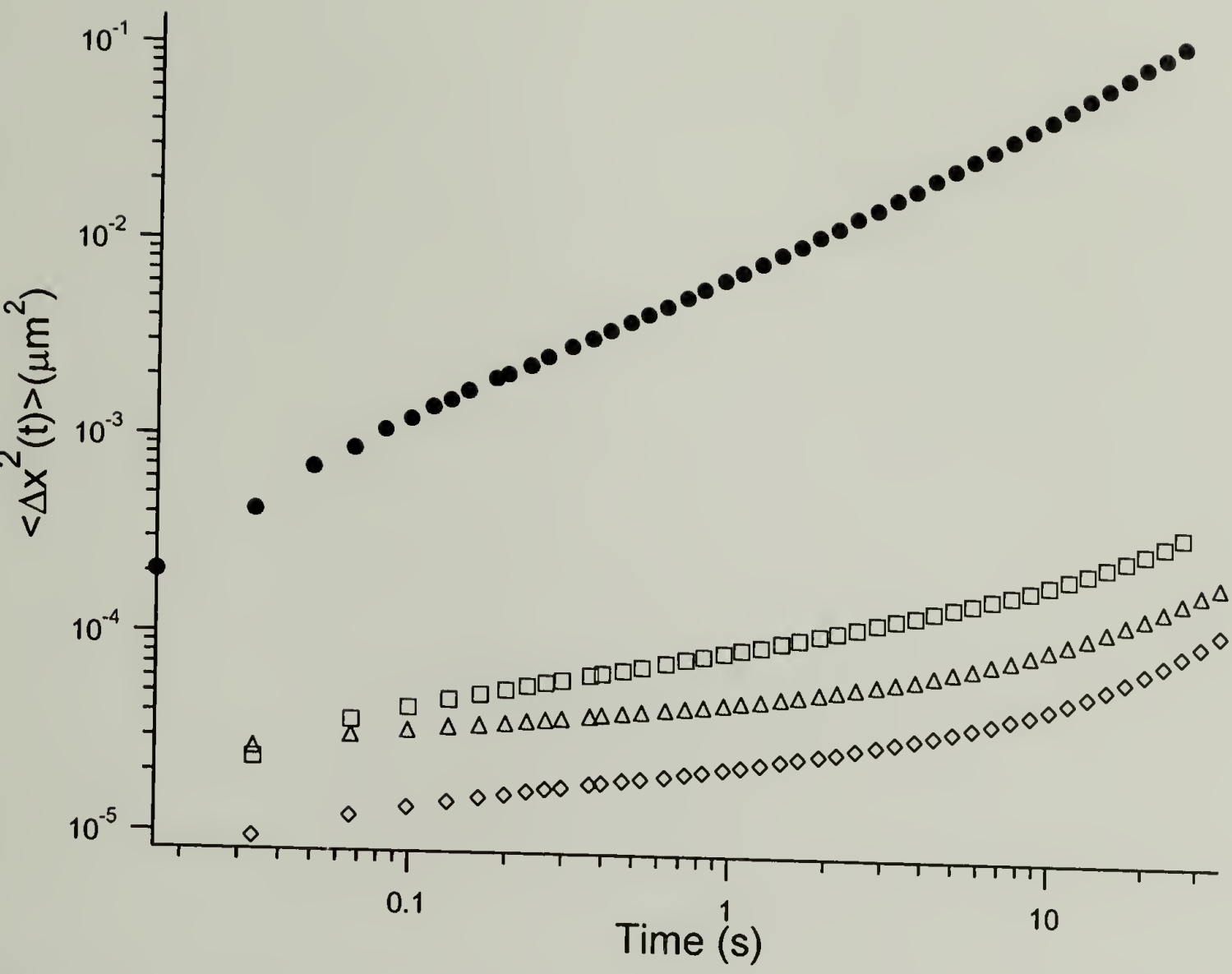

Figure 6.2 Mean square displacement vs. time for $AC_{30}Acys$, pH 8.3, 100mM tris HCl, 25 °C at 0.78 mM (●), 1.04 mM (□), 1.30 mM (△), and 1.56 mM (◇).

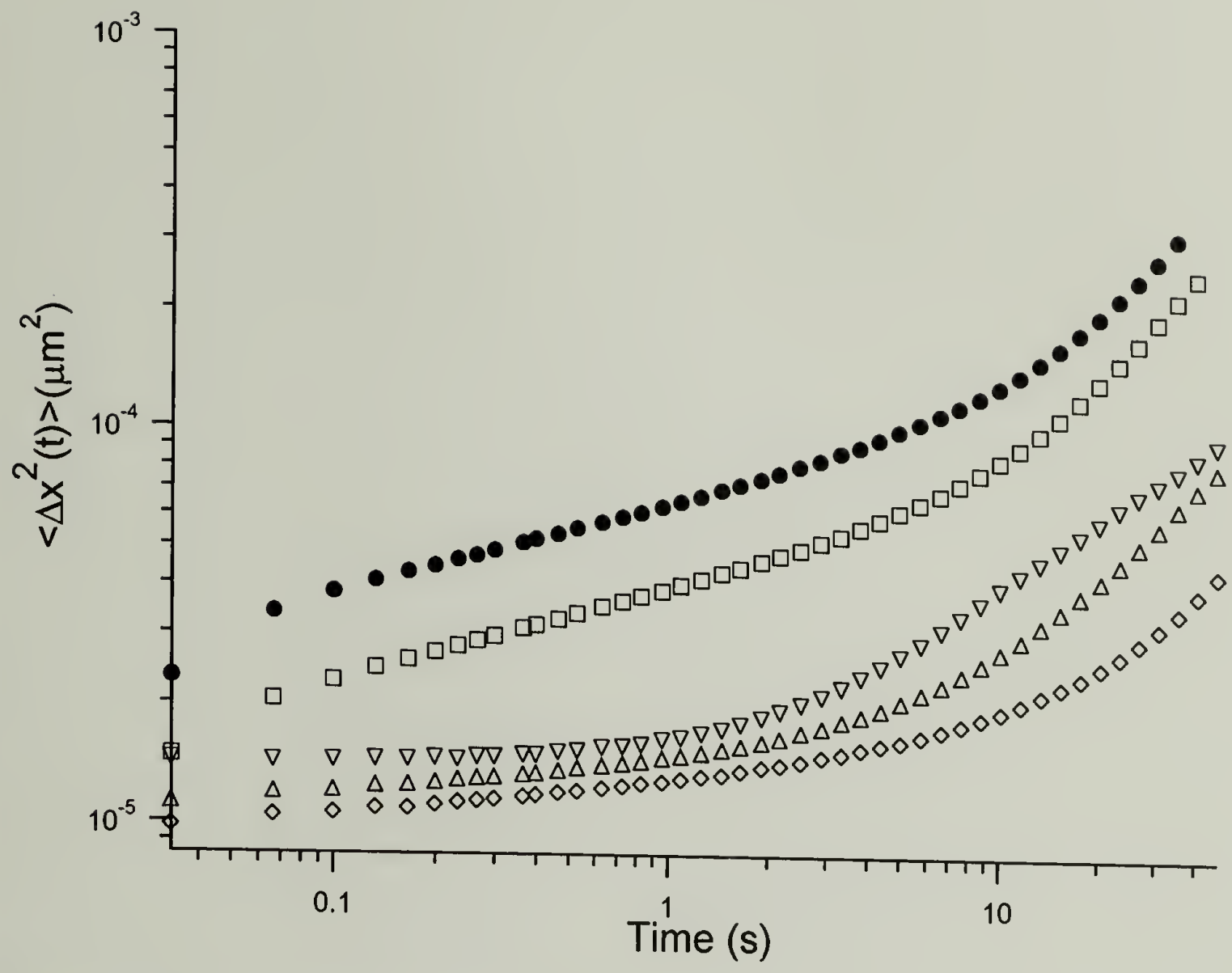

Figure 6.3 Mean square displacement vs. time for $AC_{40}Acys$, pH 8.3, 100mM tris HCl, 25 °C 0.86 mM (●), 1.07 mM (□), 1.29 mM (◇), 1.50 mM (△), and 1.93 mM (▽).

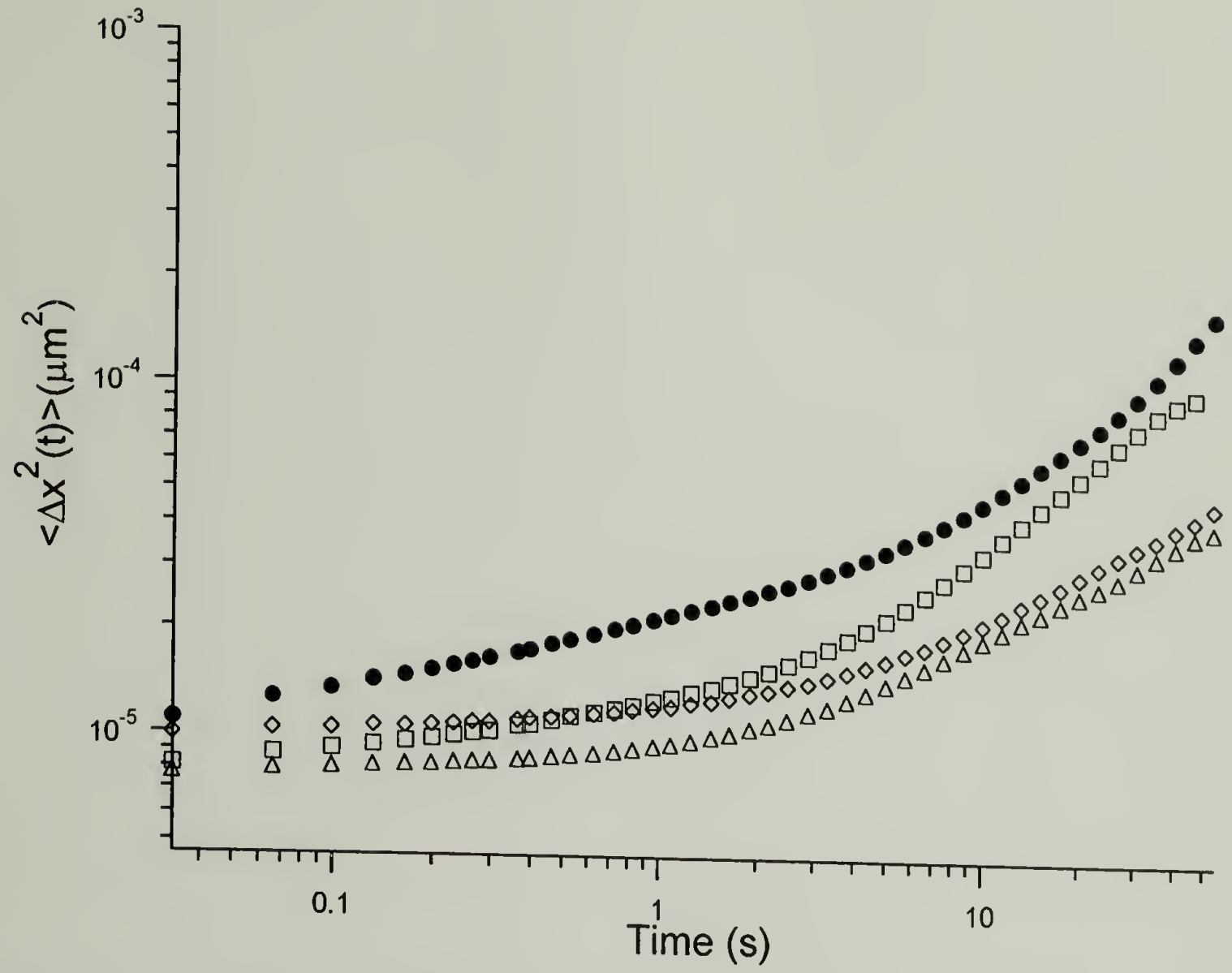

Figure 6.4 Mean square displacement vs. time for $AC_{50}Acys$, pH 8.3, 100mM tris HCl, 25 °C at 0.92 mM (●), 1.10 mM (□), 1.28 mM (◇), and 1.65 mM (△).

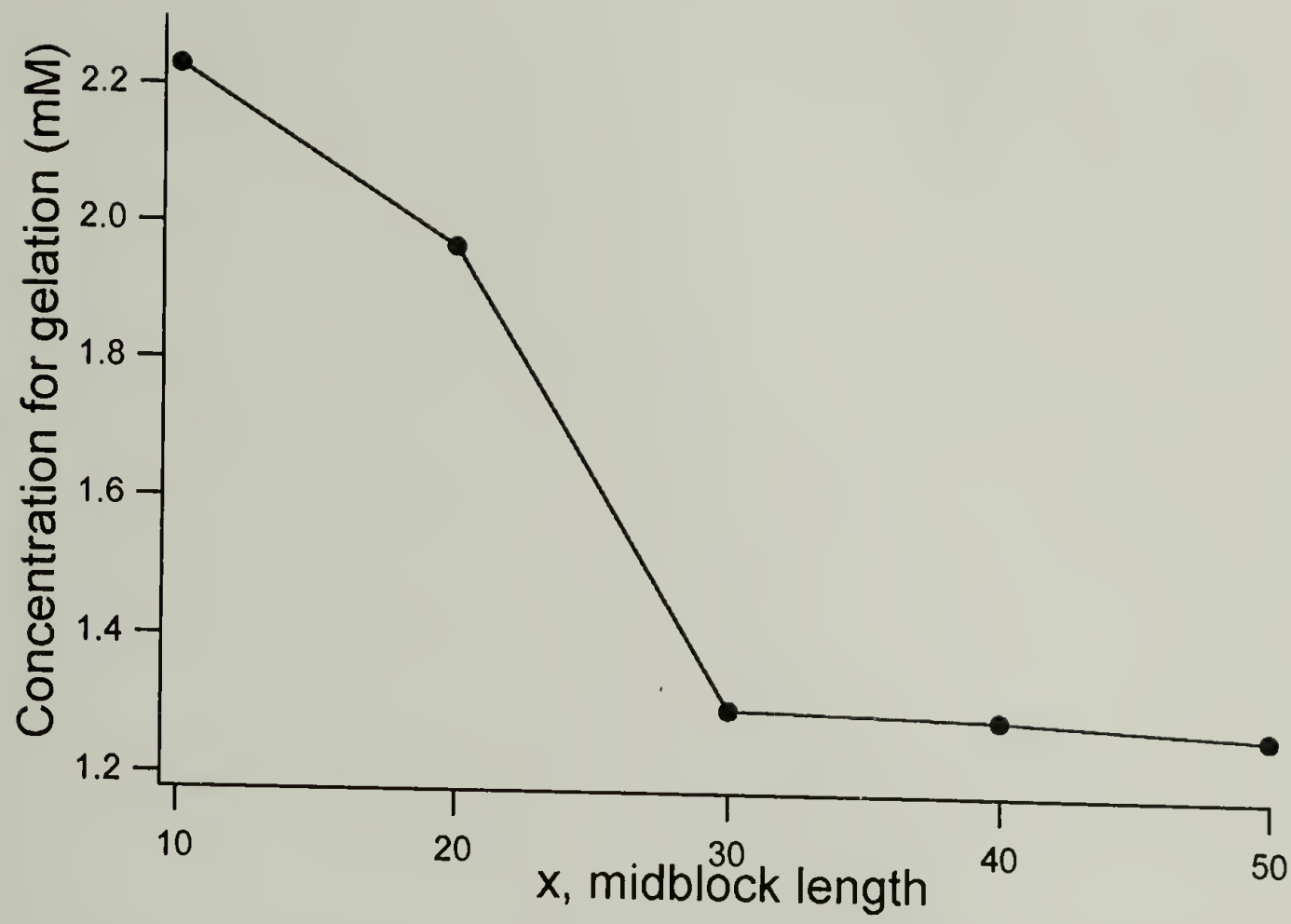

Figure 6.5 Concentration required for gelation vs. midblock length for AC_xAcys proteins.

The dependence of gelation on midblock length is displayed in Figure 6.5. Concentrations for gelation were determined by identification of the concentration at which the slope of the MSD vs. time was 0.2 or less on the log-log scale. $AC_{10}Acys$ gelation concentration was taken from DWS data by Petka and coworkers (*2*).

6.2.1.2 pH Dependence

Stock solutions prepared as described earlier were divided into 10 μL aliquots delivered to sterile microfuge tubes. Each aliquot was prepared with 0.18%(w/v) 0.56 μm fluorescent microspheres (Molecular Probes, Eugene, OR), then brought to 1.97 mM for $AC_{20}Acys$ with 100mM *tris HCl*. The other protein solutions were brought to 1.30

mM for $AC_{30}Acys$, 1.29 mM for $AC_{40}Acys$, or 1.28 mM for $AC_{50}Acys$. Acid or base was added to each aliquot to vary the pH from 6.2 to 11.4. An ISFET pH meter (Shindengen Electric Manufacturing Co, LTD, Tokyo, Japan) was used to measure the pH for each sample.

Samples were prepared for single particle tracking and the Brownian motion of fluorescent microspheres was analyzed as described earlier. MSD vs. time data are shown below for each protein at various pH.

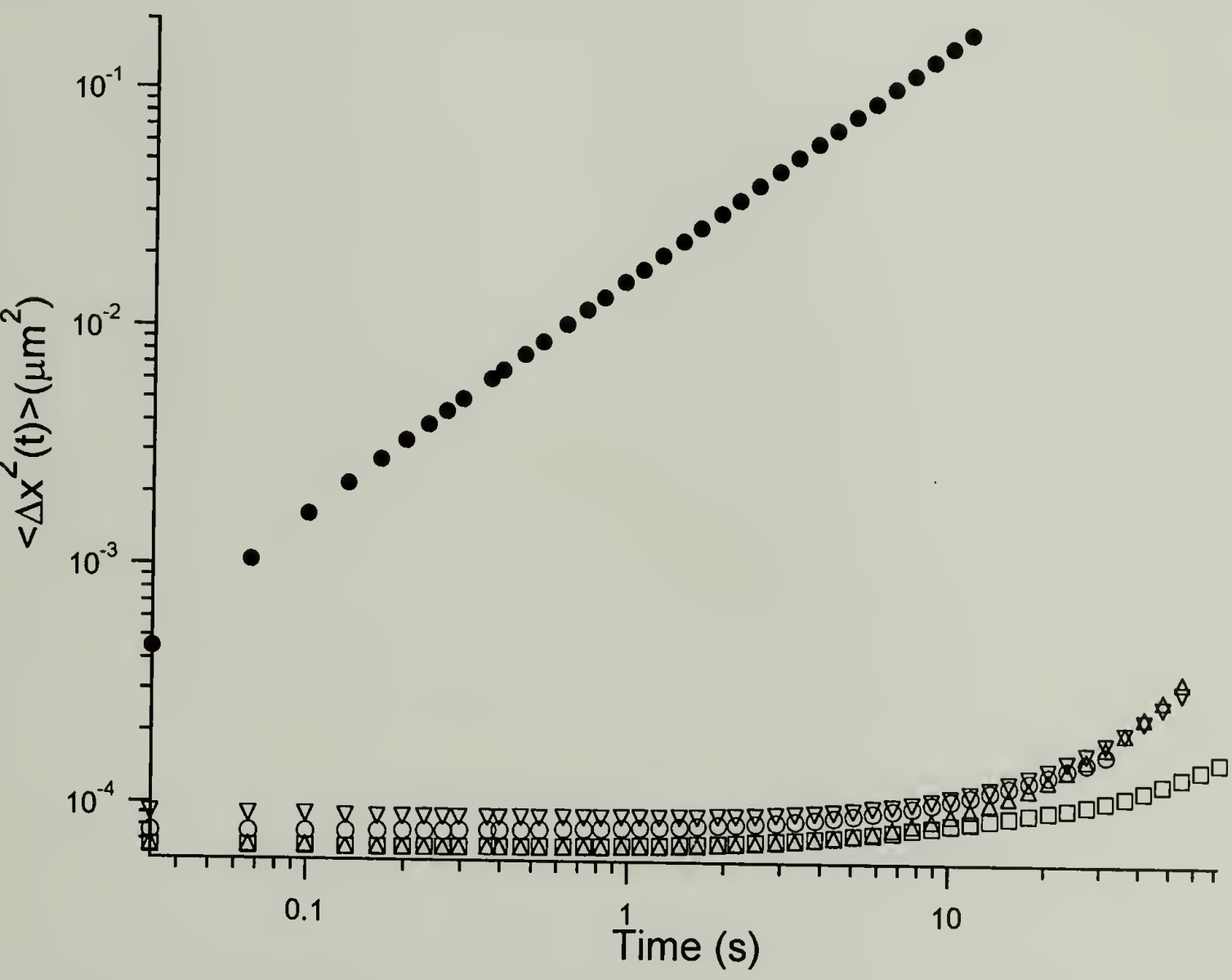

Figure 6.6 Mean square displacement vs. time for $AC_{20}Acys$, 1.97mM, 100 mM tris HCl, 25 °C, examined at pH 11.2 (●), pH 9.7 (○), pH 8.2 (□), pH 7.6 (△), and pH 6.2 (▽).

AC_{20}Acys samples (Figure 6.6) show that elastic behavior dominates for pH 9.7 or less. This observation is different than that reported for AC_{10}Acys, which showed both viscous and elastic contributions at pH 8.8 (*2*).

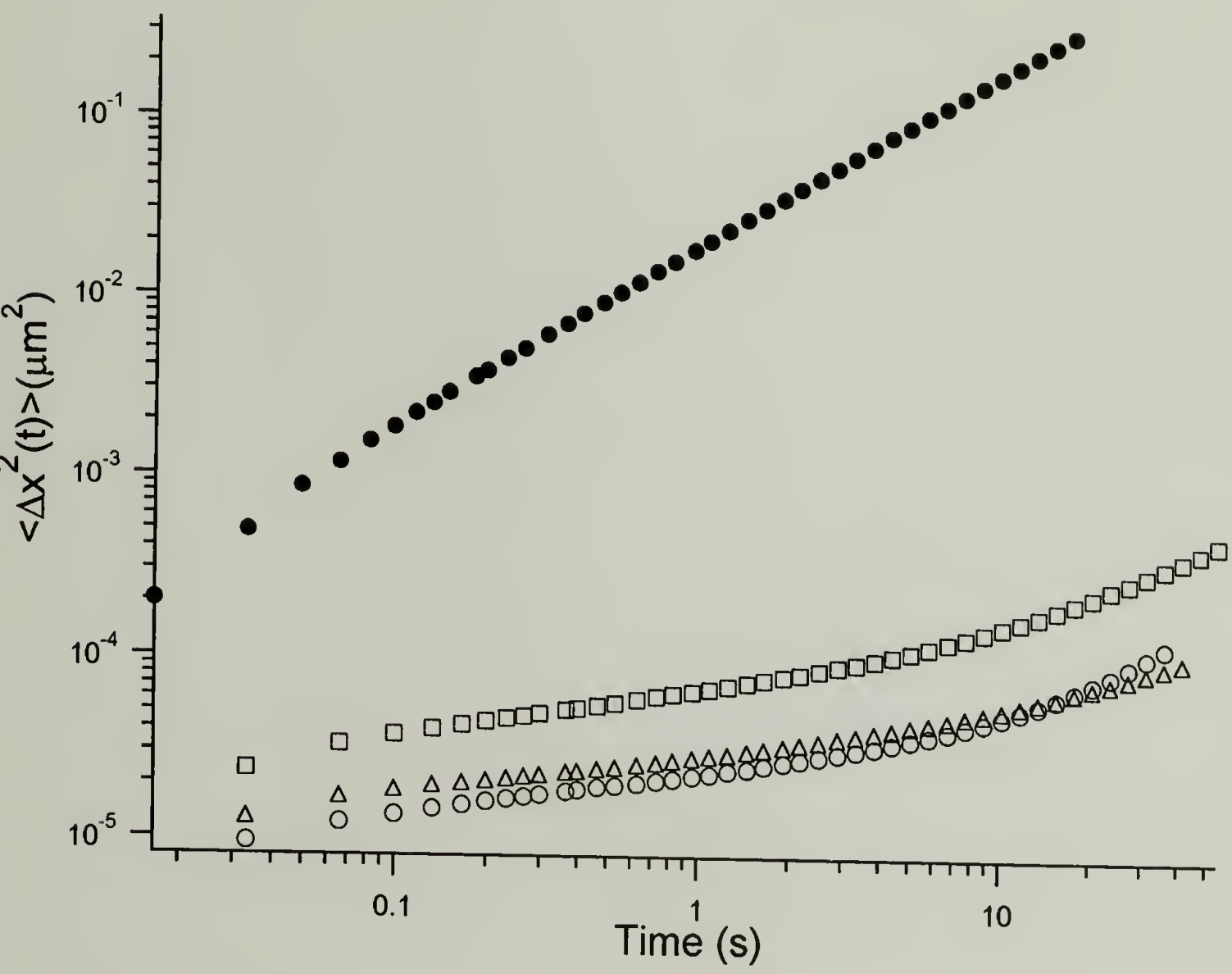

Figure 6.7 Mean square displacement vs. time for AC_{30}Acys, 1.30 mM, 100 mM tris HCl, 25 °C at pH 11.4 (●), pH 9.0 (□), pH 8.5 (○), and pH 7.7 (△).

The shape of the MSD vs. time in pH 7.7 and pH 8.5 samples of AC_{30}Acys (Figure 6.7) show similar characteristics. Viscous behavior characterizes the pH 11.4 sample, whereas the pH 9.0 sample displays largely elastic character.

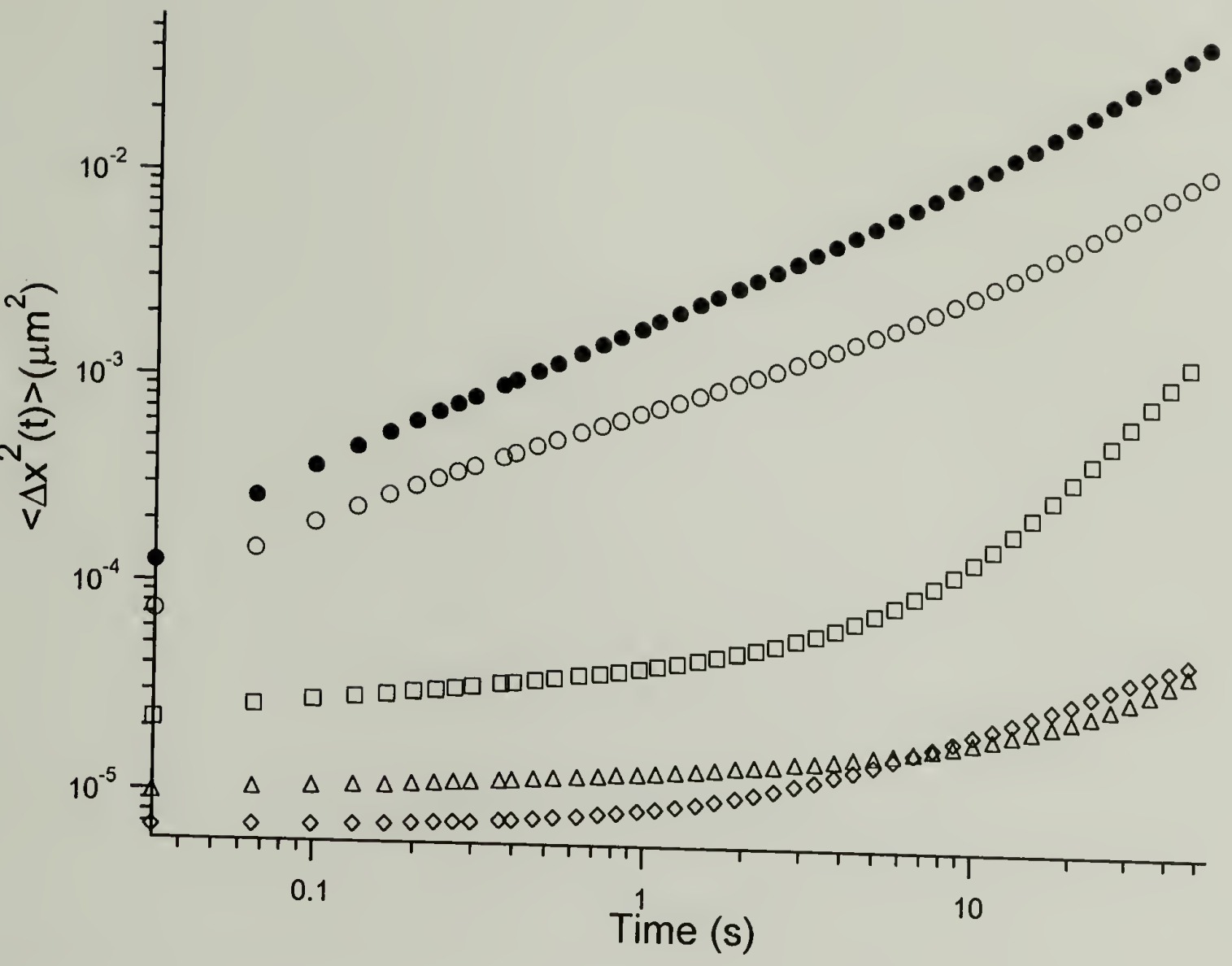

Figure 6.8 Mean square displacement vs. time for $AC_{40}Acys$, 1.29 mM, 100 mM tris HCl, 25 °C examined at pH 10.3 (●), pH 10.2 (○), pH 9.5 (□), pH 8.5 (△), and pH 7.7 (◇).

Figure 6.8 shows that elastic behavior is observed for $AC_{40}Acys$ samples less than pH 9.5. In the case of pH 8.5 and 7.7, the plateau in MSD vs. time extends beyond ~5 seconds and increases slowly. The pH 9.5 sample has a viscous onset with a larger slope than the samples of lower pH.

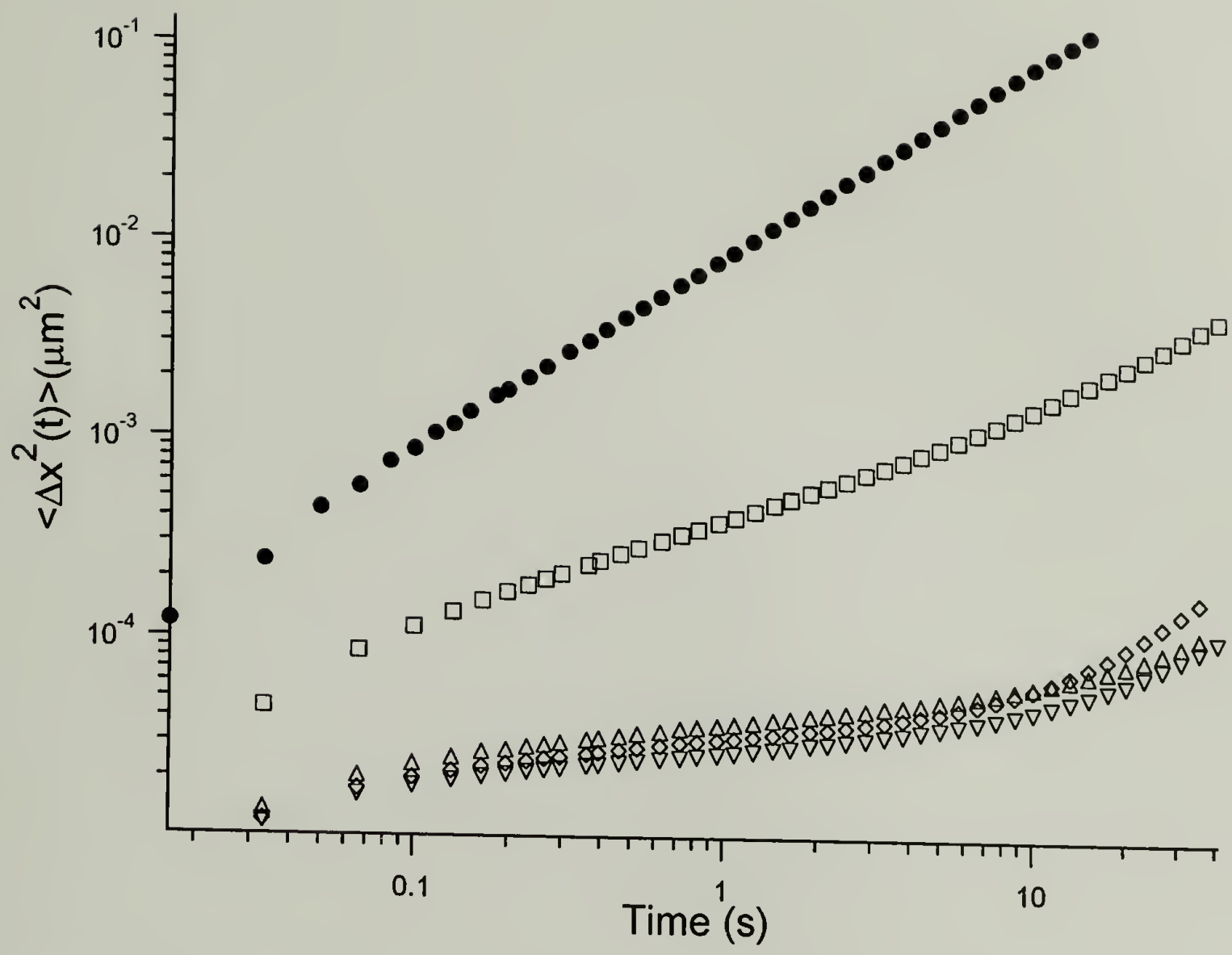

Figure 6.9 Mean square displacement vs. time for $AC_{50}Acys$, 1.29 mM, 100 mM tris HCl, 25 °C at pH 11.2 (●), pH 10.2 (□), pH 8.5 (◇), pH 8.0 (△), and pH 7.7 (▽).

Viscous behavior characterizes pH 11.2 and 10.2 $AC_{50}Acys$ samples, as observed in Figure 6.9. Samples at pH 8.5 or less generally show the same elastic plateau and viscous onset.

6.3 Discussion

Eight new proteins of the general form, AC_xAcys were used to prepare protein hydrogels. Single particle tracking was used to characterize the gel point as a function of concentration or pH. Viscoelastic behavior was illustrated by MSD vs. time plots, in

which a viscous solution is characterized by constantly increasing MSD vs. time, whereas an elastic network is described by a plateau in the MSD as a function of time. The gel point was observed to decrease as a function of molecular weight of the midblock length, comparing $AC_{10}Acys$, $AC_{20}Acys$ and $AC_{30}Acys$, which form gels at 2.23mM (*2*). 1.97 mM and 1.30 mM, respectively. Gel points for $AC_{40}Acys$ and $AC_{50}Acys$ were observed to be similar to that for $AC_{30}Acys$, at 1.29 mM and 1.28 mM, respectively.

Although a 5%(w/v) solution—equivalent to 2.23 mM—of $AC_{10}Acys$ is required for gelation (*2*), a lower concentration allows $AC_{20}Acys$ to display elastic behavior. A solution of $AC_{20}Acys$ at 1.80 mM (Figure 6.1) shows restricted bead motion, however, an elastic plateau is not observed. In contrast, the 1.64 mM solution clearly shows viscous behavior, characterized by an increasing MSD as a function of time. A concentration of 1.97 mM was used to define the gel point, since it is the lowest concentration examined that displays a plateau in the MSD over the time scale on the order of seconds.

$AC_{40}Acys$ was observed to undergo gelation at 1.29 mM, as indicated in figure 6.3 by the plateau extending to ~2 seconds. The viscous onset appears to be earlier and of larger magnitude than that observed for either $AC_{20}Acys$ or $AC_{30}Acys$. Higher concentrations, 1.93 mM in particular show a viscous onset on the order of 10-12 seconds, with a smaller slope than the 1.29 mM sample.

Each sample in the $AC_{50}Acys$ sample set shown in Figure 6.4 has a large elastic component, as indicated by the small slope in MSD vs. time. The 1.28 mM sample (open diamonds) was the lowest concentration to display a plateau in MSD up to ~3-5 seconds. In the case of 1.64 mM $AC_{50}Acys$, a viscous onset appears around the same time as observed in the 1.28 mM sample.

The decrease in the relative amount of protein needed to form an elastic network may be attributed to the difference in the number of loops and bridges in the system. Data in Chapter 5 suggest that the number of elastically effective chains can be affected by combining two molecules that prefer intermolecular bonds over intramolecular loops. In the absence of the forced intermolecular bonding, higher concentrations or longer midblock domains may be required to reduce the number of loops. Figure 6.5 illustrates the dependence of gelation on midblock length, indicating that the longer molecules require less protein to form an elastic gel.

Jacobson and Stockmayer relate the number of rings in a condensation reaction as $R_n \sim Vn^{-5/2}$, where R_n is the number of *n*-mer rings in a volume, V (*11, 12*). With either an increase in concentration, or an increase in the ring size, the total number of rings should decrease. Applying this theory to the AC_xAcys family of proteins, the number of loops should decrease with the increasing midblock length. Since the formation of a loop does not contribute to the network, then the gelation concentration should scale with the loop concentration. As the probability to form a loop decreases, the concentration for gelation should decrease. Figure 6.5 illustrates the drop in concentration required for gel formation, increasing the midblock length from $AC_{10}Acys$ to $AC_{30}Acys$. Around a midblock length of C_{30}, the probability to form a loop is low enough that the difference in the number of loops does not affect the gel point.

The pH dependence of the gel point generally illustrated that above pH 10.2, both viscous and elastic behavior are observed (Figures 6.6 – 6.9). For solutions above pH 11, all proteins could be described as viscous solutions. In contrast to the behavior of $AC_{10}Acys$, which was observed to have viscous behavior by pH 9.5, each of the proteins

examined here were characterized by more elastic than viscous behavior. It was hypothesized that the pH behavior for the longer coil length variants would be similar to that observed for $AC_{10}Acys$ (*2*), where elastic and viscous behavior was observed at 2.23 mM, pH 8.5. The increased elasticity at pH 9.5 observed for $AC_{40}Acys$, as shown in Figure 6.8, suggested that the $AC_{40}Acys$ gel has an increased stability, even at pH values higher than observed for $AC_{10}Acys$.

One architectural difference among the longer coil length variants is the charge. As the coil length increases, so does the number of glutamic acid residues in the midblock domain. Under high pH, the glutamic acids are deprotonated, so it is likely that this increase in charge will also lead to an increase in swelling ability.

6.4 References

1. K. P. McGrath, M. J. Fournier, T. L. Mason, D. A. Tirrell, *J. Am. Chem. Soc.* **114**, 727-733 (1992).

2. W. A. Petka, J. L. Harden, K. P. McGrath, D. Wirtz, D. A. Tirrell, *Science* **281**, 389-392 (1998).

3. H. H. Winter, M. Mours, Eds., *Rheology of Polymers Near Liquid-Solid Transitions*, vol. 134 (Springer-Verlag, Berlin, 1997).

4. J. M. Yu, S. Blacher, F. Brouers, G. L'Homme, R. Jerome, *Macromolecules* **30**, 4619-4625 (1997).

5. J. M. Yu *et al.*, *Macromolecules* **29**, 5384-5391 (1996).

6. B. Shnurr, F. Gittes, F. C. MacKintosh, C. F. Schmidt, *Macromolecules* **30**, 7781-7792 (1997).

7. T. G. Mason, H. Gang, D. A. Weitz, *J. Mol. Struct.* **383**, 81-90 (1996).

8. D. A. Weitz, J. X. Zhu, D. J. Durian, H. Gang, D. J. Pine, *Phys. Scripta* **T49**, 610-621 (1993).

9. W. A. Petka, Ph.D. dissertation, University of Massachusetts, Amherst (1997).

10. B. R. Dasgupta, S. Y. Tee, J. C. Crocker, B. J. Frisken, D. A. Weitz, *Phys. Rev. E* **65**, 1-10 (2002).

11. H. Jacobson, W. H. Stockmayer, *J. Chem. Phys.* **18**, 1600-1606 (1950).

12. H. Jacobson, C. O. Beckmann, W. H. Stockmayer, *J. Chem. Phys.* **18**, 1607-1612 (1950).

APPENDIX A

PROCEDURES FOR SINGLE PARTICLE TRACKING CHARACTERIZATION TECHNIQUE

Crocker and Grier (*1*)describe the development of a particle tracking analysis software package written in IDL, Research Systems, Inc. (Boulder, CO). The process for analysis can be divided into five procedures: acquiring a digital movie, exporting the movie as uncompressed TIFF files, determining the particle positions in each movie frame, determining the trajectories from particle positions, and analyzing the trajectories to determine mean squared displacement vs. time. This appendix will outline the individual procedures in detail. A tutorial, written by Eric Weeks, is provided at http://glinda.lrsm.upenn.edu/~weeks/idl/tracking.html, which should be used with this manual, as the procedures are explained with more detail as well as with images that contribute to the understanding of the analysis program.

Acquiring a Digital Movie

Movies are digitally recorded onto mini-digital video (DV) tapes by direct transfer from the CCD camera displaying the fluorescent image. Upon recording the data to tape, the movie is downloaded to the hard drive on the iMac-DV using Adobe Premiere software.

1. Prepare sample by mixing red fluorescently labeled microspheres, Molecular Probes (Eugene, OR), to achieve a concentration from 0.05- 0.18 % (w/v). Use a No. 1 ½

coverslip (0.17-mm thickness and $n_D = 1.515$) over the top of the sample if using an oil objective (*2*).

2. Turn on the power source to the ORIEL high pressure Hg lamp, then ignite the lamp. Record the time used; each lamp has a lifetime of ~ 150 hours. See the ORIEL manual for instruction on lamp replacement and alignment.
3. Turn on the power to the monitor, the DAGE-MTI 72 camera (located in the back of the control box), and the JVC digital video deck.
4. If using the 40x 1.4NA Plan-Neofluar oil immersion objective, a drop of oil is required to index match the objective to the coverslip. Lightly place a small drop of immersion oil, (Carl Zeiss, Inc., Thornwood, NY) on the top of objective, then invert the microscope slide such that the coverslip is above the objective. Slowly bring the objective up to the coverslip until the oil drop forms a meniscus between the objective and the sample.
5. Bring the sample into focus using the fine adjustment knob by viewing through the oculars or by observing the recorded image from the camera, as displayed on the monitor.
6. Although the GAIN and BLACK LEVEL can be used to adjust the brightness and contrast of the image, the highest quality image is achieved by proper light alignment and illumination. Use the iris on the fluorescence port and the focusing lens on the lamp housing to form the most even illumination possible, keeping the GAIN and BLACK LEVEL constant.
7. After a reasonable image is observed on the monitor, it can be downloaded directly to the iMAC-DV to analyze the quality of the image.

8. If the computer is running off of the OS-X start-up disk, use the Control Panel menu to choose Start Up Disk. Choose the OS-9 disk and restart the computer in OS-9.
9. Open Adobe Premiere 5.1 (in the *Applications (OS-9)* folder on the *OS-X* disk). A new project will open. Load the saved settings labeled jill's settings. The project window can be closed at this time. From the File menu, choose Movie Capture. A window displaying the live image will open.
10. Use the mouse to start recording a movie, which will be directly written to the scratch disk on the iMAC-DV. Record a few seconds of the beads imaged under fluorescence. Click the mouse a second time to stop recording.
11. An untitled clip will open. Export a few frames as uncompressed TIFF images to determine the quality of the image. Use the IN and OUT markers to set the points to start and end the movie for export. Choose the following settings when exporting:
    - Make: In to Out
    - Video: 640 x 480 (select fix 4:3 ratio) at 29.97 frames per second(fps)
    - Compression: TIFF (100%)
    - Audio: Disabled
12. Save the exported file on the desktop with the name test.
13. Open NIH Image v1.62 (in the *Applications (OS-9)* folder on the *OS-X* disk). Use the File menu to choose Open file. From the desktop, open the test movie file.
14. Choose *Show Histogram* under the *Analyze* menu to display the distribution of pixel values for the image. There should be a continuous distribution if the exported movie is uncompressed. The digital video compression is a 4:1 ratio, so that a compressed

movie would display discrete populations of pixel values by this analysis. Use this procedure to check that the movie was exported under the correct settings.

15. Click the line select tool and select a line that passes over an imaged bead and extends into the background. Choose *Show Plot* under the *Analyze* menu to display the variation in pixel value across the selected line. From this plot, the contrast and bead saturation can be determined. The desired shape should be roughly Gaussian, so that the particle tracking analysis will accurately map the change in brightness over the bead. If the image is saturated, then the brightest part of the bead image will not vary over two or more pixel, as indicated by a cut-off peak.
16. Adjust GAIN and BLACK LEVEL on the camera box to achieve the appropriate contrast and brightness such that the bead image appears to have a roughly Gaussian shape.
17. Move the field of view to a new area before recording the movie to reduce the effects of photobleaching. Record the motion of the beads onto a mini-DV tape using the JVC digital video deck. The movie can simultaneously be written to disk using the *Movie Capture* window under the *File* menu. Once the movie recording has started, avoid touching the microscope, vibration isolation table top, or camera cables. Record approximately 10 minutes of data. Save the clip to the *Movies* folder on the *OS-X* disk, under the *Users* folder.
18. For multiple samples, monitor the memory available as more movies are recorded to disk. As the space is filled, the movies should be transferred to the ACOM-ext 60 GB hard drive. Once a copy has been written to the external drive, the original movie can

be removed from the iMAC-DV hard drive to allow for the necessary scratch disk space needed during the movie capture process.

Exporting Movies as Uncompressed TIFF Files

After transferring the data to the computer, the digital movie must be divided into five second files containing a series of uncompressed images.

1. Change the start up disk to run OS-X.
2. Start Adobe Premiere 5.1. Load *jill's settings* for the new project, then close the project window. Open the data file. A window with the movie will appear with the title Clip:data.filename.
3. Using the timeline at the bottom of the window, move the marker using the cursor, or by clicking on the time code directly(eg. 0:00:03:20). The time code indicates the exact position along the movie by hour:minutes:seconds:frames. Two different time codes are available—non-drop frame (eg. 0;00;03;20) and drop frame (eg. 0:00:03:02). Because video is recorded at a frequency of 29.97 frames per second (fps), the display of each frame as an integer value misrepresents the real time of the movie. Using drop frame time code, this discrepancy is alleviated by labeling the frames to account for the time mismatch, thus providing the user an accurate representation of the movie length. The non-drop frame time code will label each frame consecutively, which will result in a misrepresentation of the actual length of the movie.

4. Use the non-drop frame time code to export the movie. Set the **IN** mark at least 5 seconds after the start of the movie, at the first frame of some interval of seconds (ie. 0:03:10:00, not 0:03:10:05). Move down the time line five seconds by highlighting the seconds number and entering the appropriate value (i.e. 0:03:15:00). To move to that point, press ENTER. Move back one frame using (i.e. 0:03:14:29) before setting the **OUT** mark. The length of the **IN** to **OUT** clip is indicated at the bottom right of the time line as Δ5:00, indicating the movie is five seconds long, exactly. Since the time code labels 30 frames per second, then a five second movie will contain 150 frames. Export the movie as an uncompressed TIFF file, using the following settings:
    - Make: In to Out
    - Video: 640 x 480 (select fix 4:3 ratio) at 29.97 frames per second(fps)
    - Compression: TIFF (100%)
    - Audio: Disabled
5. Create a folder in the *OS-X/Users/Username/Movies/* directory to save the series of uncompressed movies (eg. testfiles). Save the movie with the sample prefix and a four digit suffix indicating the time code of the movie in seconds followed the letter "a". For example, for a movie with a sample name *testfile*, starting at 0:03:10:00, save the file as *testfile*0190a. The format of the file name, including the "a" suffix, will be important for subsequent processing.
6. Continue to break the original data into a series of uncompressed five second movies in TIFF format until the entire movie has been exported. The last five second movie is usually discarded, to avoid any error due to the stopping and starting of the tape recording.

7. Once the movies have been exported using the Adobe Premiere 5.1 software, a second processing step is required to change the format to one that can be read in IDL. Find the "open movie and save" macro and place it in the *Movies* folder, which should also contain the folder with the series of uncompressed movies. Close all applications, then double click on the "open movie and save" macro. The NIH Image v.1.62 program should open with the macro in a new text window. Use the *Macros* → *Load Macro from Window* option to load "open movie and save."
8. Under the *Macros* menu, choose *Save movie as TIFF stack*. This option will only be available after loading the macro, "open movie and save." If it does not appear on the menu, repeat step 7.
9. Follow the series of questions to start saving the movies as TIFF files in NIH Image format. For files that have a starting time less than 1000 seconds, the prefix should be adjusted. In the example described, the prefix would be *testfil*, and the starting time would be *e*0190a. This will provide the correct filename for the new movie.
10. Upon entering the required information, the first movie file must be opened and saved manually. Check the file name in the Save As window is correct (eg. *testfile*0190). It should no longer contain the "a" suffix. After the first file is saved, then the program will automatically open and save the files as indicated by the user.
11. Once the files have been written to NIH format, each TIFF stack should be 49.3MB for a 150 frame movie. Close NIH Image and check to make sure that all movies are the same size before deleting the clips from Adobe Premiere, which are identified by the "a" suffix.

12. Transfer the folder containing the movies to the Linux workstation (datlinux.che.caltech.edu) using scp. (Use man scp in the terminal window for documentation.) Open a terminal window and change directories to move into the movies folder.

    >cd ~/Movies/

    view the files in the directory:

    >ls

    contained in the directory should be the testfiles folder, which contains all of the individual movies. To view the contents of the directory without changing folders:

    >ls testfiles

    Double check that the testfiles folder contains movies that end with a digit, not "a," indicating all files are in the NIH format, before sending the entire folder to datlinux.che.caltech.edu.

    >scp –r testfiles username@datlinux.che.caltech.edu:~/

    Before the files will be transferred, the user will be prompted for a password. If this does not occur, scp is simply writing the testfiles folder to the new name, username@datlinux.che.caltech.edu. The suffix :~/ must included to send the data to a new computer. Two 40GB hard drives are available for use on the Linux workstation. Speak with Suresh Gupta to be added to the user list.

Determining Particle Positions in Each Movie Frame

A tutuorial describing the procedure to determine particle positions using the IDL kit provided by John C. Crocker, David Grier, and Eric R. Weeks is provided on the

website, http://glinda.lrsm.upenn.edu/~weeks/idl/tracking.html, designed by Eric Weeks. This site provides a detailed description of the processing, and should be referred to for all software questions.

1. Open a terminal window on the Linux workstation. List the files on the home directory to identify the location of the testfiles folder. Change the current directory to testfiles, which contains the movies to be analyzed.

   >cd testfiles

2. Start IDL:

   >idl

3. Read in one frame of the first movie file. This command is different from that described in the tutorial in that it includes the option, **last**, which indicates the last frame read into the file, **a**.

   IDL>a=read_nih('filename0190',last=1)

   Since the first series of procedures are used to survey the parameters to fit the particles, only one frame should be considered in the interest of time. After verifying that the fitting parameters are correct, the each frame will be processed with the same values.

4. Use the **bpass** function to idealize the image, then use the feature function to identify the position of particles. Details are described in the tutorial. A second method to check the identity of the positions determined using feature is the **foverlay** procedure. Use **foverlay** when determining the feature parameters, or to check that the positions are correctly assigned to particles rather than noise.

IDL>foverlay,a,f

5. Use the **plot_hist** function, as described in the tutorial, to verify that the fitting parameters do not 'round off' the edge of the particle intensity. For slow moving particles, in solutions of high viscosity, or in elastic gels, this step is important to reduce the potential error in particle position assignment.
6. Use the **jpretrack** function to identify particle positions in one five second movie, based on the parameters determined by the **feature** and **bpass** functions. The **jpretrack** function will output a text file, 'xys.testfile0190.'
7. Again, use the **plot_hist** function to check for pixel biasing, as explained in the tutorial. In addition, one can also view the movement of the particles for five seconds, again, using **foverlay**.
8. Read the text file containing particle position data into a buffer, pt:

   IDL>pt=read_gdf('xys.testfile0190')
9. Check that **a** contains the first frame of the movie file:

   IDL>help,a

   The output should be:

   IDL>a = [640,480]

   Overlay the particle position data for all frames in the first movie:

   IDL>foverlay,a,pt

   For particles moving quickly, the positions should vary, even over 150 frames. If the solution has low viscosity, then apply the deinterlace option, increasing the frequency of the data to 60 Hz. All video is displayed at 30Hz, but the images are written with half the information at twice the frequency. Each frame is divided into two fields,

each containing alternating lines designated as odd or even. The two fields are interlaced, or combined, to form the image displayed at 30 Hz. If particles have significant displacements at 60 Hz, the deinterlace option should be used during the **jpretrack** procedure.

IDL>jpretrack,'testfile0190',[1,11,13,3000],/field

The **field** option indicates that each frame should be deinterlaced into odd and even fields.

Determining Trajectories from Particle Positions

After the particle positions have been determined for the entire set of movies, a series of text files (eg. xys.testfile0190) will be written to the folder containing the movie files. Each xys file contains a series of x and y coordinates, associated with a number that defines the frame number from the five second movie. Before comparing the coordinates from each frame to the next, the text files are concatenated into one single file, in which all frames are addressed consecutively according to their position in the original movie, as recorded on tape. The four digit suffix describing the starting time in seconds is referred to during the concatenation to bring the data together in the correct order.

1. Concatenate files using **cutcat** procedure:

   IDL>cutcat,'xys.testfile*','cat.testfile'

   If the user is not certain all files contain exactly the same number of frames, an alternative concatenation procedure, **ncutcat** may be used:

   IDL>ncutcat,'xys.testfile*','cat.testfile'

The **ncutcat** procedure will count the number of frames in each xys file to ensure the correct numbering, whereas the **cutcat** procedure will only count the first xys file to determine the frame numbering for all files.

2. View the particle positions for the concatenated file using **foverlay**.

   IDL>ptb=read_gdf('cat.testfile')

   IDL>foverlay,a,ptb

3. Before starting the **track** procedure, which will compare the particle positions in consecutive frames to determine their trajectories, the population of the data can be selected from noise or double particles. The 'cutting' option is available using the **cutcat** function:

   IDL>cutcat,'cat.testfile','cut.test',/poly

   Use the cursor to cut a population of the data that most represents the brightest and cleanest particles in the image. Again, **foverlay** may be used to identify the different populations that are cut using the **poly**, or 'cutting,' option.

   IDL>ptb=read_gdf('cut.test')

   IDL>foverlay,a,ptb

4. After a satisfactory data selection is made, the cut.test file may be renamed to cut.testfile and used to determine trajectories.

5. Various parameters are described for the **track** procedure in the tutorial. The options—good and memory—were routinely used and found to be helpful for reducing noise and maintaining long trajectories. Along with the described options, the maximum displacement must be defined:

   IDL>t=track(ptb,3,good=10,memory=3)

6. After the trajectories have been determined, **plot_hist** should be used to display the distribution of displacements for one time step.

IDL>plot_hist,mkpdf(t,1),/log

Two errors can be identified by this information. Below are two figures, the first illustrating an error in which two distinct displacement populations are observed. If this occurs, then steps 3 and 4 should be repeated to select the particles from noise.

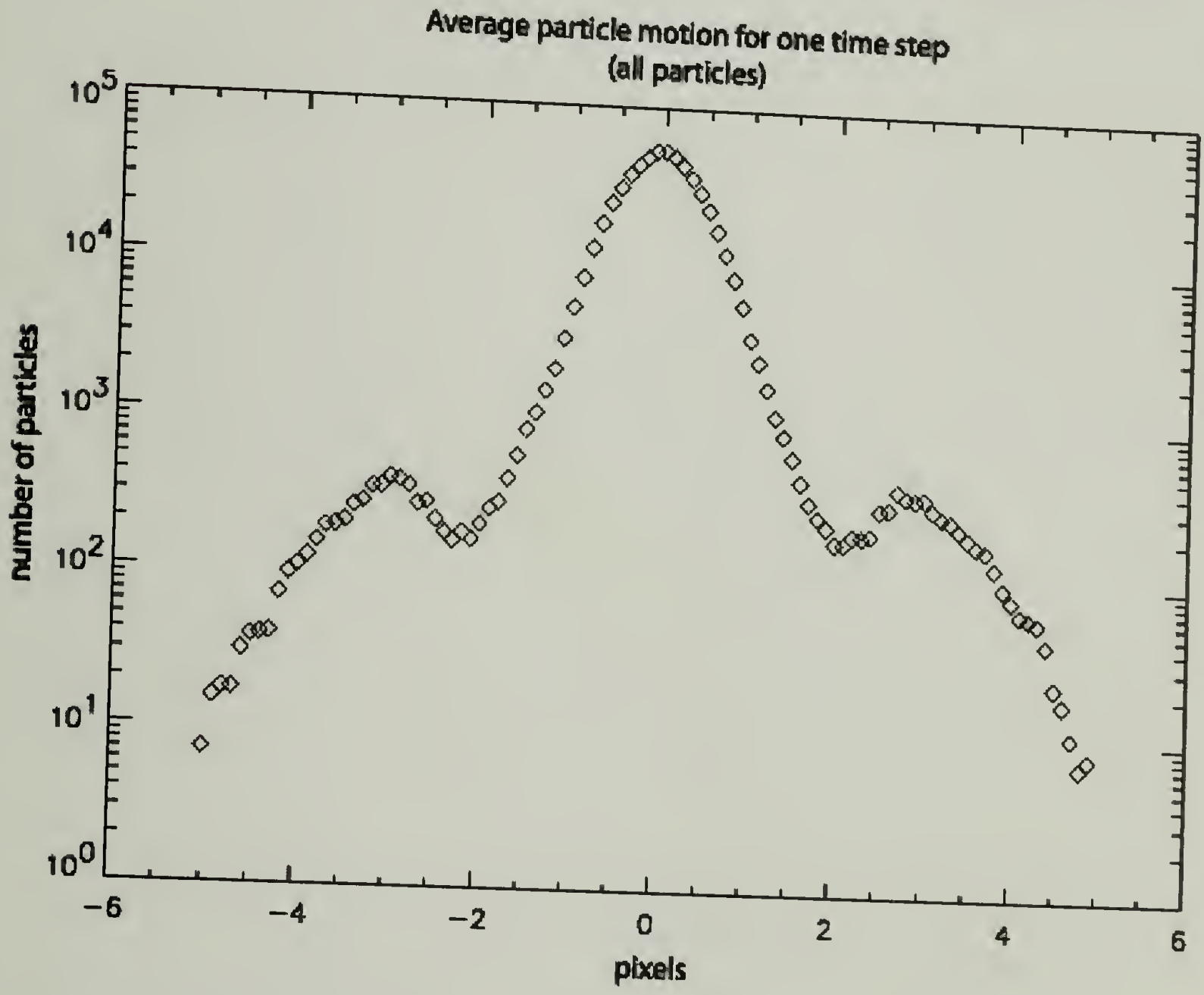

As stated in the tutorial, the histogram should go to zero before the maximum value set in the **track** procedure (eg. 3). The plot below illustrates the distribution of displacements over one time step, for a correctly set maximum diplacement and a selection of particles without noise.

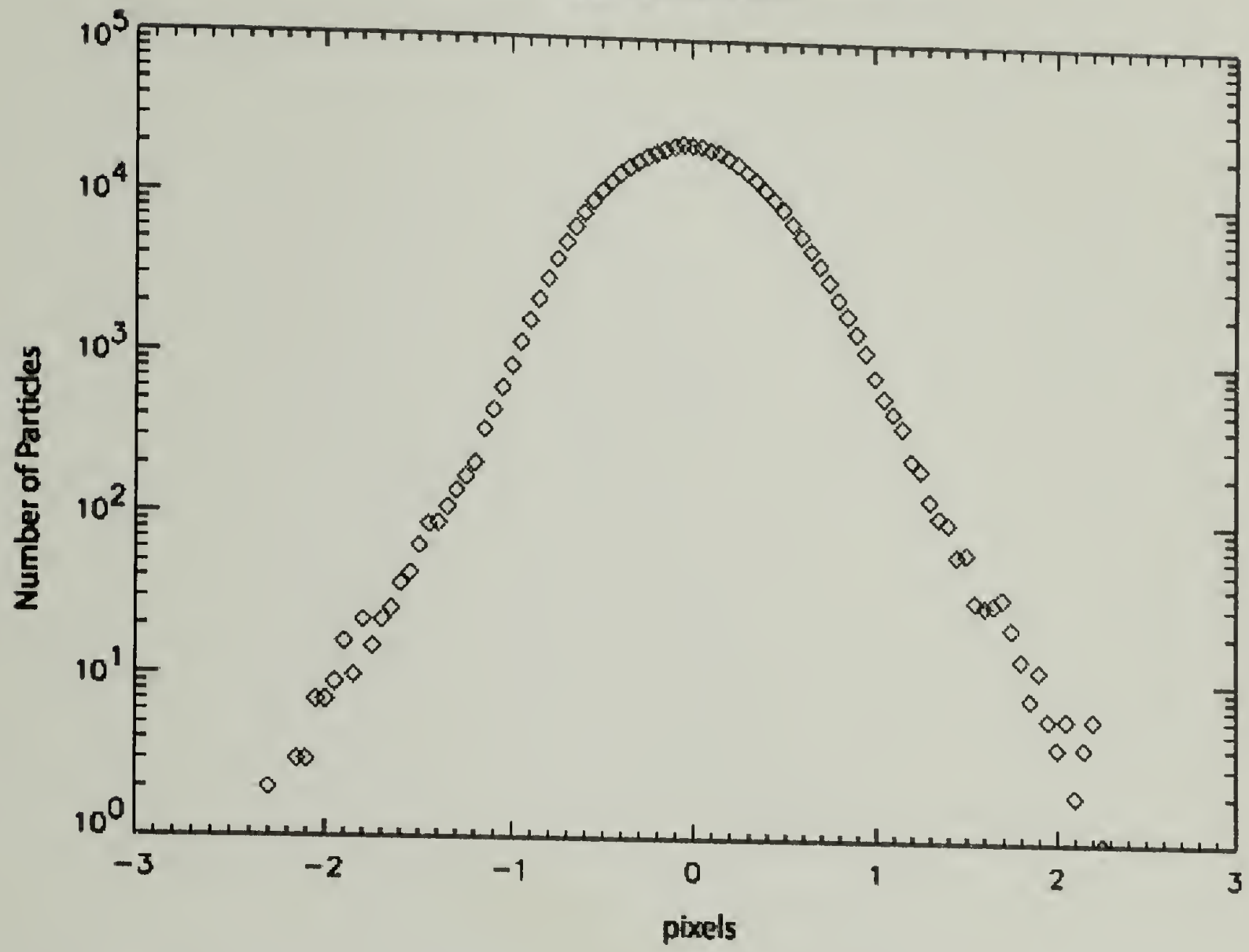

7. In some cases, particles drift during the course of the experiment. This bias can be removed using the **rm_motion** procedure. First, determine the motion in the x and y direction:

   IDL>mot=motion(t)

   drift will be indicated by lines directed in the positive or negative direction. If you think that drift is occurring, remove it using:

   IDL>trb=rm_motion(t,mot,smooth=50)

   The smooth factor can be adjusted from 1-50. 1 is best for sharp changes, such as a bump to the table, and 50 is best if the drift is gradual, as indicated by lines with little noise.

8. The trajectories may be viewed by various methods, including **seeall**, **plottr**, or **foverlay**. Refer to the tutorial for more information about these procedures.
9. Once the trajectories have been determined, the file may be saved for future reference:

   IDL>write_gdf,trb,'t-testfile'

   The gdf format is used by IDL, but cannot be viewed outside the IDL program. To write a text file, use **write_text**:

   IDL>write_text,trb,'t-testfile.txt'

Analyze Trajectories to Determine Mean Squared Displacement vs. Time

At this point, the mean squared displacement can be determined from the trajectories for the sample, testfile.

1. Use the **msd** procedure to determine the mean squared displacement:

   IDL>m=msd(trb,mic=0.083,time=0.0333,erode=2)

   - mic => microns per pixel (0.083 for the 40x objective with 4x tv tube)
   - time => time between frames (0.0166 if deinterlaced, 0.0333 for standard)
   - erode => will remove the given number of frames from the beginning and end of each movie (ie. for erode=2, the first and last two frames are removed from each track before calculating MSD. This will help remove noise introduced by mistaking noise for the beginning of a track of a real particle)

The **msd** procedure writes a file (eg. m) containing seven columns (time,dx,dy,dx^2,dy^2,$dx^2 + dy^2$, ave number of particles) labeled as 0-6

2. View the MSD vs. time on a log-log scales using **plot_oo**:

   IDL>plot_oo,m(0,*),m(3,*),psym=4

3. To overlay MSD plots, (eg. a second msd file named m1), use **oplot**:

   oplot,m1(0,*),m1(3,*),psym=5

   The second data set, m1, will be plotted over the first data set, m

4. Write the MSD files to disk in two formats:

   IDL>write_gdf,m,'m-testfile'

   IDL>write_text,m,'m-testfile.txt'

5. List files to verify that the files are saved:

   IDL>ls

6. Exit IDL

   IDL>exit

7. If satisfied with the results, remove the raw movies and the xys data.

   >rm testfile*

   The cat.testfile contains the same data as the set of xys.* files, so the cat.testfile and cut.testfile may be saved.

   >rm xys.*

8. Transfer MSD data to datserver or another computer to plot data for presentation using scp:

   >scp -r m*.txt user@131.215.228.139:~/Documents

   The computer name or the IP address may be used to identify the computer that to which the data will be sent. (e.g. 131.215.228.139 is the IP address for datserver)

References:

1. J. C. Crocker, D. G. Grier, *J. Colloid Interf. Sci.* **179**, 298-310 (1996).

2. S. Inoue, K. R. Spring, *Video Microscopy: The fundamentals* (Plenum Press, New York, ed. 2nd, 1997).

BIBLIOGRAPHY

A. J. Adler, N. J. Greenfield, G. D. Fasman, *Method. Enzymol.* **27**, 675-735 (1973).

C. M. Anderson, G. N. Georgiou, I. E. G. Morrison, G. V. W. Stevenson, R. J. Cherry, *J. Cell Sci.* **101**, 415-425 (1992).

N. Angelova, D. Hunkeler, *TIBTech.* **17**, 409-421 (1999).

T. Annable, R. Buscall, R. Ettelaie, D. Whittlestone, *J. Rheol.* **37**, 695-726 (1993).

T. Annable, R. Buscall, R. Ettelaie, *Colloid Surface A* **112**, 97-116 (1996).

R. D. Appel, A. Bairoch, D. F. Hochstrasser, *Trends Biochem. Sci.* **19**, 258-260 (1994).

V. Breedveld, D. J. Pine, *J. Mater. Sci.* **38**, 4461-4470 (2003).

J. W. Bryson *et al.*, *Science* **270** (1995).

S. A. Carr, R. S. Annan, in *Current Protocols in Molecular Biology*. (John Wiley & Sons, Inc., 1997) pp. 10.21.1-10.21-27.

T. M. S. Chang, *Biomat. Artif. Cell Im.* **21**, 291-297 (1993).

Y.-H. Chen, J. T. Yang, H. M. Martinez, *Biochemistry-US* **11**, 4120-4131 (1972).

Y.-H. Chen, J. T. Yang, K. H. Chau, *Biochemistry-US* **13**, 3350-3359 (1974).

L. Christenson, K. E. Dionne, M. J. Lysaght, Eds., *Biomedical Applications of Immobilized Cells* (CRC Press, Inc., Boca Raton, Florida, 1993).

L. G. Cima *et al.*, *J. Biomech. Eng.-T. ASME* **113**, 143-151 (1991).

S. Cohen *et al.*, *J. Am. Chem. Soc.* **112**, 7832-7833 (1990).

F. H. C. Crick, *Acta Crystallogr.* **6**, 689-697 (1953).

J. C. Crocker, *J. Chem. Phys.* **106**, 2837-2840 (15 Feb, 1997).

J. C. Crocker, D. G. Grier, *J. Colloid Interf. Sci.* **179**, 298-310 (1996).

J. C. Crocker *et al.*, *Phys. Rev. Lett.* **85**, 888-891 (2000).

D. L. Daugherty, S. H. Gellman, *J. Am. Chem. Soc.* **121**, 4325-4333 (1999).

T. J. Deming, *Adv. Mater.* **9**, 299-311 (1997).

K. DiZio, D. A. Tirrell, *Macromolecules* **36**, 1553-1558 (2003).

E. Durr, I. Jelesarov, H. R. Bosshard, *Biochemistry-US* **38**, 870-880 (1999).

G. L. Ellman, *Arch. Biochem. Biophys.* **82**, 70-77 (1959).

M. Engel, R. W. Williams, B. W. Erickson, *Biochemistry-US* **30**, 3161-3169 (1991).

P. J. Flory, *Principles of Polymer Chemistry* (Cornell University Press, Ithaca, NY, 1953).

H. Geerts *et al.*, *Biophys. J.* **52**, 775-782 (1987).

J. Gelles, B. J. Schnapp, M. P. Sheetz, *Nature* **331**, 450-453 (1988).

R. N. Ghosh, W. W. Webb, *Biophys. J.* **66**, 1301-1318 (1994).

S. C. Gill, P. H. Vonhippel, *Anal. Biochem.* **182**, 319-326 (1989).

S. C. Gill, *Anal. Biochem.* **189**, 283-283 (1990).

F. Gittes, B. Schnurr, P. D. Olmsted, F. C. MacKintosh, C. F. Schmidt, *Phys. Rev. Lett.* **79**, 3286-3289 (1997).

M. F. A. Goosen, G. A. King, Eds., *Cell Immobilization Technology: An Overview* (CRC Press, Inc., Boca Raton, Florida, 1993).

M. S. Green, A. V. Tobolsky, *J. Chem. Phys.* **14**, 80-92 (1946).

T. Gisler, D. A. Weitz, *Phys. Rev. Lett.* **82**, 1606-1609 (1999).

M. Goulian, S. M. Simon, *Biophys. J.* **79**, 2188-2198 (2000).

P. B. Harbury, T. Zhang, P. S. Kim, T. Alber, *Science* **262**, 1401-1406 (1993).

C. M. Hassan, I. Francis J. Doyle, N. A. Peppas, *Macromolecules* **30**, 6166-6173 (1997).

D. L. Hern, J. A. Hubbell, *J. Biomed. Mater. Res.*, 266-276 (1998).

R. S. Hodges, J. Sodek, L. B. Smillie, L. Jurasek, *Cold Spring Harb. Sym.* **37**, 299-310 (1972).

R. S. Hodges, J. Sodek, L. B. Smillie, L. Jurasek, *P. Natl. Acad. Sci. USA* **69**, 3800-3804 (1972).

R. S. Hodges, A. K. Saund, P. C. S. Chong, S. A. St.-Pierre, R. E. Reid, *J. Biol. Chem.* **256**, 1214-1224 (1981).

R. S. Hodges, N. E. Zhou, C. M. Kay, P. D. Semchuk, *Peptide Res.* **3**, 123-137 (1990).

R. S. Hodges, *Biochem. Cell Biol.* **74**, 133-154 (1996).

J. A. Hubbell, *Bio-Technol.* **13**, 565-576 (1995).

J. A. Hubbell, *Curr. Opin. Biotech.* **10**, 123-129 (1999).

S. Inoue, K. R. Spring, *Video Microscopy: The fundamentals* (Plenum Press, New York, ed. 2nd, 1997).

H. Iwata, in *Gels Handbook* Y. Osada, K. Kajiwara, Eds. (Academic Press, San Diego, 2001), vol. 3, pp. 248-260.

H. Jacobson, W. H. Stockmayer, *J. Chem. Phys.* **18**, 1600-1606 (1950).

H. Jacobson, C. O. Beckmann, W. H. Stockmayer, *J. Chem. Phys.* **18**, 1607-1612 (1950).

P. A. Janmey, M. D. Bale, J. D. Ferry, *Biopolymers* **22**, 2017-2019 (1983).

B. Jeong, Y. H. Bae, D. S. Lee, S. W. Kim, *Nature* **388**, 860-862 (1997).

N. R. Kallenbach, P. Lyu, H. Zhou, in *Circular Dichroism and the Conformational Analysis of Biomolecules* G. D. Fasman, Ed. (Plenum Press, New York, 1996) pp. 201-259.

J. Kopecek, *Nature* **417**, 388-389 (2002).

M. Krejchi *et al.*, *Science* **265**, 1427-1432 (1994).

W. H. Landschultz, P. F. Johnson, S. L. McKnight, *Science* **240**, 1759-1764 (1988).

R. Langer, *Science* **249**, 1527-1533 (1990).

R. Langer, J. P. Vacanti, *Science* **260**, 920-926 (1993).

S. Y. M. Lau, A. K. Taneja, R. S. Hodges, *J. Biol. Chem.* **259**, 13253-13261 (1984).

A. W. C. Lau, B. D. Hoffman, A. Davies, J. C. Crocker, T. C. Lubensky, *Phys. Rev. Lett.* **91**, art. no.-198101 (2003).

P. Lavigne *et al.*, *J. Mol. Biol.* **254**, 505-520 (1995).

A. J. Levine, T. C. Lubensky, *Phys. Rev. Lett.* **85**, 1774-1777 (2000).

A. J. Levine, T. C. Lubensky, *Phys. Rev. E* **6501**, 1-13 (2002).

K. J. Lumb, P. S. Kim, *Science* **268**, 436-438 (1995).

T. Maniatis, E. F. Fritsch, J. Sambrook, *Molecular cloning: A laboratory manual* (Cold Spring Harbor Laboratory Press, New York, 1989).

M. C. Manning, *J. Pharmaceut. Biomed.* **7**, 1103-1119 (1989).

T. G. Mason, D. A. Weitz, *Phys. Rev. Lett.* **74**, 1250-1253 (1995).

T. G. Mason, H. Gang, D. A. Weitz, *J. Mol. Struct.* **383**, 81-90 (1996).

T. G. Mason, K. Ganesan, J. H. vanZanten, D. Wirtz, S. C. Kuo, *Phys. Rev. Lett.* **79**, 3282-3285 (1997).

T. Mayata, M. Asami, T. Uragami, *Nature* **399**, 766-769 (1999).

C. R. Mayer, V. Cabuil, T. Lalot, R. Thouvenot, *Adv. Mater.* **12**, 417-420 (2000).

J. L. McGrath, J. H. Hartwig, S. C. Kuo, *Biophys. J.* **79**, 3258-3266 (2000).

K. P. McGrath, M. J. Fournier, T. L. Mason, D. A. Tirrell, *J. Am. Chem. Soc.* **114**, 727-733 (1992).

K. P. McGrath, M. M. Butler, in *Protein-Based Materials* K. P. McGrath, D. L. Kaplan, Eds. (Birkhauser, Boston, 1997) pp. 251-280.

K. P. McGrath *et al.*, *J. Bioact. Compat. Pol.* **15**, 334-356 (2000).

J. Moitra, L. Szilak, D. Krylov, C. Vinson, *Biochemistry-US* **36**, 12567-12573 (1997).

T. Narita, A. Knaebel, J.-P. Munch, S. J. Candau, *Macromolecules* **34**, 8225-8231 (2001).

A. P. Nowak *et al.*, *Nature* **417**, 424-428 (2002).

A. A. Obaidat, K. Park, *Biomaterials* **18**, 801-806 (1997).

E. K. O'Shea, R. Rutkowski, P. S. Kim, *Science* **243**, 538-542 (1989).

E. K. O'Shea, R. Rutkowski, I. Walter F Stafford, P. S. Kim, *Science*, 646-648 (1989).

E. K. O'Shea, J. D. Klemm, P. S. Kim, T. Alber, *Science* **254**, 539-544 (1991).

E. K. O'Shea, R. Rutkowski, P. S. Kim, *Cell* **68**, 699-708 (1992).

E. K. O'Shea, K. J. Lumb, P. S. Kim, *Curr. Biol.* **3**, 658-667 (1993).

N. A. Peppas, R. Langer, *Science* **263**, 1715-1720 (1994).

W. A. Petka, Ph.D. dissertation, University of Massachusetts, Amherst (1997).

W. A. Petka, J. L. Harden, K. P. McGrath, D. Wirtz, D. A. Tirrell, *Science* **281**, 389-392 (1998).

W. A. Petka, J. L. Harden, J. K. Sakata, D. A. Tirrell, *Mat. Res. Soc. Symp.* **550**, 23-28 (1999).

H. Qian, *Biophys. J.* **79**, 137-143 (2000).

H. Qian, *Protein Sci* **11**, 1-5 (January 1, 2002, 2002).

J. R. Quintana, E. Diaz, I. Katime, *Macromolecules* **30**, 3507-3512 (1997).

J. R. Quintana, E. Diaz, I. Katime, *Polymer* **39**, 3029-3034 (1998).

R. Rasmussen, D. Benvegnu, E. K. O'Shea, P. S. Kim, T. Alber, *P. Natl. Acad. Sci. USA* **88**, 561-564 (1991).

B. D. Ratner, A. S. Hoffman, F. J. Schoen, J. E. Lemons, Eds., *Biomaterials Science: An introduction to materials in medicine* (Academic Press, Inc., San Diego, CA, 1996).

S. E. Sakiyama-Elbert, J. A. Hubbell, *Annu. Rev. Mater. Res.* **31**, 183-201 (2001).

A. S. Sawhney, J. A. Hubbell, *Biomaterials* **12**, 863-870 (1992).

M. J. Saxton, *Biophys. J.* **64**, 1766-1780 (1993).

M. J. Saxton, K. Jacobson, *Annu. Rev. Bioph. Biom.* **26**, 373-399 (1997).

M. V. Sefton, W. T. K. Stevenson, in *Advances in Polymer Science* N. A. Peppas, R. S. Langer, Eds. (Springer-Verlag, New York, 1993), vol. 107, pp. 145-197.

B. Shnurr, F. Gittes, F. C. MacKintosh, C. F. Schmidt, *Macromolecules* **30**, 7781-7792 (1997).

J. Y. Su, R. S. Hodges, C. M. Kay, *Biochemistry-US* **33**, 15501-15510 (1994).

F. Tanaka, W. H. Stockmayer, *Macromolecules* **27**, 3943-3954 (Jul 4, 1994).

F. Tanaka, K. Nishinari, *Macromolecules* **29**, 3625-3628 (1996).

F. Tanaka, M. Ishida, *Macromolecules* **29**, 7571-7580 (Nov 4, 1996).

F. Tanaka, *Prog. Theor. Phys. Supp.* **126**, 257-260 (1997).

Y. Tang, D. A. Tirrell, *J. Am. Chem. Soc.* **123**, 11089-11090 (2001).

K. te Nijenhuis, Ed., *Thermoreversible Networks: Viscoelastic Properties and Structure of Gels*, vol. 130 (Springer-Verlag, New York, 1997).

K. Thuresson, S. Nilsson, B. Lindman, *Langmuir* **12**, 530-537 (1996).

K. Thuresson *et al.*, *J. Phys. Chem. B* **103**, 1425-1436 (1999).

J. G. Tirrell, D. A. Tirrell, M. J. Fournier, T. L. Mason, in *Protein-Based Materials* K. McGrath, D. Kaplan, Eds. (Birkhauser, Boston, 1997) pp. 61-102.

C. Tsitsilianis, I. Iliopoulos, *Macromolecules* **35**, 3662-3667 (2002).

C. Wang, R. J. Stewart, J. Kopecek, *Nature* **397**, 417-420 (1999).

C. Wang, J. Kopecek, R. J. Stewart, *Biomacromolecules* **2**, 912-920 (2001).

R. C. Weast, *Handbook of Chemistry and Physics* (CRC Press, Boca Raton, FL, 1988), vol. 1st Student Edition.

E. R. Weeks, J. C. Crocker, A. C. Levitt, A. Schofield, D. A. Weitz, *Science* **287**, 627-631 (2000).

D. A. Weitz, J. X. Zhu, D. J. Durian, H. Gang, D. J. Pine, *Phys. Scripta* **T49**, 610-621 (1993).

E. R. Welsh, D. A. Tirrell, *Biomacromolecules* **1**, 23-30 (2000).

H. Wendt, A. Baici, H. R. Bosshard, *J. Am. Chem. Soc.* **116**, 6973-6974 (1994).

H. Wendt, C. Berger, A. Baici, R. M. Thomas, H. R. Bosshard, *Biochemistry-US* **34**, 4097-4107 (1995).

M. A. Winnik, A. Yekta, *Curr. Opin. Colloid Interface Sci.* **2**, 424-436 (1997).

J. Xu, A. Palmer, D. Wirtz, *Macromolecules* **31**, 6486-6492 (1998).

J. Xu, V. Viasnoff, D. Wirtz, *Rheol. Acta* **37**, 387-398 (1998).

J. M. Yu *et al.*, *Macromolecules* **29**, 5384-5391 (1996).

J. M. Yu, P. Dubois, P. Teyssie, R. Jerome, *Macromolecules* **29**, 6090-6099 (1996).

J. M. Yu, S. Blacher, F. Brouers, G. L'Homme, R. Jerome, *Macromolecules* **30**, 4619-4625 (1997).

J. M. Yu, R. Jerome, P. Teyssie, *Polymer* **38**, 347-354 (1997).

S. Yu *et al.*, *Nature* **389**, 167-170 (1997).

N. E. Zhou, C. M. Kay, R. S. Hodges, *J. Biol. Chem.* **267**, 2664-2670 (1992).

N. E. Zhou, B. Y. Zhu, C. M. Kay, R. S. Hodges, *Biopolymers* **32**, 419-426 (1992).

N. E. Zhou, C. M. Kay, R. S. Hodges, *Protein Eng.* **7**, 1365-1372 (1994).

M. Zrinyi, *Trends Polym. Sci.* **5**, 280-285 (1997).